Dear Prof. Sergey A. Nizkorodov,

Thank you very much for the handling of the reviewing process for our manuscript. We have carefully addressed all of the comments by the anonymous referees # 1 and 3 in the revised manuscript. We also did our best to address the comments by anonymous referee # 2, although we found that most of them are either not fair or already addressed in the reviewed manuscript. Our point-by-point responses to the referees' comments are provided below. All the changes and corrections are highlighted in the revised manuscript and in the Supplementary Material which are also provided below. We hope that you will find the revisions satisfactory and sufficient.

Respectfully,

Igor Konovalov

on behalf of all the authors

Authors' response to the comments of Anonymous Referee # 1

We thank the Referee for the constructive comments. We tried to address them in the best way possible in the revised manuscript. Our point-by-point responses to the Referee's comments are provided below.

Referee's comment: *1. How is plume rise included in Chimere? What is the maximum vertical height of injection?*

As noted in the reviewed manuscript (page 11, lines 1, 2, 10), the fire emissions in our simulations were specified using a methodology that included calculations of the emission heights using the parameterization proposed by Sofiev et al. (2012) and was detailed in our previous papers. In response to the Referee's comment, a concise description of this parameterization and the information on its validation are provided in Sect. 2.3 of the revised manuscript. In particular, we note that the maximum injection heights of biomass burning (BB) emissions were calculated for each FRP pixel as a function of the observed FRP, the boundary layer height, and the Brunt–Väisälä frequency. In other words, the maximum vertical height of injection was not assumed to be constant but varied both in time and space. We also explain that the emissions for a given model layer were computed proportionally to the weighted number of pixels yielding the maximum injection height corresponding to this layer, with the weight of each pixel evaluated proportionally to the corresponding FRP. The average heights of the BB plumes considered in our analysis are reported in Figs. S8b and S6b in the Supplementary Material for the reviewed and revised versions of our manuscript, respectively.

Referee's comment: *2. A lot of model measurement evaluation is based on satellite data that have their own challenges as described in this study. Are there any in-situ measurements of organic aerosols at source/receptor sites? These would be valuable to constrain surface and vertical profiles of OA simulated by Chimere.*

Indeed, the satellite data which were used in our analysis are certainly not perfect. However, as pointed out in the reviewed manuscript (page 9, lines 6-12), the OMI (OMAERUV) AAOD retrievals were evaluated, both directly and indirectly (through the modeled BB emissions constrained with these retrievals), using AERONET, aircraft, and in situ data in Siberia as part of our previous study (Konovalov et al., 2018) which revealed no serious biases in these retrievals. The uncertainties in the MODIS AOD data are well documented and are relatively small (Levy et al., 2010). Accordingly, we see no evidence that the strong changes in the BB aerosol optical properties, which are identified in our analysis, can be an artifact of biases in the satellite data. Random uncertainties in the satellite data are, of course, quite considerable, but they are taken into account in our estimates of the confidence intervals for the derived tendencies in the analyzed characteristics.

Regrettably, we do not have any measurements of organic aerosols in the study region in the analyzed period at our disposal. But even if such measurements were available, they would hardly be sufficiently informative for our study: as we argue in the introduction, field studies show a very diverse picture of atmospheric transformations of BB aerosol, reflecting big diversity in fuel type and burning conditions, and so the sparse and often contradictory results of these studies can hardly provide consistent observational constraints for model representations of the effects of atmospheric aging of BB aerosol originating from multiple fires from a big region, specifically Siberia.

Taking into account the Referee's comment, we extended the discussion of possible uncertainties in our analysis, including those associated with the analysis of satellite data and the modeling, and provided a caveat concerning potential biases in the satellite data. This discussion is presented in the newly-introduced section (Sect. 3.4) of the revised manuscript.

Referee's comment: *3. Biomass burning emissions inventories like GFED often severely under-predict POA emissions from biomass burning. Can the authors provide any discussions/evaluations of primary BBOA emissions used in the model? Along the same lines, if inventories are missing a large BB-POA source, one could simply increase POA by a factor of 3 to 5, turn off BB-SOA formation and just age POA. This may result in different size evolutions (e.g. SSA, scattering efficiency), AAOD and AOD evolution. Would be interesting to see how this could affect the results and interpretations of this study.*

We thank the Referee for this insightful comment. Indeed, there is evidence (partly based on multiple studies that reported underestimation of AOD by models) that GFED and other inventories strongly underestimate POA (or OC) emissions from biomass burning. At the same time, the underestimation of AOD by a model can, at least partly, be caused by missing SOA sources in the model representation of organic aerosol, as argued, in particular, in one of our previous papers (Konovalov et al., 2015). So, in our understanding, there is a general problem concerning the evaluation of POA (OC) emissions provided by inventories. The results of our study have some implications in the context of this problem, even though the evaluation of the BB emission inventories is not its primary objective.

To address the Referee's comment, we provided a comparison of our "top-down" estimates of OC and BC emissions in the study region in July 2016 (Sect. 2.6 of the revised manuscript) with the bottom-up estimates obtained from the GFED4.1s inventory (van der Werf et al., 2017). While the top-down OC emission estimate for the 'bb_vbs' simulation scenario is found to agree well with the GFED data, the top-down estimate obtained using the 'bb_trc' simulation (which does not take into account the SOA formation) is almost a factor of 3 bigger than the corresponding bottom-up estimate (similar to what was found in our previous study (Konovalov et al., 2018)). As a caveat, we note that the good agreement of the bottom-up and top-down estimates of the OC emissions does not necessarily indicate that the emission inventory is accurate: ideally, the consistency of top-down and bottom-up estimates of the BB OC emissions should be examined by taking into account the partitioning of the measured emissions between gases and particles, but the corresponding data are not provided as part of emission inventories.

Following the referee's instructions, we also performed an additional simulation (referred to as 'bb_poa') in which the SOA formation was turned off but POA emissions were strongly increased (specifically, by a factor of 4.3) to retain the consistency between the simulated and observed AOD in the source region. The results of this simulation are summarized in Sect. 3.3 and presented in more detail in the Supplementary Material (Sect. S5). Consistently with our conclusions about the major role of SOA formation in the evolution of BB aerosol during the analyzed event, the simulations for the 'bb_poa' scenario are not found to exhibit any qualitative nonlinear features of the behavior of SSA and EnR for AOD, which were identified in the analysis of the satellite observations and were reproduced in the simulations for the 'bb_vbs' scenario. We consider this result as evidence that the proposed joint analysis of satellite and model data can be used to distinguish between the two possible reasons for the underestimation of AOD by a model, such as (1) an underestimation of OC emissions in the emission inventory and (2) missing SOA sources in the model.

Referee's comment: *4. Page 18: Its confusing as written: " We selected only those simulations that have the same ranks as the subset of CO observations matching (as described above) the OMI AAOD data". Please elaborate. How did the authors calculate ranks? Did they consider different simulations driven by different renalyses to minimize plume dispersion errors?*

We are sorry that the sentence indicated by the referee was confusing, and we tried to explain our procedure more clearly in the revised manuscript. As it is common in statistics (https://en.wikipedia.org/wiki/Ranking), the ranking of a set of data points was done in our case by assigning the order number to values arranged in ascending order. We'd like to note that while the selection procedure based on the ranking of the CO columns retrieved from satellite observations and simulated with CHIMERE was introduced to ensure more accurate quantitative results of our analysis, our main conclusions concerning the qualitative features of the BB aerosol evolution do not depend on the application of this procedure.

Unfortunately, we could not perform simulations based on different reanalyses in the framework of this study due to computational limitations. We are also not sure that the use of different reanalyses could result in a major reduction of the differences between the simulated and observed data, since these differences appear to be more due to uncertainties in the temporal and spatial variability of fire emissions rather than due to model transport errors.

Referee's comment: *5. Table2: In equation R3 how were coefficients 0.33 and 0.30 determined? Also in R5 and R6 85% of SOA is lost by fragmentation. Is the fragmented SOA recirculated or does it react to yield some MV-SOA/LV-SOA?*

The coefficients 0.33 and 0.3 were defined to retain the same total SOA yields for HV-SOA and LV-SOA from the oxidation of NTVOCs (~ 43 g mol^{-1}) as in Ciarelli et al. (2017) (page 14, lines 16, 17 of the reviewed manuscript), taking into account that the assumed molecular weights of HV-SOA and LV-SOA are 131 and 144 g mol^{-1}. In the revised manuscript (Sect. 2.4), we additionally explain that we took into account the ratio of the molar masses of these species (131/144 ≅ 0.30/0.33). The products of the fragmentation pathway of reactions (R5) and (R6) were considered as volatile and did not contribute to the SOA formation (page 14, line 27 of the reviewed manuscript).

Referee's comment: *6. Figure 2: Why does Chimere have too high AOD compared to MODIS is South-Eastern part of domain?*

We addressed this question in Sect. 3.1 of the revised manuscript. We suppose that the simulated AOD is biased high outside of the study region in the south-eastern part of the model domain as a result of spatial variations in any parameters determining (or affecting) the relationship between the real biomass burning rate and the calculated aerosol emissions. Such parameters include, in particular, the emission factors, volatility distributions for the POA emissions, and empirical factor relating FRP to the BB rate. The variations in these parameters may, in turn, be due to the inhomogeneity in the spatial distribution of the vegetation species across the study region and model domain. It is noteworthy that the high bias in AOD is not mirrored in the spatial distribution of the simulated CO columns (see Figs. S1 and S2 in the Supplementary Material of the reviewed and revised versions of the manuscript, respectively).

Referee's comment: *7. Page 22 Before section 3.2: Can the authors comment on relative importance of various processes affecting decrease of AOD to AAOD from source to receptor, e.g. fragmentation, evaporation etc.?*

Our in-detail interpretation of the processes affecting the changes in AOD to AAOD during the transport of BB plumes from the source to receptor regions is provided in Sect. 3.3 of both the reviewed and revised versions of the manuscript. In the revised manuscript, we provided an additional remark in Sect. 3.1 that the additional changes (that cannot be explained by dilution) in AOD to AAOD are primarily caused by the losses of the medium-volatility fraction of SOA due to fragmentation.

Referee's comment: *8. Figure 10: Seems we need another case showing BC core with absorbing OA shell and lensing effects.*

Figure 10 shows our computations only for several test cases. The respective results for the base case (where, as suggested by the referee, the BC core is surrounded by the absorbing OA shell and the lensing effects are taken into account) are shown in Fig. 7a. In the revised manuscript, a corresponding explanatory remark is introduced in the caption of Fig. 10.

Referee's comment: *9. How does particle water affect calculated optical properties, especially if water is on the shell?*

Since the relative humidity (RH) characterizing ambient conditions for the BB plumes analyzed in our study typically remained below 70 % (see Figs. S8a and S6a in the reviewed and revised versions of the manuscript, respectively), we did not expect, based on the common knowledge (e.g., Reid et al., 2005), that the water uptake by particle could significantly affect BB aerosol optical properties and their evolution. Indeed, according to our simulations, the water mass fraction stays, on the average, below 15% as long the photochemical age is less than 60 h, eventually increasing up to 26% toward the end of the evolution period considered (see Fig. 8a in the revised manuscript). Possible effects of the water uptake on our simulations are discussed in Sect. 3.3 of the revised manuscript. Specifically, we argue that water and inorganic ions increase the scattering cross-section of BB aerosol particles, thereby increasing AOD and SSA, although the contribution of a unit mass of water to the scattering efficiency is expected to be considerably smaller than that of the organic matter because the real component of the refractive index for water is substantially smaller than for the organic species. We also point out that a substantial increase in the water uptake occurs in our simulations only after 60 h, and therefore it could not contribute significantly to the strong increase in EnR for AOD before 30 h. The water uptake by the organic shell of the particles can also contribute to the lensing effect, thereby increasing AAOD, but the evolution of EnR for AAOD in our case was found to be determined by other factors anyway, as illus-

trated in Fig. 10. In addition to this discussion, we explicitly estimated the effects of water on AOD, SSA, and the scattering efficiency in the 'bb_poa' test simulation mentioned above. These estimates, which are discussed in Sect. S5 of the revised Supplementary Material and are presented in Fig. S8, confirm that the water uptake of particles was not among the key factors that drove the evolution of the optical properties of BB aerosol during the analyzed episode.

5 Referee's comment: *10. It would be intuitive to see a map of particle water over the domain, especially given discussion of potential importance of heterogeneous oxidation of biomass burning OA. I would think that even with hygroscopicity of 0.2 water content of BBOA will be large due to its high concentration.*

The calculated mean water content in the BB particles is shown in Fig. 8a of the revised manuscript as a function of the photochemical age. As noted above, it turned out to be relatively small, since the ambient relative humidity in the
10 center of mass of the BB plumes typically did not exceed 70 %. We presumed that Fig. 8a would be more informative than a map suggested by the referee, because the calculated mean water fraction takes into account the spatial inhomogeneity of the aerosol mass loadings in the atmospheric columns, giving larger weights to the high loadings. As the manuscript and Supplementary Material are already lengthy, we opted to not provide one more figure (which would also entail additional discussion). Note that Fig. 8a provided in the reviewed manuscript was meant to implicitly show
15 the contribution of water among "other" components. However, thanks to the Referee's comment we noticed that the model output data for these components were not processed properly. We apologize for this oversight. A corrected and improved version of Fig. 8a, in which the contribution of water is shown explicitly, is provided in the revised manuscript.

Referee's comment: *11. Can the authors comment on role of photolysis of biomass burning SOA as its loss process?*

20 A corresponding comment is provided in Sect. 3.4 of the revised manuscript. In particular, we mention the available global-scale estimates (Hodzic et al., 2015) of the SOA lifetime with respect to the in-particle photolysis, and also note that if the in-particle SOA photolysis were a primary driver for the decrease of AOD in our analysis, then the rate of the decrease in EnR$_{ext}$ would not be expected to strongly decelerate after about 70 h, as it does according to Fig. 5b.

Referee's comment: *12. Page 28: If SOA is glassy, it may not mix with POA. How are the authors treating absorptive*
25 *gas-particle partitioning of POA-SOA mixtures. One could envision treating them as two separate solutions from Raoult's law perspective.*

We made it clear in the revised manuscript (Sect. 2.4) that following Ciarelli et al. (2017) we assumed, for definiteness, that all organic species within particles form a well-mixed liquid and inviscid solution. Possible implications of this assumption – which cannot be validated or invalidated using available observations in Siberia – are briefly dis-
30 cussed in Sect. 3.4 of the revised manuscript. In particular, we note that if POA and SOA species do not mix in reality but form two separate solutions (as assumed, e.g., in Shrivastava et al., 2015), then our model is likely prone to overestimation of their concentrations in particles. It is, however, hard to see how these potential biases can invalidate our qualitative interpretation of the major changes in the BB aerosol optical properties. We plan to address the possible effects of viscosity and non-ideality of organic solutions on the Siberian BB aerosol evolution in our future studies.

35 Referee's comment: *13. Would the increase of brown carbon with BC to OA ratio imply LV-SOA is more absorbing (brown) than MV-SOA? I recall this was implied in Saleh et al. study referenced by the authors. But this is contrary to the author's hypothesis that LV-SOA is much less absorbing than MV-SOA. This may need some discussions.*

This point is briefly discussed in Sect. 2.4 of the revised manuscript. Specifically, we note that our assumption that LV-SOA is non-absorbing does not contradict the experimental findings indicating high absorptivity of low-volatility
40 organic compounds (Saleh et al., 2014), because the contributions of POA and SOA species to absorption were not isolated in these experiments, and the effect of SOA addition was found there to be comparable to measurement uncertainties.

SSA was evaluated in the standard way as 1-AAOD/AOD according to Eq. (6). So, as both AOD and AAOD decrease (due to various processes, including those indicated by the referee) to about the same extent, SSA is not significantly affected. The average size distributions of BB aerosol particles for different processing times are shown in Figs. S9 and S7 of the Supplementary Material of the reviewed and revised versions of the manuscript, respectively. We are sorry if we did not understand this comment of the Referee properly.

References

Ciarelli, G., El Haddad, I., Bruns, E., Aksoyoglu, S., Möhler, O., Baltensperger, U., and Prévôt, A. S. H.: Constraining a hybrid volatility basis-set model for aging of wood-burning emissions using smog chamber experiments: a box-model study based on the VBS scheme of the CAMx model (v5.40), Geosci. Model Dev., 10, 2303-2320, https://doi.org/10.5194/gmd-10-2303-2017, 2017.

Hodzic, A., Madronich, S., Kasibhatla, P. S., Tyndall, G., Aumont, B., Jimenez, J. L., Lee-Taylor, J., and Orlando, J.: Organic photolysis reactions in tropospheric aerosols: effect on secondary organic aerosol formation and lifetime, Atmos. Chem. Phys., 15, 9253–9269, https://doi.org/10.5194/acp-15-9253-2015, 2015.

Konovalov, I. B., Beekmann, M., Berezin, E. V., Petetin, H., Mielonen, T., Kuznetsova, I. N., and Andreae, M. O.: The role of semi-volatile organic compounds in the mesoscale evolution of biomass burning aerosol: a modeling case study of the 2010 mega-fire event in Russia, Atmos. Chem. Phys., 15, 13269-13297, https://doi.org/ 10.5194/acp-15-13269-2015, 2015.

Konovalov, I. B., Lvova, D. A., Beekmann, M., Jethva, H., Mikhailov, E. F., Paris, J.-D., Belan, B. D., Kozlov, V. S., Ciais, P., and An-dreae, M. O.: Estimation of black carbon emissions from Siberian fires using satellite observations of absorption and extinction optical depths, Atmos. Chem. Phys., 18, 14889-14924, https://doi.org/10.5194/acp-18-14889-2018, 2018.

Levy, R. C., Remer, L. A., Kleidman, R. G., Mattoo, S., Ichoku, C., Kahn, R., and Eck, T. F.: Global evaluation of the Collection 5 MODIS dark-target aerosol products over land, Atmos. Chem. Phys., 10, 10399–10420, https://doi.org/10.5194/acp-10-10399-2010, 2010.

Reid, J. S., Eck, T. F., Christopher, S. A., Koppmann, R., Dubovik, O., Eleuterio, D. P., Holben, B. N., Reid, E. A., and Zhang, J.: A re-view of biomass burning emissions part III: intensive optical properties of biomass burning particles, Atmos. Chem. Phys., 5, 827–849, https://doi.org/10.5194/acp-5-827-2005, 2005.

Shrivastava, M., Easter, R., Liu, X., Zelenyuk, A., Singh, B., Zhang, K., Ma, P-L, Chand, D., Ghan, S., Jimenez, J. L., Zhang, Q., Fast, J., Rasch, P., and Tiitta, P.: Global transformation and fate of SOA: Implications of low volatility SOA and gas phase fragmentation reac-tions, J. Geophys. Res.-Atmos., 120, 4169–4195, https://doi.org/10.1002/2014JD022563, 2015.

Sofiev, M., Ermakova, T., and Vankevich, R.: Evaluation of the smoke-injection height from wild-land fires using remote-sensing data, Atmos. Chem. Phys., 12, 1995–2006, https://doi.org/10.5194/acp-12-1995-2012, 2012.

van der Werf, G. R., Randerson, J. T., Giglio, L., van Leeuwen, T. T., Chen, Y., Rogers, B. M., Mu, M., van Marle, M. J. E., Morton, D. C., Collatz, G. J., Yokelson, R. J., and Kasibhatla, P. S.: Global fire emissions estimates during 1997–2016, Earth Syst. Sci. Data, 9, 697–720, https://doi.org/10.5194/essd-9-697-2017, 2017.

Authors' response to the comments of Anonymous Referee # 2

We thank the Referee for the critical comments. We regret that the Referee did not find worth mentioning any of the features and results of our study, which highlight a high degree of its novelty and originality, and apparently did not pay attention to the supportive analysis presented in the Supplementary Material. Nonetheless, we tried to address the Referee's comments to the best degree possible in the revised manuscript. Our point-by-point responses to the Referee's comments are provided below.

Referee's comment: *Similarly to their previous study Konovalov et al., 2017 (https://doi.org/10.5194/acp-17-4513-2017), authors use the enhancement ratios in AOD, AAOD and SSA due to the formation of organic aerosols from BB emissions relative to the corresponding enhancement of an inert aerosol tracer to investigate processes that occur during atmospheric aging of BB plumes.*

We regret that the Referee apparently misunderstood the degree of novelty of our study. Contrary to the referee's statement, our previous paper (Konovalov et al., 2017), as evident from its abstract (https://doi.org/10.5194/acp-17-4513-2017), addressed the enhancement ratios only for AOD. This major difference between this study and the previous one is explicitly explained in the introduction of the reviewed manuscript (page 4, lines 6-9, page 5, lines 26, 27). This implies detailed work on the evolution of the optical and absorptive properties of aerosol in this work, by using a Mie code. Another major novel feature of this study is the development of an original analytical framework involving the use of satellite observations as constraints to the adjustable VBS parameterization of the biomass burning (BB) organic aerosol evolution (see the abstract of the discussion paper, and also page 3, lines 30, 31, page 5, lines 4, 11-15, page 29, lines 4-9 in the reviewed manuscript).

Referee's comments: *1) The representation of organic aerosol chemistry and processes within the CHIMERE model is expected to play a key role in the interpretation of the satellite observations, and in the conclusions of this paper. My concern is that the parameterizations used in this study are either somewhat outdated i.e. for biogenic and anthropogenic precursors, or have not been previously evaluated i.e. biomass burning precursors. For instance, the VBS parameterization used in this study for BB precursors was derived from the VBS proposed by Ciarelli et al., 2017 that provided a hybrid volatility basis-set model for aging of wood-burning emissions. It seems that organic compounds were lumped over several volatility bins, and given different properties and aging reactions (Table 2), and this was done without any constraint from experimental data. It is critical for this paper to demonstrate that the derived simplified mechanism provides accurate results.*

We are not aware of any state-of-the-art parameterizations for biogenic and anthropogenic precursors that have been shown to allow improving 3D-model simulations of biogenic and anthropogenic aerosol in Siberia compared to simulations based on relatively simple parameterizations similar to those implemented in the standard version of CHIMERE. At the same time, we believe that our analysis could not be significantly affected by possible uncertainties in the modeled concentrations of anthropogenic and biogenic aerosol. This is specifically indicated by the facts that (1) the AOD level during the analyzed episode exceeded the background AOD level on the average by at least a factor of 6 (see Fig. 4 c, d in the reviewed manuscript) and (2) that the AOD simulations performed without fire emissions fit well the AOD observations in the periods when fire emissions were small (see Fig. S2). The sensitivity of the inferred evolution of the enhancement ratios for both AAOD and AOD to the assumed background conditions was examined in the supplementary section S3 of the reviewed manuscript. Regrettably, we see no evidence that the results of this analysis were taken into account by the referee.

Concerning the modeling of biomass burning precursors of aerosol, we argued in the introduction of the reviewed manuscript (page 3, lines 26-28 and above), that "… the sparse and often contradictory results of field and laboratory studies available so far can hardly provide consistent observational constraints for representations of the effects of atmospheric aging of BB aerosol in chemistry-transport and climate models". We also noted that "using the different VBS oxidation schemes partly constrained by laboratory measurements or atmospheric observations to simulate the

multi-day BB aerosol evolution under fixed ambient conditions has been found to result in major quantitative and even qualitative differences between the simulations (Konovalov et al., 2019)" and that "it is not given that any of the available schemes can adequately describe the BB aerosol evolution specifically in Siberia" (page 13, lines 5-8). So, instead of using data of specific laboratory experiments (which are always representative of particular fuel types and a particular range of burning and ambient conditions), we constrained our simulations by satellite observations which are representative of numerous BB plumes in the real atmosphere. These constraints are shown to successfully take the role of the more traditional but sparse and limited constraints provided by "experimental" data from chamber experiments. The BB aerosol evolution simulated with the proposed VBS scheme is demonstrated to be consistent with the satellite observations as evidenced by results shown in Fig. 7 of the reviewed manuscript. Regrettably, we have no evidence that these results were taken into account by the Referee.

Referee's comment: *Authors should provide a box model simulation comparing their simplified VBS parameterization with the original one for various aging experiments, as well as comparing it with previously published experimental measurements (e.g. total yields) and/or other VBS parameterizations used for BB precursors (e.g. Shrivastava et al. 2017, Majdi et al., 2017).*

Regrettably, we do not see how the suggested comprehensive comparison of box model simulations involving different parameterizations could help us to "demonstrate that the derived simplified mechanism provides accurate results". Indeed, to the best of our knowledge, neither of the alternative VBS parameterizations proposed in the literature so far has been shown to enable an adequate model representation of the atmospheric evolution of BB aerosol in Siberia. Specifically, the original VBS scheme proposed by Ciarelli et al. (2017) was evaluated only against the measurements of organic aerosol (OA) produced from several burns of a particular type of fuel (beech logs) in a residential wood burner. Hence, there is no evidence that the original scheme is applicable to simulations of BB aerosol in Siberia.

In this situation, any difference or resemblance of results obtained with different mechanisms could hardly be indicative of any shortcomings in either of them. Furthermore, a numerical analysis employing a microphysical box model and several VBS schemes of various complexities have already been performed in Konovalov et al. (2019) for a wide range of conditions representative of BB plumes in Siberia. The main conclusions of the previous box model analysis, which are relevant for the present study, are summarized in the introduction and Sect. 2.4 of the reviewed manuscript, and we tried to improve this summary in the revised manuscript.

That said, we agree that a comparison of box model simulations with our simplified parameterization to similar simulations with the original (C17) scheme can be useful as it can provide evidence on whether or not our VBS parameterization enables a realistic representation of the initial stage of the BB aerosol evolution, which is poorly represented in the satellite observations used as constraints for our model. To this end, using the microphysical box model described in Konovalov et al. (2019) with both the VBS scheme used in this study and the original C17 scheme, we simulated the BB OA evolution under the conditions of chamber experiments reported in Ciarelli et al. (2017). The results of these simulations are mentioned in Sect. 2.4 of the revised manuscript and are presented in more detail in the newly introduced supplementary section S2. Briefly, we found that the BB OA concentration initially increases more rapidly in the simulation with our scheme than in the simulation with the original scheme, and so the BB OA concentration predicted by our scheme after about 10 hours of evolution is about 40% larger than the corresponding concentration predicted by the original scheme. Nonetheless, taking into account the range of the experimental variability of BB OA concentrations, the BB OA evolution simulated with our VBS scheme does not look unrealistic. A major qualitative difference between the two simulations is that the original scheme demonstrates a monotonically saturating increase of BB OA concentration, whereas the simplified scheme yields a non-monotonic behavior of BB OA concentration (a rapid increase followed by a gradual decrease due to fragmentation of SOA). Accordingly, a smaller concentration (also by about 40 %) is found in the simulation with our scheme after 110 hours of evolution. These two types of behavior of BB OA were earlier identified and explained in Konovalov et al. (2019).

Referee's comment: *The term "mechanistic (p4, p13, p30)" should not be used here to refer to the representation of BB organic aerosols in the CHIMERE model given that there is not process level representation of the underlying chemistry and optical properties.*

The meaning of the term "mechanistic model" is somewhat uncertain and varies across different branches of science. Here we specifically meant that our scheme is expected to take into account basic physical "mechanisms" (such as oxidation/evaporation, a decrease or increase of the volatility of semi-volatile organic species, destruction of chromophores) driving the BB aerosol evolution rather than individual chemical processes (such as e.g., the oxidation chain of naphthalene). To avoid misunderstanding, we are not using this term in the revised manuscript, following the Referee's instruction.

Referee's comment: *2) The term "BB aerosol photochemical age" is misused in this study. As defined on page 7, this term does not account for the photochemical reactions or the chemical aging of the BB plume. It only accounts for the sunlight exposure of the plume, and should be referred to as "hours of sunlight exposure". This needs to be corrected throughout the manuscript and for corresponding figures (e.g. Figure 5).*

We thank the Referee for this concrete comment. Since we do not have any observable photochemical "clock" at our disposal and cannot be sure that the model predicts OH concentration within the plumes accurately, we approximately quantify the exposure of BB aerosol to photochemical processes by assuming that OH concentration in the BB plumes is constant during daytime and is zero during the nighttime. Such an approximate estimate of the BB aerosol photochemical age accounts for the well-known fact that the photochemical processing of organic aerosol is typically much faster during the daytime than during the night time (with exceptions for highly unsaturated forested emissions which are efficiently oxidized also by NO_3 and O_3). In the revised manuscript, the corresponding definition in Sect. 2.1 is corrected accordingly, and an additional caveat is provided. The term "hours of sunlight exposure" is rather cumbersome and is difficult to use throughout the text, although we agree that it is more accurate (as it was noted in the reviewed manuscript).

Referee's comment: *Also, it is unclear how the transport time from the source region of a given BB plume was determined for the satellite data, and for the model. Please add this explanation to the methods section.*

We presume that the Referee refers to Sect. 3.2 where we identified a strong association between the photochemical age of BB aerosol and the geographical location (specifically, the longitude) of the BB plumes transported westward. This association, which is illustrated in Fig. 6 of the discussion paper, allowed us to estimate the ranges of the photochemical age of BB aerosol in the source and receptor regions. This analysis does not involve any other definitions apart from those already introduced in Sects. 2.1 and 2.3 (the photochemical age or hours of sunlight exposure of BB aerosol) and in Sect. 2.5 (coordinates of the source and receptor regions).

Referee's comment: *3) This study uses a large number of assumptions, e.g. parameterizations of aging of organic compounds, their optical and absorptive properties, fire emissions, averaging in time and space to match satellite measurements, etc. Please make a table that summarizes all the assumptions used in this manuscript, and quantify the associated sensitivity of the conclusions to this assumption. This is needed to show that the conclusions of this study are robust.*

A table summarizing distinctive features and parameterizations of our modeling system is provided in the revised manuscript (Table 3). Furthermore, to address the Referee's comment, we have presented the discussion of the uncertainties in a more focused way in a new section (Sect. 3.4). This new section brings together the relevant content of Sects. 3.2, S3, and 3.3 of the reviewed manuscript, and also it includes some additional discussion.

We dedicated considerable efforts to ensure that the conclusions of our analysis are robust, and these efforts were comprehensively described in the reviewed manuscript. In particular, we quantified the uncertainties in the derived trends of the optical characteristics using a statistical (bootstrapping) method as described in Sect. 2.1. The obtained confidence intervals were shown in all our figures presenting the evolution of the optical characteristics according to

both the satellite data and model results. Furthermore, a special section (Sect. S3) was dedicated to the analysis of test cases addressing possible biases associated with the processing of the satellite data in our study. The results of this analysis allowed us to conclude that "the tests overall confirm the robustness of our major findings". Regrettably, we see no evidence that these efforts were noticed and appreciated by the Referee.

5   While the main results of our analysis of the satellite data are quantitative, our simulations involving the VBS parameterization are mainly used to get insights into qualitative patterns of the BB aerosol transformations, rather than for quantitative characterization of any processes. This feature of our modeling analysis is emphasized in the introduction (page 5, lines 3-5) of the reviewed manuscript and rephrased in the next sections (page 11, lines 1, 2; page 24, lines 12-18; page 28, lines 32, 33). To "quantify" the associated sensitivity of the qualitative conclusions to any assumptions involved in our study is logically not feasible. Furthermore, we emphasized that our interpretation of the detected changes in AAOD, AOD, and SSA is not necessarily unique (page 27, line 30). At the same time, a discussion of several major factors which can potentially affect our conclusions (page 28) allowed us to conclude that "that although our model representation of BB aerosol evolution involves strong assumptions (which yet need to be verified in future research), our qualitative interpretation of the inferred major changes of the optical properties of BB aerosol in Siberia

15   is sufficiently robust and realistic". We regret that this discussion also apparently went unnoticed by the Referee.

Referee's comment: *4) Does the proposed method allow separating between the changes in AOD due to oxidation and gas-particle partitioning vs. those due to dry and wet removal of organic gases and particles and subsequent evaporation/condensation. This needs to be clearly explained and justified.*

As explained in Sect. 2.1 (page 6, lines 14-16) of the reviewed manuscript, "the analysis of EnRs is expected to reveal

20   the differences between the dynamics of AAOD or AOD in the real BB plumes and in a hypothetical simulation in which BB aerosol is assumed to consist of only non-volatile material and SOA formation processes are disregarded". This explanation implies that, by design, our method does not allow separating between the processes indicated by the Referee. We noticed, however, that the simplified formulation of the idea of our analysis in the reviewed manuscript (page 6, lines 11-14) could be somewhat confusing. In the revised manuscript, we clarified that the objective of our

25   analysis was to identify the differences between changes in AAOD or AOD due to aging of BB aerosol in the real BB plumes (including, first of all, the changes associated with oxidation and condensation/evaporation and also the changes that can be indirectly induced by the dry and wet deposition of organic gases and particles) and those in a hypothetical simulation in which the organic fraction of BB aerosol is composed of only non-volatile, inert and hydrophobic material and the SOA formation is negligible.

30 Referee's comment: *5) Can the CHIMERE model capture the emissions and transport of the smoke plume during the studied period before all the corrections have been applied to the model? In particular, I am concerned about the coarse vertical resolution with only 12 levels up to 200hPa. What is the uncertainty in the transport and vertical distribution of smoke associated with this poor model resolution?*

The performance of our model in capturing the emissions and transport of the smoke plume during the studied period

35   was validated by comparing our simulations and satellite observations of CO columns, but maybe the Referee did not notice this. This comparison was introduced in Sect. 3.1 and was presented in more detail in the supplementary section S2 of the reviewed manuscript (see also Sect. S3 of the revised manuscript). The spatial and temporal distributions of CO are driven predominantly by emissions and transport since the effects of other processes on the time scales considered are small. The spatial distributions of the CO columns during the analysis period according to the IASI observa-

40   tions and the CHIMERE simulations were shown in Fig. S1, while the corresponding temporal variations of CO in the source and receptor regions were compared in Figs. S3 and 4 (e, f) of the reviewed version (see Figs. S3 and S4 in the revised version). The satellite retrievals of CO columns are known to be sensitive to the CO vertical distribution (e.g., George et al., 2009), and this sensitivity has been taken into account in our simulations by applying the averaging kernels (page 17, lines 29, 30 of the reviewed manuscript). Hence, the comparison is indicative of the performance of

45 CHIMERE in capturing not only the spatial distributions of emissions and horizontal transport of BB plumes but also

the vertical distribution of CO. As evident in Fig. S1 (in the reviewed version), our model captures the observed spatial distribution of CO columns quite adequately, including the large-scale smoke plume extending from Siberia into the European territory of Russia. Fig. S3 further demonstrates a good quantitative agreement between the temporal variations of CO columns over both source and receptor regions (the correlation coefficient exceeds 0.9 in both cases). Finally, very small differences between the regional averages of observed and modeled CO columns (Fig. 4 e, f) indicate that the overall uncertainty in our simulations of the BB fraction of the CO columns over the receptor region (that is, within the strongly aged BB plume), including its part associated with a limited vertical resolution of our simulations is far less than the relative magnitudes of the variations in AAOD and AOD identified in our analysis. We would like to note that the vertical discretization of the simulations in our study was defined by taking into account not only available computational resources but also probable large random uncertainties associated with the vertical distribution of BB emissions (Sofiev et al., 2012). Given these uncertainties, a higher vertical discretization of our simulations would not necessarily result in smaller errors in the modeled vertical distribution of the smoke. We extended the discussion of our simulations of CO columns in the revised manuscript (specifically, in Sect. 3.1), taking into account the Referee's comment.

Referee's comment: *In addition, BB emissions were estimated using the satellite FRPs, and emission factors. What is the total amount of OA, BC, CO emitted by these fires during the period of interest, and how does this emission estimate compares with other publicly available emission inventories e.g. GFED or FINN. By how much were these emissions adjusted to match the satellite AOD data?*

Estimation of emissions of aerosol and trace gases from fires is a subject of numerous dedicated studies (including our previous study (Konovalov et al., 2018)) but is not the focus of this one. Nonetheless, to address the Referee's comment, we have provided our top-down estimates for BB emissions of BC and OC in the study region and compared them with the corresponding estimates from the GFED4.1s inventory in Sect. 2.6 of the revised manuscript.

Referee's comment: *6) The analysis performed in this study are following very closely the approach used in the previous study by Konovalov et al., 2017 (except for the estimate of the photochemical age, and the study of a different Siberian fire even). The originality and significance of the present study needs to be well justified with regard to the previous one in the discussion section.*

We regret that the originality and significance of the present study went unnoticed by the Referee. As stated in the introduction of the reviewed manuscript (page 4, lines 6, 7), "this study substantially extends the scope of the previous one by analyzing satellite observations of both absorption and extinction characteristics of BB aerosol". We further noted (page 5, lines 26, 27) that "to the best of our knowledge, this is the first study attempting to constrain simulations of the aging behavior of BB aerosol with satellite observations of both absorption and extinction AODs". Hence, we believe that our study is highly original and that its main original features are clearly explained in the introduction of both the reviewed and revised versions of the manuscript.

The significance of our study is primarily associated with its general objective, such as "to find a way to infer statistically reliable information on the impact of aging processes on the optical properties of BB aerosol from available satellite measurements" (page 3, lines 28-30). We argue that achieving this objective is important because laboratory and field studies do not "provide consistent observational constraints for representations of the effects of atmospheric aging of BB aerosol in chemistry-transport and climate models" (page 3, lines 27, 28). The significance of the study is also emphasized in the last paragraph of the conclusions. Specifically, we note that "the presented analytical framework can be helpful in identifying and interpreting manifestations of the BB aerosol aging processes far beyond the time scales that can currently be addressed in aerosol chamber experiments" and that the proposed methods of the analysis of satellite data are sufficiently general and can be applied to different satellite observations.

The original results of our analysis include an identification of the statistically significant downward parts of the trends of the enhancement ratios for both AOD and AAOD during the multi-day aging of BB plumes as well the simultaneous increase of SSA and the enhancement ratio for AOD during the initial 20-30 hours of the evolution under daytime

11

conditions. These are, to the best of our knowledge, unique results in the literature, and at least highly original. The interpretation of the detected changes using a VBS parameterization is certainly also a major novel point. These new results are discussed in the context of other studies (including our previous ones) in Sect. 3.2 and 3.3. Regrettably, we do not see any indications that the scientific content of these sections was examined and taken into account by the
5   Referee.

Finally, we would like to note that although our idea to analyze satellite observations using modeled tracers was indeed introduced earlier, the concrete methods proposed in the reviewed manuscript are highly original. In particular, unlike Konovalov et al. (2017) we use a general algorithm for the nonlinear trend analysis. Differences between the analysis procedures used in Konovalov et al. (2017) and this study are discussed in the Supplementary Material, Sect. S1. The
10 use of an adaptive VBS parameterization and explicit modeling of the optical properties of aerosol are also important novel methodological features of this study.

Taking into account the Referee's comment, we made an additional effort to emphasize the novel points of our study throughout the revised manuscript. We also tried to better explain the differences between this study and the study by Konovalov et al. (2017) in the introduction and conclusions of the revised manuscript.

15 Referee's comment: *The introduction is quite long and dense. Please try to shorten by avoiding the redundancies. Also the description of the modeling approach should be moved into the methodology section (p4 line 19 to p6 line5).*

The introduction is indeed relatively lengthy, but this is unavoidable because our study addresses not just one but several directions of research (such as modeling of BB organic aerosol, investigations of brown carbon, applications of satellite measurements of atmospheric aerosol, the role of aerosol from Siberian fires for the environment and climate).
20 We tried but could not find any redundancies. However, following the recommendation of the referee, we have removed, for the most part, the description of our modeling approach from the introduction. In this way, the introduction has been noticeably shortened.

Referee's comment: *p1 line: 13: please remove "including the Arctic". p1 line 13: change "Atmospheric evolution" to "changes that occur in". p3 line 20 remove "recalcitrant" p5 line 1: take a step further instead of forward? p5 line 21*
25 *– remove "clockwise, and counterclockwise". p9 line 21: Remove the parenthesis after tabs. p10 line 17: remove "numerous"*

All the above textual changes suggested by the referee are done in the revised manuscript.

Referee's comment: *p10 line 22: provide a reference for the melchior2 chemical mechanism, and for Fast-JX. p12 line 10: provide a reference for LMDZ-INCA boundary conditions.*

30 The requested references are provided in the revised manuscript.

Referee's comment: *p17 line 11: What is the model resolution used in this study? And for this regridding?*

The horizontal resolution of the model grid was 1 by 1 degree (page 11, line 19 of the reviewed manuscript). By saying that satellite data were projected on the model grid we implied that the regridding was done with the same spatial resolution (page 17, line 11), that is, 1 by 1 degree.

35 Referee's comment: *p22 line 5-8: these account for different airmasses?*

Yes, the conclusions in Sect 3.1 account for different airmasses, since the averaging of the observed characteristics over the big regions and period of several days allows us to suppress the variability associated with individual airmasses. A corresponding remark is added to the first paragraph in Sect. 3.1.

Referee's comment: *Figure 4, should these AODs be compared quantitatively given all the adjustments that are ap-*
40 *plied to the emissions (p19 e.g. equation 9)?*

As explained in the reviewed manuscript (page 21, lines 3-5), the goal of the comparison presented in Fig. 4 and Sect. 3.1 was to "examine the aging-changes in the optical properties of BB aerosol by considering the satellite and simulated data for the "source" and "receptor" regions. In this context, while the adjustments applied to the BB emissions allowed us to bring the simulations close to observations in the source region, they obviously could not ensure the agreement of the simulations with the observations in the receptor region where the optical properties of BB aerosol could be affected by aging processes. Hence, we consider the discrepancies between the satellite observations and simulated data for the 'bb_trc' scenario in the receptor region as an indication for the BB aerosol aging, and we do not see any reason why these discrepancies should not be evaluated quantitatively. The comparison presented in Fig. 4 was, in our opinion, sufficiently discussed in Sect. 3.1 of the reviewed manuscript.

References

Ciarelli, G., El Haddad, I., Bruns, E., Aksoyoglu, S., Möhler, O., Baltensperger, U., and Prévôt, A. S. H.: Constraining a hybrid volatility basis-set model for aging of wood-burning emissions using smog chamber experiments: a box-model study based on the VBS scheme of the CAMx model (v5.40), Geosci. Model Dev., 10, 2303-2320, https://doi.org/10.5194/gmd-10-2303-2017, 2017.

George, M., Clerbaux, C., Hurtmans, D., Turquety, S., Coheur, P.- F., Pommier, M., Hadji-Lazaro, J., Edwards, D. P., Worden, H., Luo, M., Rinsland, C., and McMillan,W.: Carbon monoxide distributions from the IASI/METOP mission: evaluation with other space-borne remote sensors, Atmos. Chem. Phys., 9, 8317–8330, doi:10.5194/acp-9-8317-2009, 2009.

Konovalov, I. B., Beekmann, M., Berezin, E. V., Formenti, P., and Andreae, M. O.: Probing into the aging dynamics of biomass burning aerosol by using satellite measurements of aerosol optical depth and carbon monoxide, Atmos. Chem. Phys., 17, 4513-4537, https://doi.org/10.5194/acp-17-4513-2017, 2017.

Konovalov, I. B., Lvova, D. A., Beekmann, M., Jethva, H., Mikhailov, E. F., Paris, J.-D., Belan, B. D., Kozlov, V. S., Ciais, P., and Andreae, M. O.: Estimation of black carbon emissions from Siberian fires using satellite observations of absorption and extinction optical depths, Atmos. Chem. Phys., 18, 14889-14924, https://doi.org/10.5194/acp-18-14889-2018, 2018.

Menut, L., Bessagnet, B., Khvorostyanov, D., Beekmann, M., Blond, N., Colette, A., Coll, I., Curci, G., Foret, G., Hodzic, A., Mailler, S., Meleux, F., Monge, J.-L., Pison, I., Siour, G., Turquety, S., Valari, M., Vautard, R., and Vivanco, M. G.: CHIMERE 2013: a model for regional atmospheric composition modelling, Geosci. Model Dev., 6, 981–1028, https://doi.org/10.5194/gmd-6-981-2013, 2013.

Sofiev, M., Ermakova, T., and Vankevich, R.: Evaluation of the smoke-injection height from wild-land fires using remote-sensing data, Atmos. Chem. Phys., 12, 1995–2006, https://doi.org/10.5194/acp-12-1995-2012, 2012.

Authors' response to the comments of Anonymous Referee # 3

We thank the Referee very much for the positive evaluation of our manuscript and for the useful comments, which are addressed in the revised manuscript. Our point-by-point responses to the Referee's comments are provided below.

Referee's comment: *At P17L9, the approach to harmonize the model and satellite data, in terms of temporal and spatial sampling is described in detail. One important aspect, which I did not see described: as part of the satellite/model harmonization, how was the model data filtered for retrieval quality, by which, masking out of retrievals under cloudy conditions is meant? At P5L23, the predominantly cloudless conditions during this period are mentioned, but a quick inspection of the MODIS true color imagery and retrieved AOD show a mix of cloudy and clear sky conditions during the second half of July 2016. Under cloudy conditions, much of the AOD is masked out, as is the case for the OMI AOD and AAOD retrievals (for L3, at least, and presumably for many of the L2 pixels and individual CO retrievals). Is CTM filtered accordingly to not introduce a discrepancy due to the inclusion of simulated data under cloudy conditions where the retrievals fail? This could even be as basic as an ad-hoc threshold of cloud fraction or cloud optical depth, depending on what is available, so that the CTM data are 'biased' toward clear sky conditions in the same way as the satellite data. Or are the CTM cloud fields in sufficient enough agreement with those seen by the satellites that the retrieval co-location sampling handles this?*

First of all, we would like to clarify our remark concerning "predominantly cloudless conditions" during the BB aerosol outflow event. According to the Level-3 AIRS retrievals (see Fig. C1 below), the cloud fraction was indeed typically less 0.5 over the region (40-80°E, 55-65°N) and period (17-27 July) most affected by the outflow of BB plumes from Siberian fires. Furthermore, the cloud fraction was smaller and clouds were less dense than typical for a summer period in the same region (cf. panels (a) and (c) with panels (b) and (d) in Fig. C1). That said, we recognize that our remark could be confusing, particularly because the cloud fractions inferred from different observations can differ significantly. The corresponding sentence is corrected in the revised manuscript.
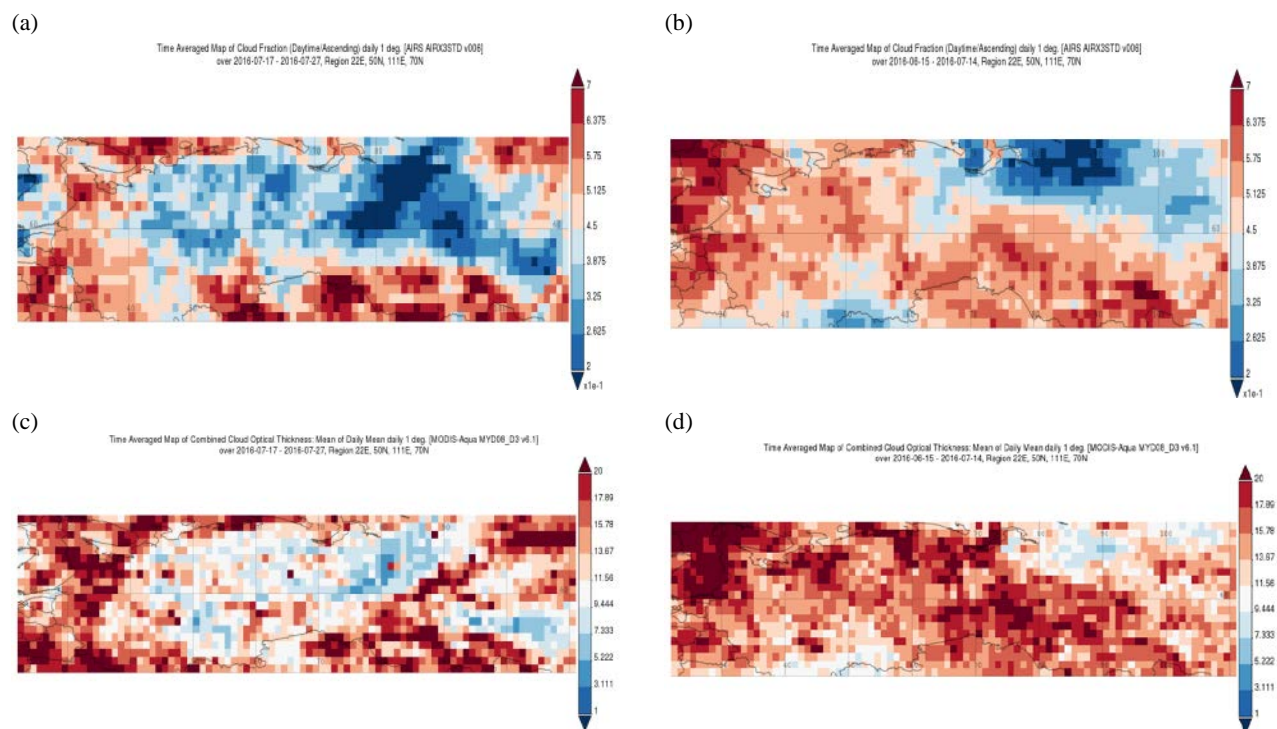
(a)

(b)

(c)

(d)

Figure C1. Time-averaged maps of (a, b) the cloud fraction and (c, d) the cloud optical depth according to the data retrieved from the AIRS and MODIS observations, respectively, for the periods (a, c) 17 - 27 July 2016 and (b, d) 15 June – 14 July 2016. The data are shown only for the study region. Source: Giovanni, https://giovanni.gsfc.nasa.gov/giovanni/, last access: 1 November 2020.

Our satellite/model harmonization procedure did not involve any filtering of the model data with respect to the cloud coverage. However, since each available retrieval falling into a given grid cell was matched with the corresponding simulations in time and since grid cells/hours corresponding to the continuous cloud coverage are barely represented in the satellite observations, both the satellite data and simulations are "automatically" weighed towards the clear sky
5   conditions. Furthermore, as part of a preliminary analysis, we examined whether or not the lack of satellite retrievals for cloudy scenes could introduce significant systematic discrepancies between the simulated and modeled data fields by plotting the relationship between the difference of the observed and retrieved values of AOD in a given grid cell in the study region and period and the number of retrievals per grid cell. This analysis is illustrated in Fig. C2 provided below. If there were strong systematic discrepancies between the observations and simulations due to the lack of ob-
10   servations for cloudy scenes, then the difference of the observed and retrieved values would probably depend on the number of retrievals per grid cell (since this number is inversely proportional to the fraction of cloudy scenes). However, we did not observe such a dependence and therefore concluded that biases introduced into our analysis by cloudy scenes in the satellite observations are not significant. We included a concise discussion of this point in Sect. 2.5 of the revised manuscript.
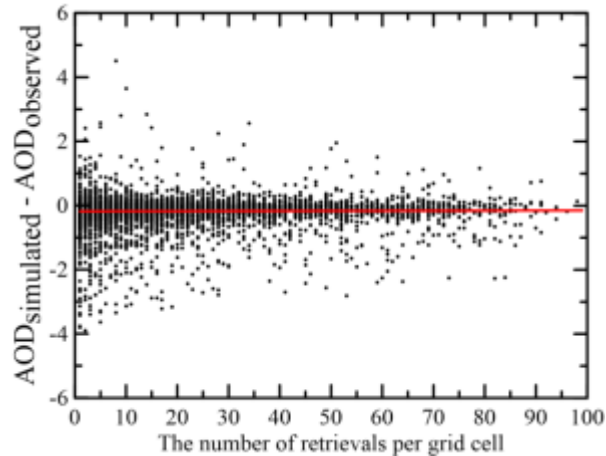
15

Figure C2. The differences between the simulated AOD values (for the 'bb_vbs' scenario) and their counterparts retrieved from the MODIS observations as a function of the number of AOD retrievals per grid cell. Both the simulated and retrieved data were gridded on a $1° \times 1°$ model grid with the hourly temporal resolution and were not subject to any pre-selection procedure. The red line shows the best linear fit to the data. Only each 10th data point is shown in the plot to preserve its readability. Note that the simulations shown here do not include the background part, which is the reason for a small negative bias in the simulated values.

Referee's comment: *P1L12: In the abstract, consider a basic description of importance of how the VBS scheme improved agreement between the model and satellite data (i.e. in Fig 4 b,d). This point is worth mentioning.*

We thank the referee for this useful suggestion. The corresponding remark is included in the abstract of the revised
20   manuscript.

Referee's comment: *P21L6: In Figure 2b and 2d, I would suggest that the AOD scale range from, say, 0-2, to get a better sense of the AOD enhancement over the receptor region centered on Moscow.*

We have re-drawn Fig. 2 using the scale suggested by the referee. The AOD enhancement associated with anthropogenic emissions from Moscow (if this is what the referee meant) is now clearly seen in the simulations (Fig. 2d), but

15

the corresponding enhancement in the observations is more smeared (Fig. 2c). These spatial differences between the observed and simulated AOD values are typically less than 0.1 and are likely due to either a minor positive bias in the MODIS retrievals or underestimation of the AOD associated with biogenic aerosol by the model. These minor differences could not significantly affect the results of our analysis. In addition, we would like to note that the receptor region is somewhat shifted from the center of the plume northward in order to exclude the impact of minor local fires (in the south-western part of the domain, see Fig. 1) on the analysis results.

Referee's comment: *P21L9: by correlation, do you mean spatial pattern correlation or something else?*

We meant the correlation between the daily values of the spatially averaged retrievals and simulations. This is clarified in the revised manuscript.

Referee's comment: *Minor editorial point throughout: use the word 'rather' fewer times.*

We thank the referee for this useful suggestion. We tried to avoid using the word 'rather' in the revised manuscript unless it is necessary.

Insights into the aging of biomass burning aerosol from satellite observations and 3D atmospheric modeling: Evolution of the aerosol optical properties in Siberian wildfire plumes

Igor B. Konovalov[1], Nikolai A. Golovushkin[1], Matthias Beekmann[2], and Meinrat O. Andreae[3,4,5]

[1]Institute of Applied Physics, Russian Academy of Sciences, Nizhniy Novgorod, Russia
[2]LISA/IPSL, Laboratoire Interuniversitaire des Systèmes Atmosphériques, UMR CNRS 7583, Université Paris Est Créteil (UPEC) et Université Paris Diderot (UPD), France
[3]Max Planck Institute for Chemistry, Mainz, Germany
[4]Scripps Institution of Oceanography, University of California San Diego, La Jolla, CA 92093, USA
[5]Department of Geology and Geophysics, King Saud University, Riyadh, Saudi Arabia

Correspondence to: Igor B. Konovalov (konov@ipfran.ru)

Abstract. Long-range transport of biomass burning (BB) aerosol from regions affected by wildfires is known to have a significant impact on the radiative balance and air quality in receptor regions~~, including the Arctic~~. However, the changes that occur ~~atmospheric evolution of~~ in the optical properties of BB aerosol during the long-range transport events ~~is~~ are insufficiently understood, limiting the adequacy of representations of the aerosol processes in chemistry transport and climate models. Here we introduce a framework to infer and interpret changes ~~of~~ in the optical properties of BB aerosol from satellite observations of multiple BB plumes. Our framework includes (1) a procedure for analysis of available satellite retrievals of the absorption and extinction aerosol optical depths (AAOD and AOD) and single scattering albedo (SSA) as a function of the BB aerosol photochemical age, and (2) a representation of the AAOD and AOD evolution with a chemistry transport model (CTM) involving a simplified volatility basis set (VBS) scheme with a few adjustable parameters. We apply this framework to analyze a large-scale outflow of BB smoke plumes from Siberia toward Europe that occurred in July 2016. We use AAOD and SSA data derived from OMI (Ozone Monitoring Instrument) satellite measurements in the near-UV range along with 550 nm AOD and carbon monoxide (CO) columns retrieved from MODIS (Moderate Resolution Imaging Spectroradiometer) and IASI (Infrared Atmospheric Sounding Interferometer) satellite observations, respectively, to infer changes in the optical properties of Siberian BB aerosol due to its atmospheric aging and to get insights into the processes underlying these changes. Using the satellite data in combination with simulated data from the CHIMERE CTM, we evaluate the enhancement ratios (EnR) that allow isolating AAOD and AOD changes due to oxidation and gas-particle partitioning processes from those due to other processes, including transport, deposition, and wet scavenging. The behavior of EnRs for AAOD and AOD is then characterized using nonlinear trend analysis. It is found that the EnR for AOD strongly increases (by about a factor of 2) during the first 20-30 hours of the analyzed evolution period, whereas the EnR for AAOD does not exhibit a statistically significant increase during this period. The increase in AOD is accompanied by a statistically significant enhancement of SSA. Further BB aerosol aging (up to several days) is associated with a strong decrease of EnRs for both AAOD and AOD. Our VBS simulations constrained by the observations are found to be more consistent with satellite

observations of strongly aged BB plumes than "tracer" simulations in which atmospheric transformations of BB organic aerosol were disregarded. The simulation results indicate that the upward trends in EnR for AOD and in SSA are mainly due to atmospheric processing of secondary organic aerosol (SOA), leading to an increase in the mass scattering efficiency of BB aerosol. Evaporation and chemical fragmentation of the SOA species, part of which is assumed to be absorptive (to contain brown carbon), are identified as a likely reason for the subsequent decrease of the EnR for both AAOD and AOD. Hence, our analysis reveals that the long-range transport of smoke plumes from Siberian fires is associated with major changes in BB aerosol optical properties and chemical composition. Overall, this study demonstrates the feasibility of using available satellite observations for evaluating and improving representations in atmospheric models of the BB aerosol aging processes in different regions of the world at much larger temporal scales than those typically addressed in aerosol chamber experiments.

1 Introduction

Open biomass burning – including wildfires, controlled fires, and agricultural burns – is an important source of aerosol particles that are a key agent in the processes controlling regional and global climate (e.g., Bond et al., 2013; Jacobson, 2014; Sand et al., 2015). Climate effects of biomass burning (BB) aerosol are associated, in particular, with the scattering of the solar radiation by organic matter, which is typically a dominant component of BB aerosol (Reid et al., 2015a), as well as with absorption of solar radiation by black carbon (BC) and brown carbon (BrC), which are also ubiquitous components of BB aerosol (Andreae and Gelencsér, 2006), both within the atmosphere and on snow and ice surfaces (Gustafson and Ramanathan, 2016; Jiang et al., 2016; Wang et al., 2016). Acting as cloud condensation nuclei (CCN), BB aerosol particles can affect the formation and radiative characteristics of clouds (e.g., Hobbs et al., 1969; Petters et al., 2009; Lu et al., 2018). Apart from being an important agent in the climate system, BB aerosol is a major contributor to air pollution episodes that have been caused by wildfires worldwide (e.g., Konovalov et al., 2011; Keywood et al., 2013; Gupta et al., 2018) and represent a major human health problem (Lelieveld et al., 2020). These facts highlight the importance of having adequate representations of the physical and chemical properties of BB aerosol in models of various complexities for climate and air pollution studies. However, developing such representations is an extremely challenging task, given the high diversity of BB aerosol composition and optical properties (e.g., Reid et al., 2005a,b; Tsigaridis and Kanakidou, 2018), and the dynamic, nonlinear nature of the atmospheric evolution of its organic component (e.g., Bian et al., 2017; Konovalov et al., 2019).

The composition of primary BB smoke is strongly dependent on fuel type and highly variable burning conditions (McMeeking et al., 2009; Levin et al., 2010; Liu et al., 2014; Laskin et al., 2015). For example, smoldering fires have been reported to favor higher emissions of organic aerosol (OA) and semi-volatile organic gases, but lower BC emissions, compared to flaming conditions (Jen et al., 2019). In turn, the BC-to-OA ratio has been identified as a key factor controlling BrC contribution to light absorption by BB aerosol (Saleh et al., 2014; Lu et al., 2015; Pokhrel et al., 2017; McClure et al., 2020).

Furthermore, results of laboratory and field studies show a very diverse picture of atmospheric transformations of BB aerosol, suggesting that oxidation of volatile and semi-volatile organic gases or heterogeneous oxidation of particles can lead, in different cases, to either enhancements or losses of organic matter by BB aerosol (e.g., Yokelson et al. 2009; Cubison et al., 2011; Hennigan et al., 2011; Akagi et al., 2012; Jolleys et al., 2015; Konovalov et al., 2015; Tiitta et al., 2016; Ciarelli et al.,

5   2017; Vakkari et al., 2018). Besides, some observational studies reported that atmospheric aging of BB aerosol did not result in changes of mass concentration (corrected for dilution) of OA (e.g., May et al.; 2015; Sakamoto et al. 2015; Zhou et al., 2017). This diversity, which is presently not well understood and is not reproduced in chemistry transport and climate models, can, at least partly, be associated with differences in fuel types, burning conditions, initial parameters of BB smoke plumes, and the dilution rate (Hennigan et al., 2011; Ahern et al., 2019; Lim et al., 2019; Hodshire et al. 2019; Konovalov et

10   al., 2019).

There is still no consensus on the patterns of the changes of absorptive properties associated with brownness of organics in BB aerosol in the real atmosphere, although findings from many laboratory and field studies indicate that these changes can be very significant (e.g., Kumar et al., 2018; Browne et al., 2019; Fan et al., 2019; Li et al., 2019; Sumlin et al., 2019). Based on both a BB aging experiment with an outdoor smog chamber and an analysis of field observations, Zhong and Jang (2014)

15   reported an initial increase in light absorption by BrC under natural sunlight, followed by a decrease. The same BrC aging effects, that is, an initial photo-enhancement of BrC absorption and ~~an~~ eventual bleaching of OA under the UV irradiation, have also been found in more recent laboratory experiments with water-soluble organic extracts from BB aerosol (Wong et al., 2017; 2019). However, only rapid bleaching of BrC (on the time scale of 9 to 15 hours) has been detected in age-resolved aircraft observations of BB aerosol (Forrister et al., 2015). ~~ ~~Furthermore, while these aircraft observations suggest that BrC

20   almost fully disappears from BB aerosol after about 40 hours of atmospheric aging, an analysis of the AErosol RObotic NETwork (AERONET) data by Wang et al. (2016) indicates that a sizeable fraction of BrC "survives" during a much longer atmospheric exposition. Laboratory data (Di Lorenzo et al., 2017; Wong et al., 2017; 2019; Fleming et al., 2020) indicate that this ~~recalcitrant~~ fraction is likely formed by high-molecular-weight chromophores (while low-molecular-weight chromophores are more rapidly destroyed), suggesting that the atmospheric fate of the BrC fraction of BB aerosol is dependent

25   on fuel type and burning conditions. Finally, it should be noted that the atmospheric relevance of various processes, which, according to laboratory studies, can affect formation and bleaching of chromophores in BB aerosol, is so far not sufficiently clear (Fleming et al., 2020); this fact constitutes an additional obstacle for developing adequate modeling representations of BB aerosol aging processes.

The discussion above indicates that the sparse and often contradictory results of field and laboratory studies available so far

30   can hardly provide consistent observational constraints for representations of the effects of atmospheric aging of BB aerosol in chemistry-transport and climate models. The general objective of the present study is to find a way to infer statistically reliable information on the impact of aging processes on the optical properties of BB aerosol from available satellite measurements. To this end, we developed an analytical framework enabling the synergetic combination of satellite and model

data on the BB aerosol optical properties and composition. Unlike the inevitably sparse field observations that are available only for a tiny fraction of wildfires occurring in the world each year, satellite instruments provide abundant observations of BB plumes associated with virtually any major vegetation fire worldwide. Accordingly, satellite observations of BB plumes can enable statistical characterization of the BB aerosol aging effect in a given region, encompassing a wide range of BB aerosol sources and burning conditions. A similar concept was initially exploited in our previous study (Konovalov et al., 2017a), focusing on the analysis of the MODIS (Moderate Resolution Imaging Spectroradiometer) observations of extinction aerosol optical depth (AOD) (Levy et al., 2013) in Siberia. We found, in particular, that after being corrected for dilution, AOD increases almost two-fold in BB plumes aged between 15 and 20 hours, compared to fresher plumes, indicating strong secondary organic aerosol (SOA) formation. This study substantially extends the scope of the previous one by analyzing satellite observations of both absorption and extinction characteristics of BB aerosol. Specifically, along with the MODIS AOD observations, we analyze near-UV retrievals of the absorption aerosol optical depth (AAOD) and single scattering albedo (SSA) from the OMI (Ozone Monitoring Instrument) measurements (Torres et al., 2007; 2013). Taking into account that the OMI observations of AAOD at the 388 nm wavelength are sensitive to the BrC content in the BB aerosol (Jethva et al., 2011; Mok et al., 2016), these observations can be expected to provide useful insights into the changes of the absorptive properties of the organic fraction of BB aerosol. At the same time, the MODIS AOD observations are expected to bring light to a possible role of SOA formation (Saleh et al., 2013) in these changes. Note that the OMI AAOD and MODIS AOD observations were earlier found to provide consistent information on BB aerosol optical properties, enabling their use as observational constraints on BB emissions of BC and OC (Konovalov et al., 2018). The OMI AAOD retrievals were also found to provide useful constraints on anthropogenic BC emissions over southeastern Asia (Zhang et al., 2015). Similar to Konovalov et al. (2017a), we additionally use CO column amounts retrieved from IASI (Infrared Atmospheric Sounding Interferometer) satellite observations (Clerbaux et al., 2009) to account for the effects of dilution.

To analyze and interpret the satellite observations, we use the CHIMERE chemistry transport model (Mailler et al., 2017) in combination with an external module, OPTSIM (Stromatas et al., 2012), enabling Mie calculations of the light absorption and extinction for both core-shell and homogeneous morphologies of particles. ~~The CHIMERE simulations are also used to estimate the photochemical age of BB aerosol. A mechanistic (highly simplified) representation of evolution of the organic fraction of BB aerosol within the VBS framework (Robinson et al., 2007) is used to simulate the behavior of mass concentrations of primary and secondary organic components of BB aerosol. It should be noted that there is currently no uniform way to represent atmospheric transformations of BB OA and its optical properties in models. Furthermore, differences between the available VBS schemes (e.g., Shrivastava et al., 2015; Konovalov et al., 2015; Ciarelli et al., 2017; Tsimpidi et al., 2018), which have been proposed for simulations of BB aerosol and are, to some extent, constrained by observational or experimental data, have been shown to result in major quantitative and qualitative differences in the simulated multi-day evolution of BB OA mass concentration (Konovalov et al., 2019). There is also no uniform way to represent sources and evolution of BrC.~~ Typically, BrC has been introduced in previous modeling studies as an absorbing fraction of otherwise non-absorbing OA (e.g., Park et al., 2010; Saleh et al., 2015; Jo et al., 2016), with pre-defined absorptive properties that are not affected by

atmospheric aging. More recently, Wang et al. (2018), Brown et al. (2018), and Zhang et al. (2020) assigned empirical estimates of absorption properties for all OA in their global modeling studies, and also assumed that the absorption of OA is decreasing with a constant rate as a function of the BB aerosol photochemical age, irrespective of the simulated evolution of the chemical composition of the particles. In this study, we largely follow the latter approach but take a step ~~forward~~ further

5   by considering evolution of BrC consistently with simulated changes of both primary organic aerosol (POA) and SOA within the volatility basis set (VBS) framework (Robinson et al., 2007). Several parameters of our model are adjusted to meet the observational constraints. Nonetheless, because our representation of BB aerosol aging is highly simplified and associated with large uncertainties, we use our simulations mainly to get insights into qualitative patterns of the BB aerosol transformations, rather than for quantitative characterization of any processes.

10   Aerosol particles emitted from vegetation fires in Siberia can be transported in the atmosphere over thousands of kilometers and significantly affect atmospheric composition in receptor regions, such as, e.g., East Asia (Agarwal et al., 2010; Matsui et al, 2013, Ikeda et al., 2015; Yasunari et al., 2018~~-~~), the Western USA (Laing et al., 2016), and Alaska (Warneke et al., 2009). Siberian fires have been estimated to contribute, on average, up to 40 % of total BC deposited annually in the Arctic (Evangelio et al., 2016), where BB aerosol can significantly affect the climate processes (Sand et al., 2015) associated with an

15   observed rapid increase of the annual surface temperature in this region (Bekryaev et al., 2010). As the role of fires in boreal regions is projected to increase in a warmer climate (Oris et al., 2014), there is a need for better quantitative understanding of the climate impact of BB aerosol emitted in these regions ~~specifically from Siberian fires~~, which can be achieved, in particular, through the use of stronger observational constraints to represent of BB aerosol optical properties and their evolution in chemistry transport and climate models. A way to obtain and exploit such constraints is proposed in this paper.

20   In this study, we analyze aging effects on the evolution of BB aerosol from Siberian fires by considering a relatively short period – from 15 to 31 July 2016. This analysis period is chosen to include a spectacular event of an anomalous outflow of optically dense BB plumes from Siberia to the European part of Russia. Different aspects of this event have already been addressed in the scientific literature (e.g., Sitnov et al., 2017; 2020; Gorchakov et al., 2017). It has been shown, in particular, that this event was associated with the formation of a so-called dipole structure of the atmospheric circulation, with the

25   westward transport of air masses being a result of anticyclonic ~~(clockwise)~~ and cyclonic ~~(counterclockwise)~~ circulations to the north and the south of the air transport trajectory, respectively. The outflow of the BB plumes took place in a relatively dry~~, predominantly~~ and cloudless atmosphere, providing ~~nearly ideal~~favorable conditions for observing the evolution of BB smoke plumes from space. Importantly, the geographical isolation of aged and young plumes during this event allows us to minimize the effects of possible uncertainties associated with the estimation of photochemical age.

30   To the best of our knowledge, this is the first study attempting to constrain simulations of the aging behavior of BB aerosol with satellite observations of both absorption and extinction AODs. Using the constrained simulations, we attempt to get insights into the key physical and chemical processes driving changes of the optical characteristics of BB aerosol from Siberian wildfires during its long-range transport. By examining the changes in the absorption properties of BB aerosol through

21

the joint analysis of the corresponding satellite retrievals and Mie calculations, this study significantly extends our previous analysis of the evolution of BB aerosols in Siberia (Konovalov et al., 2017a), which ~~was~~had been focused on the evolution of only the extinction AOD. Although this study addresses ~~only~~ a relatively short period and a specific region, we believe that the analytical framework developed here, as well as insights into the effects of atmospheric aging of BB aerosol during a

5   period spanning its typical lifetime, will be beneficial for other studies involving modeling of aerosol processes and their climate impacts, especially in Northern Eurasia and in the Arctic.

2 Method and data

2.1 Analysis method

We analyze the atmospheric evolution of BB aerosol by considering the enhancement ratio (EnR), which is defined as the

10   ratio of the enhancement of actual AAOD or AOD due to fire emissions to the corresponding enhancement of an ~~inert~~ aerosol tracer that ~~is assumed to be~~ represents the atmospheric evolution of a hypothetical BB aerosol in which the organic fraction is composed of inert, non-volatile and non-hygroscopic matter. ~~In accordance to~~Under this definition, the enhancement ratio for AAOD (EnR_{abs}) is evaluated as follows:

$$EnR_{abs} = \eta_0 \frac{\tau_{abs} - \tau_{abs}^{bgr}}{\tau_{abs}^{t}}, \tag{1}$$

15   where τ_{abs} is the AAOD retrieval, τ_{abs}^{bgr} is the estimate of the background part of AAOD, τ_{abs}^{t} is the estimate of AAOD associated with the inert aerosol tracer, and η_0 is a constant normalization factor defined below. The enhancement ratio for extinction AOD (EnR_{ext}) is evaluated similar to EnR_{abs}, by substituting the observed and estimated AOD values (τ_{ext}, τ_{ext}^{bgr}, and τ_{ext}^{t}) into Eq. (1) instead of τ_{abs}, τ_{abs}^{bgr}, and τ_{abs}^{t}. The ~~idea behind the use of~~objective of ~~these EnRs in~~ our ~~study~~ analysis involving these EnRs ~~is~~ ~~to isolate changes of AAOD and AOD due to oxidation and condensation/evaporation processes~~

20   ~~from those due to any other processes, such as, e.g., advection, eddy diffusion, dry deposition, and wet scavenging, which~~ ~~can affect AAOD and AOD associated with~~BB plumes. In other words, the analysis of EnRs is expected to ~~reveal~~ identify the differences between ~~the dynamics of~~changes in AAOD or AOD due to aging of BB aerosol in the real BB plumes (including the changes that occur due to oxidation and condensation/evaporation and can also be indirectly induced by the dry and wet deposition of organic gases and particles) and ~~and in~~those in a hypothetical simulation in which the organic fraction

25   of BB aerosol is ~~assumed to consist~~composed of only non-volatile, inert, and hydrophobic material and SOA formation processes are ~~disregarded~~negligible. In our analysis involving EnRs, we largely follow Konovalov et al. (2017a) and Konovalov et al. (2019), but it should also be noted that the meaning of EnR defined by Eq. (1) is very similar to that of the normalized excess mixing ratio (NEMR), which was employed in previous studies (e.g., Yokelson et al., 2009; Vakkari et al., 2018; Junghenn Noyes et al., 2020) to analyze the evolution of mass concentrations (or mixing ratios) of aerosol species.

In the framework of this study, Eq. (1) is also used to analyze the simulated evolution of BB aerosol. To this end, AAOD (or AOD) retrievals are replaced in Eq. (1) by the corresponding simulated values.

~~As the main option for our analysis,~~ Tthe BB aerosol tracers (τ_{abs}^t and τ_{ext}^t) are evaluated using AAOD and AOD values obtained from simulations with a chemistry transport model (CTM) as explained in Sect. 2.3. An advantage of the BB aerosol "optical" tracers in comparison with more traditional tracers based on CO concentration is that they are affected not only by transport and eddy diffusion but also by dry deposition, wet scavenging, and coagulation, thereby representing BB aerosol in the aforementioned hypothetical simulation. Note that coagulation is not considered as one of the BB aerosol aging processes addressed in this study.

However, the BB aerosol simulated tracers can be affected by model transport errors that can lead to biases in EnRs for both fresh and aged BB plumes observed from satellites (Konovalov et al., 2017a). To address this potential issue, we employ a simple correction procedure involving satellite observations of CO columns. Specifically, we introduce a correction factor, f_c, defined as follows:

$$f_c = ([CO]^{obs} - [CO]^{bgr}) ([CO]^{mod})^{-1}, \tag{2}$$

where $[CO]^{obs}$ and $[CO]^{mod}$ are the observed total CO column amounts and the corresponding modeled contribution of fire emissions to the CO columns, respectively, and $[CO]^{bgr}$ is the background value of ~~-~~[CO] in the absence of fires.

This factor is applied to the simulated tracers. In particular, the simulated values of τ_{abs}^t are corrected as follows:

$$\tau_{abs}^t[corrected] = \tau_{abs}^t[simulated] \times f_c \tag{3}$$

This correction implies that the simulated CO column amounts in a BB plume are affected by the same multiplicative transport errors as the BB aerosol components determining AAOD and AOD. Note that a similar procedure was used in Konovalov et al. (2017a), where advantages of using the observed and simulated CO columns in the estimation of EnR for AOD are discussed in detail; similar arguments apply for our estimations of EnRs for AAOD and AOD in this study. Estimation of the background values of τ_{abs}, τ_{ext}, and [CO] in this study is described in Sect. 2.3.

The normalization factor η_0 does not affect the results of our analysis and is introduced mainly for illustrative purposes. Here, we define it such that the average of all values of EnR_{abs} (or EnR_{ext}) over the ensemble of the data considered is equal to one:

$$\eta_0 = \langle \frac{\tau_{abs} - \tau_{abs}^{bgr}}{\tau_{abs}^t} \rangle^{-1}, \tag{4}$$

where the angular brackets denote averaging over the data ensemble.

As part of our analysis, we infer trends of EnRs for AAOD and AOD in the process of BB aerosol aging from the ensemble of available estimates of EnR_{abs} and EnR_{ext}. To characterize the BB aerosol age, we evaluate the time, t_e, of exposure of a given BB plume to solar irradiation. In other words, t_e is the integral time of the transport of a given BB plume since emission, during daytime hours. <u>Unlike the BB aerosol photochemical age evaluated in Konovalov et al. (2017a), the solar irradi-</u>

ation exposure time – which ~~was~~has been previously employed by Forrister et al. (2015) to evaluate the photo-degradation of BrC in observed BB plumes – is not affected by potential major uncertainties in the simulated OH concentration. At the same time, t_e ~~This characteristic~~ also quantifies the exposure of BB aerosol to the photochemical processing through oxidation by OH under the assumption that the OH concentration inside the plumes is constant ~~in the~~during daytime and zero ~~in~~

~~the~~during nighttime. We believe that this is a reasonable simplifying assumption in our case, where ~~the~~ observations of OH are unavailable and the accuracy of the simulated OH concentration in the BB plumes is unknown. ~~is evaluated as detailed in Sect. 2.3.~~Accordingly, ~~F~~for brevity, we refer below to t_e as the photochemical age of BB aerosol. ~~Note that t_e is equivalent to the more conventional definition of the BB aerosol photochemical age (e.g., Konovalov et al., 2017a) in the case where the latter is evaluated with constant daytime and zero nighttime OH concentrations within the BB plume. Unlike the BB aerosol photochemical age evaluated in Konovalov et al. (2017a), the solar irradiation exposure time – which was previously employed by Forrister et al. (2015) to evaluate the photo-degradation of BrC in observed BB plumes – is not affected by potential major uncertainties in the simulated OH concentration.~~ A ~~p~~Potential drawback~~s of U~~using ~~such defined~~a photochemical age defined in this way ~~the solar irradiation exposure time~~ as a predictor for the atmospheric evolution of BB aerosol in an analysis such as ours has the potential drawbacks ~~is~~that it can result in losing some observational information about the oxidation processes controlled by OH and that it disregards possible effects of the nighttime oxidation processes (specifically involving NO_3 and O_3 as oxidation agents). A concrete method which is used to evaluate t_e in this study is detailed in Sect. 2.3.

The trends in EnR_{abs} and EnR_{ext} (that is, the corresponding dependences on t_e) are fitted with a nonlinear function, $y(t_e)$, which is constructed as a sum of sigmoids:

$$y(t_e) = \sum_{k=1}^{N} \frac{w_{k1}}{(1+\exp(w_{k2} t_e + w_{k3}))} + w_0, \tag{5}$$

where $w_{\sim1k\sim1}$, $\sim-w_{\sim2k\sim2}$, $w_{\sim3k\sim3}$, and w_0 are the weight coefficients, and N is the number of sigmoids. In essence, the function $y(t_e)$ represents a neural network (of the perceptron type), which is known as a universal approximator (Hornik et al., 1989). The optimal values of the weight coefficients are found by minimizing the root mean square difference between the individual values of EnR_{abs} or EnR_{ext} and the corresponding values of $y(t_e)$. Following Konovalov et al. (2010), the optimization of the weight coefficients is achieved using the Nelder-Mead simplex algorithm (Press et al., 1992). Although the number of neurons (N) used for the trend approximation can also be optimized in a regular (albeit more complicated) way (Konovalov et al., 2010), here we simply tried the fits with $N=1$, $N=2$, and $N=3$. We found that while the fits with $N=2$ manifested statistically significant features that are missing in the approximations with $N=1$, the use of three neurons instead of two did not reveal any new statistically significant features of the analyzed trends. Therefore, only results obtained only with $N=2$ are reported in this paper. The nonlinear fit function given by Eq. (5) is also applied to the SSA retrievals described in Sect. 2.2 as well as to model data described in Sect. 2.3. Similar to Konovalov et al. (2017a), the confidence intervals for the approximations $y(t_e)$ were evaluated with the bootstrapping method (Efron and Tibshirani, 1993) involving a random selection of sample estimates. To ensure the reliable evaluation of the confidence intervals in terms of the 95th percentile, the analysis

involved 300 random samples. Note that the method employed in this study to approximate the tendencies in the optical properties of BB aerosol is more general and objective than the one used in our previous analysis of the AOD observations (Konovalov et al., 2017a). ~~Some~~ The ~~m~~Main technical differences between the analysis procedures used in Konovalov et al. (2017a) and this study are ~~discussed~~ outlined in Supplementary Material, Sect. S1.

5   **2.2 Satellite data**

Our analysis described in the previous section makes use of aerosol optical properties and total CO column amounts, which are retrieved from satellite observations performed by the three satellite instruments: OMI (Levelt et al., 2006), MODIS (Salomonson et al., 1989), and IASI (Clerbaux et al., 2009). Various combinations of these satellite retrievals were used in our previous studies of the atmospheric impacts of Siberian fires (Konovalov et al., 2014; 2017a; 2018) and are only briefly

10   described below. Pre-processing and harmonization of the different satellite data sets are explained in Sect. 2.5.

Specifically, we used the AAOD and SSA retrievals for the 388 nm wavelength, which are available as part of the Level-2 OMAERUV (v. 1.8.9.1) data product (Torres et al., 2007, 2013) derived by NASA from the OMI observations onboard the EOS Aura satellite. The OMAERUV algorithm exploits the observed departure of the spectral dependence of the near-UV upwelling radiation at the top of the atmosphere from that of a hypothetical pure molecular atmosphere and derives AAOD,

15   AOD, and SSA following a look-up table approach with assumed aerosol models, aerosol layer height and surface albedo. Importantly, the OMAERUV data product used in this study accounts for the wavelength-dependent aerosol absorption associated with BrC (Jethva et al. 2011; Torres et al., 2013). While the OMAERUV algorithm identifies one of the three assumed aerosol types (biomass burning, desert dust, and urban/industrial), we consider the AAOD and SSA data only for the first aerosol type. The data are retrieved assuming a set of five different vertical locations of the aerosol center mass: at the sur-

20   face and 1.5, 3.0, 6.0, and 10 km above the surface. We also used the "final" AAOD OMAERUV product, which is derived using the OMI-CALIOP (Cloud-Aerosol Lidar with Orthogonal Polarization) joint dataset (Torres et al., 2013) for the monthly climatology of the aerosol layer height. An important feature of the OMAERUV data product is that the AAOD data are less affected by sub-pixel cloud contamination than the AOD and SSA data, due to partial cancellation of errors in the AOD and SSA retrievals. Accordingly, the quality assured AOD and SSA data (which are associated with the quality

25   flag "0") are much less abundant than the quality assured AAOD data (which are associated with the quality flag "0" and "1").

Both AOD and SSA data were found to be in ~~a rather~~ good agreement with corresponding AERONET data worldwide (Ahn et al., 2014; Jethva et al., 2014), indicating that the AAOD data associated with the quality flag "0" are also sufficiently accurate. Besides, in our previous study (Konovalov et al., 2018), CTM simulations based on BB black carbon (BC) and organ-

30   ic carbon (OC) emissions in Siberia, which were inferred from the OMI AAOD data associated with the quality flag of both 0 and 1 and from the MODIS AOD observations, were found to be consistent with AERONET, aircraft, and in-situ aerosol measurements. Furthermore, the relationship between AAOD and AOD values retrieved from, respectively, the OMI and

MODIS satellite observations was found to be virtually the same as that between AAOD and AOD values derived from the AERONET measurements in Siberia, confirming that sub-pixel cloud contamination, which can affect the less reliable retrievals (with the quality flag "1"), is not likely to result in serious biases in the OMI AAOD retrievals. Therefore, the previous results provide evidence for the reliability of the OMAERUV AAOD data corresponding to both values of the quality flag.

We also used AOD at 550 nm derived from the MODIS observations onboard the Aqua and Terra satellites (Levy et al., 2013). The AOD data are obtained as the merged "dark target" and "deep blue" AOD retrievals from the Collection 6.1 MYD04 and MOD04 Level-2 data products (Levy et al., 2015). Validation studies (e.g., Levy et al., 2010) indicated the high quality of the MODIS AOD data, with the multiplicative and additive errors of MODIS-retrieved AOD of ~15% and 0.05 (or less), respectively.

In this study, the OMI AAOD and MODIS AOD retrievals are analyzed independently as described in Sect. 2.1. Besides, a similar analysis was performed for the SSA estimates obtained by combining the AAOD and AOD data as follows:

$$\omega_0 = \frac{\tau_{ext}^{inferred} - \tau_{abs}}{\tau_{ext}^{inferred}}, \tag{6}$$

where ω_0 is an estimate of SSA at 388 nm, τ_{abs} is AAOD retrieved from the OMI measurements, and $\tau_{ext}^{inferred}$ is AOD at 388 nm inferred from the MODIS observations at 550 nm using a power-law approximation. The extinction Ångström exponent necessary for this calculation was estimated in two ways. First, it was evaluated as the average ratio of the logarithms of the 388-nm AOD and 550-nm AOD retrievals from the matching OMI and MODIS satellite observations, respectively. Since the OMI AOD data correspond to the quality flag "0" and are therefore very sparse, the Ångström exponent could be estimated only as a constant number being independent ~~on~~ of the BB aerosol age. The different AOD retrievals were matched in space and time as described below in Sect. 2.5. Second, the Ångström exponent was calculated using the simulated AOD values (see Sect. 2.3) matching both the AAOD and AOD observations. The advantage of the second approach is that it allowed us to take into account the dependence of the Ångström exponent on the BB aerosol photochemical age, but an obvious drawback of the model estimates is that they can be affected by various model errors.

The total CO columns used in our analysis were retrieved using the FORLI (Fast Optimal Retrievals on Layers for IASI) algorithm (Hurtmans et al., 2012) from the IASI observations onboard the METOP-A satellite (Clerbaux et al., 2009) and are provided by LATMOS/CNRS and ULB (ESPRI, 2020). Following Konovalov et al. (2014; 2016; 2017a), the IASI CO data were pre-selected based on the degree of freedom of the signal (DOFS), which is considered as an indicator of the IASI sensitivity to CO in the boundary layer (George et al., 2009): we only considered the CO observations with DOFS exceeding 1.7.

In addition to the satellite observations of aerosol and CO, we use MODIS retrievals of the fire radiative power (FRP), which are available as the Collection 6 Level-2 MYD14/MOD14 data products (Giglio and Justice, 2015a, b). Following Konovalov et al. (2018), these FRP data were used to evaluate fire emissions, as briefly explained in the next section.

2.3 Chemistry transport model simulations: basic configuration and fire emissions

The chemistry transport model (CTM) is a key component of our analytical framework, serving three main objectives. First, we use the model to evaluate the BB aerosol tracers and photochemical age. Second, it is used to characterize the background conditions for aerosol and CO. Third, simulations of BB aerosol evolution help interpreting the results of the satellite
5   data analysis.

The simulations are performed with the CHIMERE CTM, version 2017 (Mailler et al., 2017). The same version of this model was successfully used in our previous analysis of satellite observations of BB aerosol (Konovalov et al., 2018). Previous versions of the CHIMERE model proved to be useful in other ~~numerous~~ studies of BB aerosol and fire emissions (e.g., Hodzic et al., 2010; Konovalov et al., 2012; Péré et al., 2014; Majdi et al., 2019). In this study, the configuration of the model
10 was almost the same as that in Konovalov et al. (2018), although there are some differences mainly concerning the representations of the organic fraction and optical properties of BB aerosol. These model representations are described in Sect. 2.4. The basic features of the model configuration used in this study are outlined later in this section.

Specifically, the chemical transformations of gaseous species, including OH, are simulated with the MELCHIOR2 chemical mechanism (Schmidt et al., 2001). Photolysis rates are computed with the FAST-JX module (Wild et al., 2000; Bian and
15 Prather, 2002), taking into account the attenuation of solar radiation by both clouds and aerosols. The representation of dry deposition follows Zhang et al. (2001). Wet scavenging and coagulation of aerosol particles are simulated using the standard parameterizations described in Mailler et al. (2017) and Menut et al. (2013). The formation of SOA from biogenic emissions of isoprene and terpenes is simulated with an oxidation scheme based on Kroll et al. (2006) and Zhang et al. (2007). Anthropogenic SOA is represented as a result of the oxidation of a few specific volatile SOA precursors (Bessagnet et al., 2008).
20 The anthropogenic emissions of gaseous and aerosol species are specified using the Hemispheric Transport of Air Pollution (HTAP) v2 global emission inventory (Janssens-Maenhout et al., 2015). Biogenic emissions of several organic gases and NO are calculated using the Model of Emissions of Gases and Aerosols from Nature (MEGAN v2.04) (Guenther et al., 2006).

Fire emissions are derived from satellite FRP data following the methodology detailed in Konovalov et al. (2014; 2017a; 2018). Briefly, the rate of emissions of a given aerosol or gaseous species from fires per ~~a~~ unit area is assumed to be propor-
25 tional to the FRP density. The proportionality coefficients include, in particular, the emission factor (depending on a vegetation land cover type), the empirical factor relating FRP to the BB rate, and the adjustable correction factor (F_s), which is allowed to take different values for different species s. The emission factors for gaseous species are specified using the data from Andreae (2019). However, to simplify the auxiliary – for the given study – task of optimizing BB aerosol emissions, the BC and organic carbon (OC) emission factors are taken to be the same as in Konovalov et al. (2018; see Table 1 therein).
30 The emission rates are modulated with the diurnal profile of BB emissions, which was derived directly from the MODIS FRP data (Konovalov et al., 2014, 2015). The correction factors are adjusted against the satellite data as explained in Sect. 2.6.

Following Konovalov et al. (2018), Tthe maximum emission injection heights of BB emissions are calculated for each FRP pixel using the "two-step" parameterization by of Sofiev et al. (2012). as a function of the observed FRP, the boundary layer height, and the Brunt–Väisälä frequency. The calculations of the injection heights of the BB emissions were validated by Sofiev et al. (2012; 2013) against vertical profiles of BB plumes derived from satellite observations by the Multi-angle Imaging SpectroRadiometer (MISR) and CALIOP instruments (Mazzoni et al., 2007; Omar et al., 2009) and were found to be in a reasonable quantitative agreement with these observations. In our simulations, the emissions for the given model layer are computed proportionally to the weighted number of pixels yielding the maximum injection height corresponding to this layer, with the weight of each pixel evaluated proportionally to the corresponding FRP. Konovalov et al. (2018) found that BB aerosol simulations whichthat were constrained by the OMI and MODIS satellite observations of AAOD and AOD were consistent with in situ measurements of BC and OC (Mikhailov et al., 2017) at the 300-m tall mast at the Zotino Tall Tower Observatory (ZOTTO) situated at a remote location in central Siberia (within our study region). Taking into account that the AAOD and AOD observations provide constraints to only columnar concentrations of BC and OC, this finding can be regarded as indirect evidence that the calculated BB emission vertical profiles within the boundary layer are reliable.

To estimate the BB aerosol photochemical age (or, more strictly speaking, the solar radiation exposure time as defined in the previous sectionSect. 2.1), the chemical mechanism in CHIMERE is extended to include two gaseous tracers that have the same emissions as BB OC. One of the tracers, T_1, is treated as an inert gas, while another tracer, T_2, decays with time, but only when the local solar zenith angle is less than 90°. The decay rate, k_T, is set to be equal to $2.3 \cdot 10^{-5}$ s^{-1} to represent – for definiteness – the mid-range of the half-lives for the decay of BrC in BB aerosol (12 h) according to the observational estimates by Forrister et al. (2015). Using the columnar mass concentrations of the tracers, $[T_1]$, and $[T_2]$, the BB aerosol photochemical age (or, more strictly speaking, the solar radiation exposure time), t_e, is estimated as follows:

$$t_e = k_T^{-1} \ln([T_1]\,[T_2]^{-1}).$$ (7)

The simulations are performed using a 1 by 1 degree model mesh covering a major part of Northern Eurasia (22.5–136.5 ° E; 38.5–75.5 ° N) with 12 non-equidistant model layers in the vertical. The top of the upper layer is fixed at the 200 hPa pressure level. The model was run for the period from 28 May to 15 August 2016, but the first 18 days (until 15 June) are withheld as the spin-up period. Note that BB aerosol evolution in 2016 had not been addressed in our previous studies mentioned above. The CHIMERE simulations are driven with the meteorological data from the WRF (Weather Research and Forecasting; version 3.9) model (Skamarock et al., 2008) simulations with nudging toward the FNL reanalysis (NCEP, 2017).

Similar to Konovalov et al. (2015; 2017a), the simulations considered in this study are performed for three main scenarios. The first and second main scenarios (labeled here as 'bb_vbs' and 'bb_trc', respectively) represent the conditions with predominating air pollution from fire emission. For these scenarios, all sources of gases and aerosol, except for those due to fire emissions inside the CHIMERE domain, were disregarded. The 'bb_vbs' scenario corresponds to the BB OA representation formulated within the VBS framework as described in Sect. 2.4. In the 'bb_trc' scenario, which is ancillary in the framework of the given study, the BB OA representation largely follows that for anthropogenic OA in the "standard" version of CHI-

MERE (Menut et al., 2003), presuming, in particular, that primary OA consists of non-volatile material. In this study, this representation is further simplified by entirely neglecting SOA formation, which turned out to be ~~rather~~ negligible anyway in our previous BB aerosol simulations with the standard version of CHIMERE (Konovalov et al., 2015; 2017a; 2018). The simulations for the 'bb_trc' scenario are used to evaluate the BB aerosol tracers involved in Eq. (1). For both scenarios, par-

5 ticulate fire emissions of OC were distributed following a fine-mode log-normal distribution with a mass median diameter (MMD) of 0.3 μm and a geometric standard deviation of 1.6 (Reid et al., 2005a) among 10 size sections. A smaller value of MMD of 0.25 μm was assumed for BC emissions, partly based on the recent measurements by Morgan et al. (2020). Taking into account that a contribution of the coarse mode of aerosol particles to the optical properties of BB aerosol at the UV and visual wavelengths is likely negligible (Reid et al., 2005b), this mode was disregarded in our simulations. This simplification

10 allows us to avoid large uncertainties associated with the representation of emissions and the evolution of coarse particles.

The third scenario (labeled below as 'bgr') represents the hypothetical conditions that are background with respect to the air pollution caused by fire emissions. The corresponding simulations were made with anthropogenic and biogenic emissions of particles and gases, but without fire emissions. Monthly climatology for gas and aerosol concentrations from the LMDZ-INCA chemistry transport model (Folberth et al., 2006) was used as the boundary conditions. The AOD values in our analy-

15 sis were computed in CHIMERE under the assumption that particle components are homogeneously mixed. The AAOD background values have not been evaluated in this study. As discussed in Konovalov et al. (2018), the main reason is that it is not known how the background part can be accounted for in the OMI AAOD retrievals for the "biomass burning" type of aerosol. Furthermore, the CHIMERE simulations of AAOD at 388 nm for the scenes dominated by anthropogenic pollution are probably highly uncertain particularly due to poorly known and variable values of the imaginary refractive index for OA.

20 Hence, a contribution of the background part of AAOD to the OMI AAOD retrievals is effectively neglected and is disregarded (unless indicated otherwise) in the analysis involving Eq. (1). To evaluate the total CO columns and AOD representative of all sources (anthropogenic, biogenic, and pyrogenic) of gases and aerosol, the corresponding values for the 'bb_vbs' or 'bb_trc' scenarios are summed up with values for the 'bgr' scenario. Note that by doing so we disregard any effects of anthropogenic emissions on the evolution of BB aerosol: according to our simulations, concentrations of aerosol and reactive

25 gases in the analyzed situation are predominantly determined by fire emissions. Our computations of the optical properties of BB aerosol are explained in the next section.

In addition, we performed supplementary simulations for a test scenario (referred below to as 'bb_poa') in which all the oxidation reactions that were taken into account in the simulations for the 'bb_vbs' scenario were turned off but POA was still assumed to be composed of semi-volatile species. Some further details on this scenario are provided below in Sect. 3.3.

30 Figure 1 shows the model domain and illustrates the fire emissions used in our simulations by presenting the density of the total BB emissions of particulate matter (PM) according to the 'bb_vbs' scenario in the analysis period of 15-31 July 2016 (see Introduction). The same figure also introduces the study region that covers western and central parts of Siberia – where

(as evident from the figure) major fires occurred during the analysis period – and also a part of Eastern Europe, including the European territory of Russia and territories of several Eastern European countries.

2.4 Model representation of the evolution and optical properties of BB aerosol

As noted above, one of the goals of our BB aerosol simulations is to interpret the evolution of BB aerosol optical properties that can be inferred from satellite observations as described in the previous section. However, there is currently no uniform way to represent atmospheric transformations of BB organic aerosol (OA) and its optical properties in CTMs. ~~Taking into account that the real BB aerosol evolution depends on numerous variable factors, most of which cannot presently be constrained by available observations in Siberia, we do not attempt to represent the many inter-related aging processes that can affect the BB aerosol evolution in a quantitatively accurate way. Furthermore, it is also challenging to choose an appropriate model representation of BB aerosol atmospheric aging among those suggested in the literature.~~ Typically, ~~such~~ model representations of the evolution of OA aerosol involve organic aerosol (OA) oxidation schemes that are designed using the volatility basis set (VBS) framework (Donahue et al., 2006; Robinson et al., 2007)~~.~~, but it is challenging to choose an appropriate VBS scheme among those suggested in the literature. Furthermore, differences between the available VBS schemes (e.g., Shrivastava et al., 2015; Konovalov et al., 2015; Ciarelli et al., 2017; Tsimpidi et al., 2018), which have been proposed for simulations of BB OA aerosol and are, to some extent, constrained by observational or experimental data, have been shown to result in major quantitative and even qualitative differences in the simulated multi-day evolution of BB OA mass concentration (Konovalov et al., 2019). Therefore, ~~However, using the different VBS oxidation schemes partly constrained by laboratory measurements or atmospheric observations to simulate the multi-day BB aerosol evolution under fixed ambient conditions has been found to result in major quantitative and even qualitative differences between the simulations (Konovalov et al., 2019). Furthermore,~~ it is not given that any of the available schemes can adequately describe the BB aerosol evolution specifically in Siberia.

Taking into account that the real BB aerosol evolution depends on numerous variable factors, most of which cannot presently be constrained by available observations in Siberia, we do not attempt to represent the many inter-related aging processes that can affect the BB aerosol evolution in a quantitatively accurate way. ~~Hence, i~~Instead of choosing any concrete OA oxidation scheme among those previously described in the literature, we designed a highly simplified ~~(mechanistic)~~ VBS scheme, which takes into account only basic processes driving the OA evolution and can be fitted to the satellite observations by adjusting ~~only~~ a few parameters. This scheme was used in our simulations for the 'bb_vbs' scenario.

As the basis for our OA oxidation scheme, we used a relatively simple "1.5-dimensional" VBS scheme proposed and described in detail by Ciarelli et al. (2017) (abbreviated below as C17). The original scheme addresses the evolution of several surrogate organic species, each of which is given a volatility, molecular weight, and ~~the~~ oxidation state. More specifically, all semi-volatile organic compounds (SVOCs) are split into three sets, such as (1) the POA set, (2) the set of SOA species formed as a result of oxidation of the POA species, and (3) the SOA set containing products of oxidation of volatile organic

compounds (VOCs) or intermediate-volatile organic compounds (IVOCs). Real VOC and IVOC species are represented by surrogate species referred to as NTVOCs ("non-traditional" VOCs). Some parameters of the C17 scheme, including the mass ratio of NTVOC and SVOC emissions and the enthalpies of vaporizations for SVOCs, were constrained with mass-spectrometric measurements of organic gases and particles from combustion of beech logs in a residential wood burner. The

5   SVOC species are split into five volatility classes, with the volatilities (C^*) ranging from 10^{-1} to 10^3 µg m^{-3}. The constrained VBS scheme yielded a good agreement of the measurements with corresponding box-model simulations under OH exposures that are equivalent to about 10 to 15 hours of evolution under typical atmospheric conditions (Ciarelli et al., 2017).

Our simplified oxidation scheme includes only two aggregated volatility classes of the POA species, one of which aggregates the three original classes of organic compounds with relatively low volatilities (LV) ($C^* \in [10^{-1}; 1]$ µg m^{-3}), and anoth-

10   er represents mostly medium-volatility (MV) primary compounds with volatilities ranging from 10^1 to 10^2 µg m^{-3}. The corresponding model species are denoted below as LV-POA and MV-POA. The volatilities of LV-POA and MV-POA were set in our simulations at 1 and 10^2 µg m^{-3}, respectively. Note that the gas-particle partitioning of MV-POA emissions in our simulation may be similar to that of more volatile organic species, since small but dense BB plumes are effectively diluted over the size of a grid cell. Box model simulations performed with varying initial size and density of ~~a~~ the BB plume indicated that

15   such artificial dilution can unrealistically enhance SOA formation (Konovalov et al., 2019). For these reasons, the BB emissions of SVOCs species with a volatility of ~10^3 µg m^{-3} are assumed to be also represented by MV-POA. The fire emissions of POA were split between LV-POA and MV-POA species based on a ratio of ~~4~~ 3 to ~~3~~ 4 following the estimates by May et al. (2013).

In our simulations, we merged the two SOA sets that had been originally introduced in C17. Similar to primary organic

20   compounds, secondary compounds with volatilities lower than or equal to 1 µg m^{-3} are aggregated as one model species, LV-SOA. To allow for a more realistic representation of the multi-generation aging of SOA, we retained a distinct SOA species with relatively high volatility (HV) of 10^3 µg m^{-3}. Our scheme also involves an MV-SOA species with a volatility of 10^2 µg m^{-3}. The POA and SOA species were given the same molecular weight as their respective analogs from the second, fourth, and fifth volatility classes of the SVOC sets 1 and 3 from the original C17 scheme. The properties of the VBS species

25   in our model are listed in Table 1.

The reactions representing the evolution of BB OA within our simplified VBS scheme are specified in Table 2. Specifically, the POA species in the gas phase are assumed to undergo reactions (R1) and (R2), where the stoichiometric factor of 1.3 is introduced to account for the difference between the molecular weights for SOA from the second volatility class of set 2 of the C17 scheme and the merged SOA set in our model (189 and 144 g mol^{-1}, respectively). Following C17, we assume that

30   apart from the oxidation of POA, SOA species are produced from the oxidation of NTVOCs (see reaction (R3)). However, we simplified the SOA yields: the direct oxidation of NTVOCs is assumed to result in the formation of only HV-SOA and LV-SOA, while the formation of MV-SOA is disregarded. The SOA yields for HV-SOA and LV-SOA are defined to retain the same total yield of SOA mass from the oxidation of NTVOCs as in C17 (~ 43 g mol^{-1}). The stoichiometric coefficients

for these yields are determined by the factors (0.33 and 0.30) accounting for the difference between the molar masses of HV-SOA and LV-SOA (131/144 ≅ 0.30/0.33) and by the ~~The value of the stoichiometric~~ adjustable parameter ξ_1 which ~~determining HV-SOA and LV-SOA yields~~ was varied in our test simulations to enable consistency of our simulations with the satellite observations considered (see Sect. 2.6). The simulation results presented in this paper were obtained with ξ_1 equal to 0.85.

Oxidation of gas-phase HV-SOA is assumed to yield MV-SOA (reaction R4). Since the molecular weight of MV-SOA is larger than that of HV-SOA (see Table 1), functionalization is presumed to effectively dominate – although only slightly – over fragmentation in the oxidation of "high-volatility" organic species. However, fragmentation is assumed to dominate over functionalization in the oxidation of both MV-SOA and LV-SOA in (R5) and (R6): the reaction yield is controlled by another adjustable parameter, ξ_2, which is set in our simulations at the small value of 0.15 (see Sect. 2.6 for the adjustment procedure). This means that OH oxidation of MV-SOA and LV-SOA yields 15% of LV-SOA by a functionalization pathway, while the fragmentation pathway accounts for 85% of products, which are considered as volatile and do not contribute to SOA formation. ~~A l~~Lower volatility of the SOA species is associated with a higher O~~:~~/C ratio (see C17), thus making less volatile species more prone to fragmentation. The reaction rates (k_{OH}) for reactions (R1)-(R4) are taken to be the same as those for similar reactions in C17, but a smaller rate is set for reactions (R5) and (R6), presuming that they represent multi-generation fragmentation processes.

One more adjustable parameter – ξ_3 – in our simplified VBS scheme is the emission ratio of the mass concentration of NTVOCs to the sum of mass concentrations of the POA species, which was set at 14.2. The same parameter was estimated in C17: its optimal value was found to be 4.75 (that is, three times less than in our case), although a much larger value (up to 9.8) was found to be also consistent with the measurements analyzed in C17. As noted above, the results of the experiments performed in C17 do not directly apply to the case of BB aerosol from Siberian fires. Hence, it does not seem infeasible that oxidation of VOC emissions from Siberian fires indeed effectively yields more SOA than oxidation of VOCs from the combustion of beech logs.

Enthalpies of vaporization (ΔH_{vap}) of the surrogate OA species are evaluated using the estimates derived by May et al. (2013) from thermodenuder measurements of fresh BB aerosol. The same ΔH_{vap} values (depending on the volatility) are used both for POA and SOA species. Following C17, we assume, for definiteness and simplicity, that all organic species within particles form a well-mixed, liquid, and inviscid solution. This assumption implies, in particular, that POA species can affect partitioning of SOA species according to Raoult's law, and vice versa.

To get a tentative idea about whether or not our simplified VBS scheme enables a sufficiently realistic representation of the BB aerosol evolution (especially during the first few hours, which, as ~~it is~~ ~~found~~discussed below, are not represented in satellite observations), we simulated the BB OA evolution under the conditions of chamber experiments reported in C17 by using the microphysical box model described in Konovalov et al. (2019) with both the simplified and original (C17) VBS schemes. The simulations are described in Supplementary Material, Sect. S2, and the ~~simulation~~ results are presented in Fig. S1 in

comparison with available chamber measurements. These results ~~are~~ indicati~~ve~~ that the simulations of the BB OA evolutions with our simplified scheme are physically reasonable (see Sect. S2 for details).

The optical properties of BB aerosol particles (for both 'bb_vbs' and 'bb_trc' scenarios) are evaluated using the OPTSIM software (Stromatas et al., 2012) under the assumption that any particle is composed of a spherical BC core surrounded by a

5 concentric shell consisting of homogeneously mixed organic components, inorganic ~~salts~~ions, and water. Given the simulated size-resolved mass concentration and composition of BB aerosol particles, as well as the complex refractive index for each particle component, the scattering and absorbing efficiencies for the particles are computed for the core-shell mixing scenario with a Mie code based on the formulations proposed by Toon and Ackerman (1981). The scattering and absorption efficiencies are then used to compute both the AOD and AAOD values. Note that Mie core/shell models in which a BC core

10 is represented as a perfect sphere ~~have been found to be~~are prone to underestimation of the fractional contribution of BC to absorption at near-UV wavelength~~s~~ in cases where the coating is relatively thin (with the shell/core mass ratio less than 3) as a result of the fact that actual BC particles are typically non-spherical aggregates (Liu et al., 2017; Taylor et al., 2020). However, this potential underestimation is unlikely to be significant in our simulations representing typical Siberian BB aerosol, which features typical OC/BC mass ratios as large as almost 30 (Mikhailov et al., 2017).

15 The real part of the refractive index for all of the BB aerosol components resolved in our simulation (see Sect. 2.3), as well as the imaginary part of the refractive index for the inorganic components (including BC), were taken in our computations to be the same as those given in Stromatas et al. (2012) for the 532 nm wavelength (see Table 3 therein) and are assumed for simplicity to be the same for both the 388 and 550 nm wavelengths considered here. In the 'bb_trc' simulation, BB aerosol absorption was calculated under the assumption that the organic shell is non-absorbing. Evaluation of the imaginary part of

20 the refractive indexes for the POA and SOA species, k_{poa} and k_{soa}, in our simulations for the 'bb_vbs' scenario involved the following assumptions.

First, based on the experimental findings (Saleh et al., 2014) that almost all BrC absorption of fresh BB aerosol is associated with extremely low-volatility organic compounds, we assumed that MV-POA is not absorbing. Based on the estimates of the imaginary refractive index of fresh OA, k_{OA}, and their uncertainties, which have been reported by Lu et al. (2015) as a func-

25 tion of the BC-to-OA ratio, and assuming ~~an~~ average value~~s~~ of the BC-to-OC and POA-to-OC ratios ~~-~~for Siberian BB aerosol to be about 0.04 and 1.8, respectively (Mikhailov et al., 2017; Konovalov et al., 2017b), we conservatively estimated k_{OA} to be 0.013. This estimate, which is in the lower range of the corresponding k_{OA} values ($k_{OA} \approx 0.025 \pm 50\%$) given by Lu et al. (2015), is expected to ensure that the contribution of POA to BB aerosol absorption in our simulations is not overestimated. Accordingly, taking into account the assumed MV-POA / LV-POA emission ratio (see above), we estimated k_{poa} (for LV-

30 POA) to be 0.03.

Second, we assumed that, as a result of UV photodegradation, k_{poa} decreases exponentially with the BB aerosol photochemical age (t_e). Taking into account the laboratory results by Fleming et al. (2020), we assumed the lifetime of BrC chromo-

phores in the LV-POA species to UV photodegradation to be 82 h. This lifetime represents the lowest part of the range of the experimental values reported by Fleming et al. (2020, see Table 3 therein).

Third, we assumed that in contrast to POA, the low-volatility SOA, LV-SOA, is not absorbing. This assumption ~~is not based on any direct experimental findings~~does not contradict the aforementioned experimental findings (Saleh et al., 2014) that

5 indicated high absorptivity of low-volatility organic compounds, since the contributions of POA and SOA species to the absorption were not isolated in these experiments, and the effect of SOA addition was found to be comparable to measurement uncertainties. ~~However~~Furthermore, if low-volatility SOA remaining after more rapid atmospheric processing of higher-volatility SOA would be strongly absorbing, it would be difficult to explain an almost total loss of BrC absorption of aging BB aerosol (Forrister et al., 2015), in which POA is typically replaced by oxidized species (e.g., May et al., 2015).

10 While oxidation of low-volatility POA is likely to yield absorptive components (Wong et al., 2017), chemical processing of LV-POA in our simulations is very slow (as shown below), and so the corresponding source of BrC is disregarded. For simplicity, the HV-SOA and MV-SOA species are assumed to have the same constant values of the imaginary refractive index, k_{soa}. This value was adjusted in our simulations for the 'bb_vbs' scenario (see Sect. 2.6) and is taken to be equal to 0.009 for the 388 nm wavelength. Photochemical processing of HV-SOA and MV-SOA resulting in the formation of non-absorbing

15 LV-SOA implicitly accounts in our simulations for the destruction of BrC chromophores through all possible mechanisms, including gas-phase and heterogeneous oxidation and UV photodegradation. To the best of our knowledge, estimates of the imaginary refractive index for SOA formed from photo-oxidation of BB emissions have so far been reported only by Saleh et al. (2013) based on the analysis of smog chamber experiments. According to these estimates, the imaginary refractive index (at 388 nm) for SOA is at least 0.04 (as in the case of SOA from pocosin pine) or even much larger. However, these

20 estimates correspond to a very initial stage of BB aerosol aging (when the UV exposure time is less than 1.5 hours), which is not addressed in our analysis, and therefore maybe not applicable to the more oxidized SOA compounds that are probably dominating aged BB aerosol particles.

Overall, except for a slow degradation of BrC by UV in primary aerosol particles, we assume that each molecule of any given SVOC species contains a constant fraction (that can be different for different species) of chromophores and that at-

25 mospheric evolution of BrC within BB aerosol particles is determined by the condensation or evaporation of the different primary and secondary organic compounds forming BB aerosol particles. This approach allows us to parameterize the evolution of the optical properties of BB aerosol within the CTM and the evolution of its chemical composition in a consistent way.

To characterize the effects of water uptake by BB aerosol particles on our computations of their optical properties, we evalu-

30 ated the hygroscopicity parameter κ_{org} (Petters and Kreidenweis, 2007) for BB OA by assuming that all the SOA species feature a constant hygroscopicity parameter, κ_{org} (Petters and Kreidenweis, 2007), of 0.2 and that the POA species are hydrophobic. The chosen value of κ_{org} for SOA is representative of the mid-range of the set of κ_{org} measurements for oxidized organic compounds generated in a flow reactor (Lambe et al., 2011). Also, we took into account the water uptake by inor-

ganic ~~salts~~ species using the equilibrium concentrations calculated in CHIMERE with the ISORROPIA module (Nenes et al., 1998). The main features of our simulations for the different modeling scenarios defined in Sect. 2.3 are summarized in Table 3.

Finally, we would like to emphasize once again that our simplified parameterization of the physical, chemical, and optical properties of BB aerosol is not aimed at a quantitatively accurate representation of the actual very complex processes. We believe that a quantitatively accurate representation of the BB aerosol properties and their evolution in CTMs is presently not feasible in a general case due to the lack of the necessary observational constraints. However, we consider our study as a step forward towards the development of a simple and robust but yet physically sound parameterization ensuring adequate simulation of BB aerosol properties and evolution in chemistry transport and climate models.

2.5 Pre-processing and harmonization of the satellite and model data

At the preparatory stage of our analysis, the Level-2 (orbital) AAOD, AOD, and CO satellite data were projected onto the model grid with an hourly temporal resolution (corresponding to the temporal resolution of the output data from CHIMERE). Different pixels falling into the same grid cell were averaged and matched to ~~a~~the corresponding simulated value. To select a particular AAOD retrieval among those corresponding to the different altitudes of the aerosol center mass (see Sect. 2.2), the altitude of an observed BB plume was estimated using the mass concentration of the total particulate matter from the CHIMERE simulations for the "bb_vbs" scenario. In this way, we harmonized the OMI AAOD retrievals with the corresponding simulations (similar to Zhang et al. (2015) and Konovalov et al. (2018)). As noted in Sect. 2.2, we also used the "final" AAOD retrieval product, which is not affected by possible errors of our model, but still maybe not free of biases due to differences between the actual and assumed "climatological" heights of the BB plumes.

For our analysis of EnR_{abs} or EnR_{ext}, the MODIS and IASI observations collocated – at the scale of a model grid cell – with the OMI observations were selected by requiring that the absolute value of the time difference between the measurements taken by OMI and MODIS as well as by OMI and IASI is as small as possible and does not exceed two hours. The observed BB plumes are assumed to be mostly of a large spatial scale (tens of km) and slowly evolving at a scale of a few hours. Accordingly, the temporal and spatial inconsistencies between the different satellite data are expected to result mostly in random uncertainties in our estimates of the EnR_{abs} or EnR_{ext}, which can be taken into account by the corresponding confidence intervals. For the ancillary analysis that does not involve the OMI AAOD observations (which are much sparser than the MODIS AOD and IASI CO observations), we matched only the available AOD and CO observations, again requiring that the absolute value of the time difference between these observations does not exceed 2 hours.

The simulated AAOD, AOD, and CO data were matched in both space and time to the corresponding satellite data. The simulated 3-D concentration fields of CO were first processed to compute the total CO columns using the IASI averaging kernels as described in Konovalov et al. (2014; 2016). As an additional step towards the harmonization of the satellite and simulation data, we introduced a selection criterion for the simulated data, which accounts for the fact that the OMI AAOD

data considered in this study are representative only of the scenes strongly affected by fire emissions. In the framework of the OMAERUV retrieval algorithm (Torres et al., 2013), such scenes were selected based on real-time AIRS (Atmospheric Infrared Sounder) retrievals of CO. Accordingly, the grid cells for which the OMAERUV data are available correspond to larger magnitudes of the retrieved CO columns than the grid cells for which the OMAERUV are not provided. However, due to errors in the fire emissions and computations of the air pollution transport, the observed "hot spots" in the CO columns do not necessarily correspond to similarly elevated values in the simulated CO columns, AAOD, and AOD. Such a mismatch between the OMAERUV data and simulations can result in systematic biases in estimates of EnR_{abs}. To avoid these possible biases, we first arranged (ranked) the retrieved CO columns with respect to their magnitudes. A similar ranking was performed for the simulated CO columns. Then we required that the simulated CO data (and the simulated AOD and AAOD data matching the CO columns in space and time) selected for our analysis have the same ranks as the retrieved CO columns. Using this criterion, we tried to mimic the selection procedure which was applied to the OMI observations in the framework of the OMAERUV algorithm in the case of the simulated data. ~~both CO columns from the satellite observations and simulations matched in space and time were first arranged (independently) with respect to magnitudes of the total CO columns. Then, we selected only those simulations that have the same ranks as the subset of CO observations matching (as described above) the OMI AAOD data.~~ An advantage of this selection procedure is that it does not involve any subjective quantitative criteria and its outcome is rather insensitive to the mean level of the CO fire emissions in the model. Finally, some outliers (too large and too small values of EnR_{abs} and EnR_{ext}) were removed using the three-sigma rule.

Applying all the selection criteria left us with a sufficiently large number (1156) of data points (in the main data set) suitable for our statistical analysis using the method outlined in Sect. 2.2. As the OMI SSA retrievals are very sparse compared to the AAOD retrievals, we did not apply any selection criteria to the SSA data except for the common spatial and temporal windows.

Note that the harmonization procedure described above presumes that the satellite retrievals which are available only for clear sky conditions are sufficiently representative of a whole grid cell, part of which can be covered by clouds. The underlying assumption is that in the analyzed period in the middle of summer, when there was little precipitation in the study region, the fire emissions and the corresponding atmospheric loading of BB aerosol were independent, in the statistical sense, of the cloud coverage in a given location. To ensure that the masking out of cloudy scenes in the satellite retrievals does not entail any major systematic discrepancies between the retrievals and simulations, we examined the difference of the observed and retrieved values of AOD in a given grid cell in the study region and period as a function of the number of the available retrievals per grid cell and did not find any considerable relationship between the two characteristics.

Figure 2 illustrates the "ancillary" (see above) data sets of AOD observations and simulations. In addition, Figure ~~S1~~ S2 in the Supplementary Material shows similar data for the CO columns. More specifically, these figures show the AOD and CO spatial distributions averaged over the analysis period (15-31 July 2016) in comparison to the similar distributions for the preceding period (15 June -14 July 2016) when there were no strong fire emissions in the study region. These figures also

introduce two special regions used in our analysis, one of which (referred to below as the "source" region) includes the locations of major Siberian fires that emitted BB plumes transported afterward to the Eastern European part of Russia and is expected to contain relatively fresh BB aerosol, and another (referred to below as the "receptor" region), which is expected to represent aged BB aerosol. The spatial distributions shown indicate that the Siberian fires caused strong enhancements of

5   the concentrations of BB aerosol and CO in the troposphere over a big part of Eastern Europe, which is further discussed in Sect. 3.

A final step of our procedure aimed at harmonizing the satellite and simulation data involved the estimation of probable biases in the background values of CO columns and AOD. (It may be useful to recall that the background part of AAOD is neglected in our analysis.) Similar to our previous studies mentioned above, these biases were estimated by averaging the

10   differences between the simulated and observed data representative of background conditions. A given scene was assumed to be representative of the background conditions with respect to a given characteristic (CO columns or AOD) if a corresponding simulated value for the 'fires' scenario did not exceed 10 % of the respective value for the 'bgr' scenario. In this study, the averaging is done over the period from 15 June to 15 August 2016 separately for the source region, the receptor region, and the rest of the study region. The estimated biases are then applied to the simulations of AOD and CO columns for the

15   corresponding regions under the 'bgr' scenario.

2.6 Adjustment of the model parameters

As explained above (see Sect. 2.4), our model representation of the BB aerosol aging processes for the 'vbs' scenario involves the three adjustable parameters, ξ_1-ξ_3, controlling the evolution of the POA and SOA species, and the imaginary refractive index, k_{soa}, controlling the absorptive properties of SOA. Besides, we need to adjust correction factors, F_s (see Sect.

20   2.3), specifically those controlling the fire emissions of BC, POA and CO. Note that the correction factor for CO emissions, F_{CO}, is applied to the emissions of all other gaseous species, except for those of NTVOCs (which were determined by scaling the POA emissions). Taking into account that AAOD for BB aerosol in Siberia is typically an order of magnitude smaller than AOD (e.g., Konovalov et al., 2018), we expected that the modeled evolution of AOD is not sensitive to k_{soa} and also not sensitive to the correction factor for BC emission, F_{BC}. Therefore, the parameters ξ_1-ξ_3, as well as the correction factors for

25   the POA and CO emissions from fires, can be adjusted independently of k_{soa} and F_{BC}. Specifically, we required that the nonlinear trend (see Eq. 5) in EnR for the simulated AOD be consistent with the corresponding nonlinear trend in the MODIS observations:

$$\left| y_{ext}^{obs}(t_e) - y_{ext}^{sim}(t_e) \right| < \Delta_{ext}^{obs}(t_e) + \Delta_{ext}^{sim}(t_e), \ \ t_e \in [t_e^{min}; t_e^{max}], \tag{8}$$

where $y_{ext}^{obs}(t_e)$ is the approximation of EnR_{ext} for the AOD observations, $y_{ext}^{sim}(t_e)$ is a similar approximation for the AOD

30   simulations, Δ_{ext}^{obs} and Δ_{ext}^{sim} are the 95% confidence intervals for y_{ext}^{obs} and y_{ext}^{sim}, respectively, and t_e^{min} and t_e^{max} are the minimum and maximum values of the photochemical age in the selected dataset.

In the presence of significant nonlinear variations of y_{ext}^{obs}, the condition given by Eq. (8) can provide sufficiently strong observational constraints to the three parameters ξ_1-ξ_3 of our VBS scheme. To optimize the fire emissions for POA by adjusting the corresponding correction factor (F_{POA}), we further required (following Konovalov et al., 2018) that the average values of the AOD simulated using an optimal value of F_{POA}, τ_{ext}^{sim}, and of the AOD derived from MODIS observations, τ_{ext}^{obs}, be approximately equal:

$$\left|\langle\tau_{ext}^{sim}\rangle - \langle\tau_{ext}^{obs}\rangle\right|\langle\tau_{ext}^{obs}\rangle^{-1} < o, \tag{9}$$

where the angular brackets denote the averaging performed over (only) the source region and analysis period, and o is the relative error, which is set to be equal to 0.05 in this study.

Similar conditions providing observational constraints to k_{soa} and F_{BC} apply to the simulations of AAOD:

$$\left|y_{abs}^{sim}(t_e) - y_{abs}^{obs}(t_e)\right| < \Delta_{abs}^{sim}(t_e) + \Delta_{abs}^{obs}(t_e), \ t_e \in [t_e^{min}; t_e^{max}], \tag{10}$$

$$\left|\langle\tau_{abs}^{sim}\rangle - \langle\tau_{abs}^{obs}\rangle\right|\langle\tau_{abs}^{obs}\rangle^{-1} < o. \tag{11}$$

Note that the trend $y_{abs}^{sim}(t_e)$ involved in Eq. (10) is expected to depend on both the correction factor F_{BC} and the imaginary refractive indexes k_{poa} (which is fixed) and k_{soa}. Taking into account Eq. (11), larger values of F_{BC} would require smaller values of k_{soa}. In turn, smaller values of k_{soa} would suppress the variability of $y_{abs}^{sim}(t_e)$ (which is expected to depend also on parameters ξ_1-ξ_3) and, therefore, the condition (10) would require a smaller value of F_{BC}. Such reasoning shows that if y_{abs}^{obs} exhibits significant changes with t_e, then the conditions (10) and (11) allow constraining each of the two parameters, k_{soa}, and F_{BC}, independently. ~~As argued above, a similar conclusion applies to the parameters controlling the simulations of AOD.~~

It should be noted that Eqs. (8)-(11) do not imply a rigorous minimization procedure~~,~~ but ~~rather~~ impose only approximate constraints on the parameters. Indeed, constraining the six parameters controlling our simulations of AAOD and AOD within the VBS framework is a challenging (even though not infeasible) computational task. On the other hand, the relatively "loose" constraints defined above allowed us to adjust the parameter values with a reasonable accuracy manually by running the model multiple times and iteratively varying the parameter values using the trial-and-error method. More specifically, starting from a priori estimates of F_{POA} and F_{BC} based on our previous studies and estimates of ξ_1-ξ_3 based on Ciarelli et al. (2017), we first adjusted the parameters ξ_1-ξ_3 and F_{POA} in an iterative process. At the next iteration cycle, using the optimized values of ξ_1-ξ_3 and F_{POA}, we adjusted the parameters k_{soa} and F_{BC}. These iteration cycles were repeated to ensure the consistency of all the parameters. The optimized values for ξ_1-ξ_3 and k_{soa} are indicated above in Sect. 2.4 and in Tables 2 and 3.

A similar but much simpler optimization procedure was realized in the case of the simulations with the standard version of CHIMERE (that is, for the 'bb_trc' scenario). Specifically, the parameters of the VBS scheme did not need to be adjusted by definition, and only a pair of iterations ~~was~~ were needed to adjust the correction factors F_{POA} and F_{BC} under conditions (9) and (11). The CO emissions from fires were optimized in the same way as the POA and BC emission for the 'bb_trc' scenario.

~~The optimized values for ξ_1-ξ_3 and k_{soa} are indicated above in Sect. 2.4.~~

~~The optimized values of F_{POA} and F_{BC} were found to be 2.8 and 2.9, respectively, for the 'bb_trc' scenario. These values are within the range of uncertainties of the similar estimates reported in Konovalov et al. (2018) and yield a mean ratio of BC and OC mass concentrations of about 0.05, which is rather close to the average value (0.038) of the highly variable BC/ OC~~

5 ~~ratios observed for BB aerosol in central Siberia (Mikhailov et al., 2017). For the 'bb_vbs' scenario, the optimized value of F_{POA} was found to be equal to 0.9 – that is, it is much smaller than that for the 'bb_trc' scenario. This difference accounts for the strong SOA formation in our simulations, qualitatively consistent with similar findings from our previous studies (Konovalov et al., 2015, 2017a) and with underestimation of AOD by simulations in which SOA formation was treated as a minor process (e.g., Petrenko et al., 2012; Tosca et al., 2013; Reddington et al., 2016).~~

10 For the 'bb_vbs' scenario, the optimized values of F_{POA} and F_{BC} were found to be 0.9 and 1.5, respectively. ~~The optimized value of F_{BC} (1.5) is also found to be smaller than for the 'bb_vbs' scenario, indicating a significant contribution of BrC to BB aerosol absorption.~~ With ~~this~~ these factors, the 'bb_vbs' simulation yields a mean ratio of BC and OC mass concentrations of 0.035, which is a quite realistic value, given the estimate (0.036± 0.009) previously derived by Konovalov et al. (2017b) from the AERONET measurements as well the average value (0.038) of the highly variable BC/OC ratios observed

15 for BB aerosol in central Siberia (Mikhailov et al., 2017). ~~aforementioned observations by Mikhailov et al. (2017) and estimates by Konovalov et al. (2017b).~~ This ~~fact~~ finding indicates that the absorption closure carried out in our numerical experiments is sufficiently adequate. The optimized value of F_{BC} is consistent with the F_{BC} estimate (1.5±0.5) obtained in Konovalov et al. (2018) for the Siberian fires ~~which~~ that occurred in July 2012. However, F_{POA} is much smaller than the corresponding estimate of F_{OC} (2.3±0.6), which was also reported in Konovalov et al. (2018). This difference accounts for the

20 strong SOA formation in our simulations for the 'bb_vbs' scenario, which was essentially disregarded in the simulations performed in Konovalov et al. (2018) (where BrC absorption, on the other hand, was taken into account implicitly using an empirical parameterization). ~~A higher BC content in our 'bb_trc' simulation than in the 'bb_vbs' one compensates for the BrC absorption, which is not taken into account in the 'bb_trc' simulation. The F_{CO} factor was set to 1.9 for both 'bb_vbs' and 'bb_trc' scenarios.~~

25 For the 'bb_trc' scenario, the optimized values of F_{POA} and F_{BC} were found to be 2.8 and 2.9, respectively. The difference between the optimal values of F_{POA} for the two scenarios is qualitatively consistent with similar findings from our previous studies (Konovalov et al., 2015, 2017a) and with underestimation of AOD by simulations in which SOA formation was treated as a minor process (e.g., Petrenko et al., 2012; Tosca et al., 2013; Reddington et al., 2016). A much larger value of F_{BC} in the 'bb_trc' scenario compared to that in the in 'bb_vbs' is indicative of a major contribution of BrC to BB aerosol

30 absorption in the 'bb_vbs' scenario, since the organic matter was assumed to be non-absorbing in the 'bb_trc' simulation. The F_{CO} factor was set to 1.9 for both 'bb_vbs' and 'bb_trc' scenarios.

The optimized correction factors allow obtaining "top-down" estimates of the total amounts of OC and BC emissions from fires in the study region. Specifically, the total emissions of OC (in particles) in the study region in July are found to be 1.0

and 2.8 Tg, respectively, for the 'bb_vbs' and 'bb_trc' scenarios. The big difference between the estimates reflects a strong dependence of the top-down estimates of the BB OA emissions on a model representation of the OA processes (Konovalov et al., 2015). The corresponding BC emissions are estimated as 70 and 136 Gg. As noted above, the difference between the BC emission estimates is mainly due to a missing contribution of BrC to the absorption in the simulations for the 'bb_trc'

5   scenario. For comparison, according to the GFED4.1s inventory (van der Werf et al., 2017), the same fires emitted 0.96 Tg OC and 51 Gg BC. These "bottom-up" estimates are evidently much closer to our estimates for the 'bb_vbs' scenario than for the 'bb_trc' one. The good agreement of the bottom-up and top-down estimates of the OC emissions is not necessarily meaningful: as argued in Konovalov et al. (2015), the consistency of top-down and bottom-up estimates of the BB OA emissions should be examined by taking into account the partitioning of the measured OC emissions between gases and particles,

10   but the necessary data are not provided as part of emission inventories. Our estimate of the BC emissions for the 'bb_vbs' scenario is indicative of the underestimation of the Siberian BB BC emissions in the GFES4.1s emission inventory, consistent with the findings of ~~the~~ previous analyses (Hao et al., 2016; Konovalov et al., 2018). Note, however, that the present study is not designed to evaluate the uncertainties in the top-down emissions estimates. As indicated by the more detailed analysis in Konovalov et al. (2018), the uncertainty in our estimate of the BC emissions is likely at least 35 %. Accordingly,

15   the top-down emission estimates reported above do not allow us to make any certain conclusions about the accuracy of the BC or OC emission estimates provided by the GFED4.1s inventory.

3 Results

3.1 Analysis using the two-region approach

In this section, we provide some preliminary characterization of the input data for our analysis, specifically by considering

20   the spatial distributions and time series of both the satellite observations and corresponding simulations. We also ~~and~~ examine the aging-driven changes in the optical properties of BB aerosol by considering the satellite and simulated data for the two regions ("source" and "receptor") introduced above (see Sect. 2.5 and Fig. 2). The source region includes locations of major Siberian fires, and the receptor region was affected by the aged BB plumes transported from the source region (see Fig. 2 and ~~S1~~S2). Spatial averaging of the observed characteristics over a big region suppresses the variability associated

25   with individual air masses.

~~The time series corresponding to Figs. 2 and S1 (which are based on the ancillary dataset) are presented and discussed in the Supplementary Material (Sect. S2, Figs. S2 and S3). Here we only note that the simulations taking fire emissions into account are found to be in good agreement with the observations, with the correlation coefficient exceeding 0.85.~~

The analysis presented in this section allows us to get some preliminary insights into the effects of atmospheric aging on the

30   BB aerosol optical properties. The advantage of this analysis is that it does not rely on any quantitative estimates (which may be inaccurate) of the BB aerosol photochemical age and is more "transparent" than the more general analysis presented in

Sect. 3.2. However, such an analysis has serious limitations, as it can provide only crude snapshots of the evolving BB plumes and does not involve ~~a~~ the characterization of statistical uncertainties.

The spatial distributions of the simulated average values of AOD and CO columns in the study region during the analyzed period are in a reasonable (although not perfect) agreement with the corresponding fields of the satellite data, both in Siberia and Europe (see Fig. 2a, c, and Fig S2a, c). Specifically, the satellite and model data (both for AOD and CO) exhibit similar big enhancements in the source region and also similar smaller but still considerable enhancements in the receptor region (compared to the period without strong BB emissions in the study region, see Fig. 2b, d and Fig. S2b, d). It is noticeable, however, that CHIMERE yields too high AOD values compared to MODIS in the eastern and south-eastern parts of the model domain (cf. Figs. 2a and 2c), where, on the contrary, the simulated CO columns tend to be lower than those retrieved from the IASI observations in the same parts of the domain. We suppose that these differences (which ~~could~~ do not significantly affect the results of our analysis because the affected grid cells are mostly outside of the study region) ~~c~~ may ~~an~~ be caused by the spatial variations in several factors and parameters involved in our simulations, including the emission factors for aerosol and gaseous species, volatility distributions of the POA emissions, and the relationship between FRP and the BB rate. In turn, these variations may be due to the inhomogeneity in the spatial distribution of the vegetation species across the region covered by the model domain: in particular, while the dominant tree species in the forest of western Siberia are pine, spruce, fir, birch, and aspen, the most abundant tree species in eastern Siberia (including ~~an~~ the eastern part of the study region) is larch (Schepaschenko et al., 2011). According to available measurements (May et al., 2014; Hennigan et al.,~~-~~ 2011), both the BB OA emission factors and SOA formation for different tree species exhibit strong diversity, while the relationship between FRP and the BB rate can be affected by relative prevalence of crown and ground fires, which differs in forests dominated by different tree species (Schulze et al., 2012).

The time series corresponding to the spatial distributions shown in Figs. 2 and S2 are presented and discussed in the Supplementary Material (Sect. S3, Figs. S3 and S4). Similar to the spatial distributions, the time series of the simulations taking fire emissions into account are found to be in good agreement with the observations both in the source and receptor regions, with the correlation coefficient for the spatially averaged daily values of the observations and simulations exceeding 0.85. Taking into account that CO has a relatively long lifetime, typically exceeding 15 days in the troposphere over continental regions in summer (Holloway et al., 2000), we consider the results of the comparison of the simulated and retrieved CO columns as an indication of the good performance of CHIMERE in capturing both the emissions and transport of the BB plumes during the studied period. Furthermore, taking into account that satellite retrievals of CO columns are known to be sensitive to the CO vertical distribution (e.g., George et al., 2009) (and, as noted in Sect. 2.5, this sensitivity has been addressed in our simulations by applying the averaging kernels), this comparison is also indicative of the adequacy of the simulated vertical profiles of the BB plumes.

The spatial distributions of the OMI AAOD observations and corresponding simulations (for the 'bb_vbs' scenario) for the study region and analysis period are shown in Fig. 3. Note again that the AAOD data analyzed in this study represent only

41

BB aerosol. Qualitatively, these distributions are similar to the corresponding distributions of AOD and CO (see Figs. 2a, c, and ~~S1a~~S2a, c), but the data are much more sparse, especially in the receptor region. Nonetheless, both the AAOD observations and simulations show numerous "hot spots" of AAOD in the source region and are also indicative of the major outflow of BB plumes from Siberia into the European territory of Russia.

5 Figure 4 shows the time series of the spatially averaged AAOD values according to the OMI observations and our simulations for the 'bb_vbs' and 'bb_trc' scenarios. It should be recalled that the background AAOD values were not computed in our simulations and thus are not shown. As the OMI AAOD data representing BB aerosol are almost absent for both regions outside of the analysis period, only the data for the analysis period are presented in Fig. 4. Note that for the receptor region, there is not enough data to cover even the whole analysis period. The time series for the corresponding AOD and CO values

10 (that were selected consistently with the AAOD observations) are also shown in Fig. 4.

It can be seen that the simulations for both 'bb_vbs' and 'bb_trc' scenarios are in ~~a rather~~ good agreement with the AAOD observations in the source region. In the receptor region, however, the simulations for the 'bb_trc' scenario overestimate AAOD for all four days for which the data are available and are biased high by ~22 % on average. The AOD simulations for the same scenario also tend to overestimate the observations, although the bias is smaller (~16 %). In contrast, the corre-

15 sponding simulations of the CO columns are practically not biased. These results indicate that the decrease of the observed values of both AAOD and AOD in the receptor region compared to the source region cannot be fully explained by the processes (such as dilution, dry and wet deposition, and coagulation) included in the simulations for the 'bb_trc' scenario. As argued below (see Sect. 3.3), these additional changes in AAOD and AOD are primarily caused ~~to~~by ~~the~~ losses of ~~a~~the medium-volatility fraction of SOA due to fragmentation. It is noteworthy that the simulations for the 'bb_vbs' scenario, which

20 take into account BB aerosol aging, do not exhibit any bias in the case of AOD and show only a minor negative bias of ~4 % in the case of AAOD. Note that the magnitude of the biases is not quite properly illustrated in Fig. 4a, because different "daily" points represent significantly different numbers of spatial grid cells. Overall, the analysis presented in this section indicates (i) that BB aerosol transported from the source region to the receptor region was affected by aging processes that resulted in reductions of both AAOD and AOD, and (ii) that our simulations, which have been designed to account for these

25 processes, reproduce these reductions rather adequately.

3.2 Analysis of EnRs for the AAOD and AOD observations as a function of the BB aerosol photochemical age

The results of the application of our analysis method, which is described in Sect. 2.1, to the AAOD, AOD, and SSA data retrieved from the OMI and MODIS measurements are presented in Figure 5. Different panels show the nonlinear approximations (trends) of EnRs for AAOD and AOD (Figs. 5a and 5b) as a function of the BB aerosol photochemical age, as well

30 as similar nonlinear approximations for the SSA values that are either inferred from the OMI AAOD and MODIS AOD observations (Fig. 5c) or ~~are~~ available directly from the OMAERUV data product (Fig. 5d). Along with the nonlinear trends for EnRs and SSA, we show the running averages over each corresponding 15 data points (for EnRs or SSA) that were pre-

liminarily arranged with respect to the BB aerosol photochemical age. The averaging is done for illustrative purposes, as the scatter of the original data points is typically large at the scale of the trends. Note that in the special situation addressed in this study, there is a strong association between the photochemical age of BB aerosol and the geographical location (specifically, the longitude) of the BB plumes transported westward (see Fig. 6). In particular, the BB aerosol photochemical age ranges from 6 to 42 hours in the source region and from 70 to 106 hours in the receptor region. This association facilitates the interpretation of the results of our analysis and also confirms the reliability of our model estimates of the BB aerosol photochemical age.

The nonlinear trend for AAOD (Figs. 5a) reveals a statistically significant decrease in EnR_{abs} (up to ~45%) corresponding to the photochemical age (t_e) period from about 25 to 60 hours. The changes in EnR_{abs} corresponding to both fresher and older BB aerosol are not statistically significant. This trend indicates that if AAOD were simulated for the given situation without taking into account any BB aging processes (except for coagulation) and were fitted to the AAOD observations corresponding to BB aerosol aged less than 40 h, the simulated AAOD corresponding to the aged BB plumes ($t_e > 60$ h) would be overestimated by ~30%. This rough estimate is in tentative agreement with the results from the two-region analysis discussed above (see Fig. 4), taking into account the ranges of the BB aerosol age in the source and the receptor region (see Fig. 6) and the uncertainty of the trends.

Variations in EnR for AOD (EnR_{ext}) are more pronounced (see Fig. 5b). Specifically, EnR_{ext} increases by more than a factor of two during the initial 30 hours of the daytime evolution (since t_e of about 6 hours) but then decreases by ~40%. This nonmonotonic behavior is not contradictory to the relatively minor overestimation of AOD in the receptor region in our simulations for the 'bb_trc' scenario, taking into account that the major part of the increase of EnR_{ext} occurs inside the source region, which includes BB aerosol with photochemical ages less than 40 h. Interestingly, the decreasing part of the trend in EnR_{ext} almost coincides in time with the decreasing part of the trend in EnR_{abs} (cf. Figs. 5a and 5b). This observation suggests that the reductions in both EnR_{abs} and EnR_{ext} may be driven by the same processes.

It is noteworthy that a similar increase (by a factor of two) in EnR for AOD as a result of atmospheric evolution of aerosol from Siberian fires was reported in our previous study (Konovalov et al., 2017a), despite the differences in the region, period and method of analysis compared to those in the present study. Furthermore, the previous analysis indicated the presence of a decreasing part in the dependence of EnR_{ext} on the BB aerosol photochemical age, but the statistical significance of that feature was not evaluated. The quantitative difference between the BB aerosol photochemical ages corresponding to the EnR_{ext} maximum (~30 h in this study and ~15 h in Konovalov et al., 2017a) may partly be due to the different definitions of the photochemical age. To the best of our knowledge, this is the first study reporting simultaneous decreases in both the AAOD and AOD (both corrected for dilution) in strongly aged BB plumes.

It seems reasonable to expect that the major increase in EnR_{ext} in the absence of a similarly strong increase in EnR_{abs} is likely to signify an increase in SSA. Figures 5c and 5d indicate that there is indeed a significant increase of SSA (at 388 nm) during the first 20-30 hours of the daytime evolution. According to the SSA estimates inferred from both the OMI AOD and

MODIS AAOD data (Fig. 5c) under the assumption that the Ångström exponent is constant (see Sect. 2.2) and equal (in the given case) to 1.0, SSA increased with a decreasing rate from ~0.89 to almost 0.95 during the first 25 h and then continued to increase much more slowly, reaching a maximum after 67 h of the BB aerosol evolution. This assumption, however, may be too strong, because whatever processes might significantly affect AAOD and AOD will also likely affect the size distribution of the particles and the Ångström exponent. As an alternative, we also estimated variable values of the Ångström exponent for the 388 and 550 nm wavelengths by using the corresponding AOD from our simulations for the 'bb_vbs' scenario. The dependence of the derived SSA estimates on the photochemical age is found to be qualitatively similar to the dependence shown in Fig. 5c, although the amplitude of the SSA changes in the test case is smaller than in the base case (see Fig. ~~S4~~S5). Importantly, a growing dependence on t_e is also found for the direct SSA retrievals (see Fig. 5d). In this case, SSA increases from about 0.9 to almost 0.94, and the increase is statistically significant. These direct SSA retrievals are, however, very sparse, resulting in a large uncertainty of the derived trend, and have not been selected consistently with the AAOD and AOD data (see Sect. 2.5). Although the inferred SSA increase associated with the BB aerosol aging may look relatively small, it can be regarded as an indication of major changes in the optical properties of BB aerosol. For example, an increase of SSA from 0.91 to 0.95 under a constant value of AAOD would result in an enhancement of the aerosol scattering of the solar radiation by almost a factor of two. Such enhancement can likely have serious implications for the radiative effects of BB aerosol.

Note that the freshest BB aerosol considered in our analysis has already been exposed to atmospheric processing for several hours. So, on the one hand, in the context of most BB aerosol aging experiments in smog chambers (e.g., Hennigan et al., 2011; Tiitta et al., 2016; Ciarelli et al., 2017) such an aerosol would be considered as already aged. On the other hand, these experiments do not usually examine changes in BB aerosol optical properties, especially at the long time scales addressed in this study. Therefore, a comparison of the results of our analysis with available results of laboratory experiments is not straightforward, and it goes beyond the scope of this study. However, the increase of SSA in our analysis is qualitatively consistent with the persistent enhancements of SSA of BB aerosol particles after 24 hours of atmospheric aging according to a recent analysis of AERONET data (Shi et al., 2019). Significant increases of the BB aerosol mass scattering efficiency and SSA as a result of the BB aerosol aging were observed by Kleinman et al. (2020) in near-field observations of BB plumes, consistent with an earlier observation (Akagi et al., 2012) of a major increase in aerosol light scattering in BB plumes. To the best of our knowledge, the simultaneous increase of both SSA and AOD (corrected for dilution) is reported here for the first time.

~~In~~

~~addition to the analysis outlined above, we performed several sensitivity tests aimed at examining possible systematic errors in the estimated nonlinear trends. An overview of these tests and the corresponding results is presented in the Supplementary Material, Sect. S3. The results of the tests overall confirm the robustness of our major findings discussed above.~~

3.3 Interpretation of the inferred changes in the BB aerosol optical properties

In this section, we employ our simulations with the CHIMERE CTM to interpret the qualitative features of the BB aerosol evolution inferred from the satellite observations. It should be noted that our interpretation is not unambiguous, especially with respect to the quantitative aspects of the effects considered. However, to the best of our knowledge, this interpretation is the first attempt to reconcile the major changes in both absorption and scattering characteristics of BB aerosol due to multi-day atmospheric aging with the available knowledge on the atmospheric transformations of BB aerosol by using numerical simulations with a CTM. The analysis presented below may have implications for developing adequate and robust parameterizations of BB aerosol aging processes in chemistry transport and climate models.

Figure 7 shows the nonlinear approximations for the AAOD and AOD enhancement ratios calculated using the simulations for the 'bb_vbs" scenario. The corresponding approximations based on the analysis of the satellite data are also shown for comparison. Evidently, based on the criteria given by Eqs. (8) and (10), EnR_{abs} and EnR_{ext} from the simulations are overall consistent with their counterparts from the observations (see Fig. 5a, b). This fact gives credence to the representation of the BB aerosol evolution in our model.

Further insights into the processes leading to the nonlinear trends in EnR_{ext} and EnR_{abs} according to our simulations are provided by the results presented in Figs. 8-10. Specifically, Fig. 8 illustrates the evolution of the chemical composition of BB aerosol in the simulations for the 'bb_vbs' scenario, presenting the fractional contributions of the model species in the mass columnar concentration of BB aerosol (Fig. 8a) and the normalized EnRs for the columnar concentrations of organic species in the particulate phase (Fig. 8b). These EnRs were evaluated similarly to Eq. (1) as the normalized ratio of the columnar concentration of the given component originating from fires to the columnar concentration of BB BC (which was considered as a passive tracer). Figure 8b also presents the evolution of EnR for OA in the sixth section (310-630 nm) of the particle size distribution assumed in our simulations. Figure 9 shows the evolution of the mass absorption and mass scattering efficiencies, and Fig. 10 demonstrates several sensitivity tests (explained below) aimed at a better understanding of the factors governing the evolution of EnR_{abs}. Additionally, several characteristics that can affect the gas-particle partitioning and oxidation processes and AAOD and AOD enhancement ratios are discussed in Sect. S4 (see also Fig. ~~S8~~S6).

According to Fig. 8a, the BB aerosol composition is dominated by SOA species from the very beginning of the BB aerosol aging period addressed in our analysis (that is, from t_e bigger than about 6 h). This is not quite surprising, as the typical lifetime of NTVOCs, which is the major source of SOA in our simulations, is just ~2 hours (with k_{OH} of 4×10 cm^3 molec^{-1} s^{-1} and OH concentration of ~4×10^6 cm^{-3}, see Fig. ~~S8b~~S6b). The same lifetime is characteristic ~~for~~ of the gaseous fractions of POA (but note that the gaseous fraction of LV-POA is relatively very small) and HV-SOA. During the next 30 h or so, the remains of MV-POA and HV-SOA are evaporated and converted into LV-SOA and MV-SOA. At this stage, the SOA fraction remains nearly constant (~78 %), as the effects of evaporation and fragmentation are overall counterbalanced by the effects of condensation and functionalization. It is worth noticing, however, that while the MV-SOA fraction also remains nearly constant, the LV-SOA fraction increases by more than 20 %, and the ratio of the LV-SOA and LV-POA fractions

increases ~~very~~ quite significantly by about 45 %. ~~~~After about 40 h, the main processes governing the evolution of SOA are the evaporation (facilitated by dilution, see Fig. ~~S8c~~S6c) of MV-SOA, its subsequent conversion into LV-SOA, and ~~a~~ relatively slow evaporation and gas-phase fragmentation of the latter. Consequently, the MV-SOA fraction shrinks from 44 % to merely 5 %, whereas the LV-SOA fraction increases twofold. The contribution of the inorganic fraction to the BB aerosol is

5   initially small (16 %) but it increases up to ~~(~~37 % ~~)~~ (see Fig. 8a) ~~Ff~~ollowing the increase of the relative humidity (see Fig. ~~S8a~~S6a) from about 40 to 65 %. The predominant inorganic compound in particles is water, whose fraction remains below 15 % before 60 h and eventually rises to 26 %~~., the inorganic fraction (including water) also increases but still remains relatively small, contributing a maximum of 20 %~~ Similar to non-absorbing organic compounds, inorganic ions and water increase the scattering cross-section of BB aerosol particles, thereby increasing AOD and SSA, although the contribution of a

10 unit mass of water to the scattering efficiency is considerably smaller in our simulations than that of the organic matter because the real component of the refractive index for water (1.33) is substantially smaller than for the organic species (1.63). It is noteworthy that the substantial increase in the water uptake occurs only after 60 h, and therefore it could not contribute significantly to the strong increase in EnR_{ext} before 30 h. The water uptake by the organic shell of the particles can also contribute to the lensing effect, thereby increasing AAOD, but as argued in this section below, the lensing effect does not play~~s~~ a

15 key role in the evolution of EnR_{abs} ~~anyway~~.

Consistent with the results shown in Fig. 8a, the EnRs for both MV-POA and HV-SOA are rapidly decreasing and become negligible after about 60 h (see Fig. 8b). In contrast, the EnR for LV-SOA exhibits a growing tendency during the whole period of evolution, increasing by ~70 %, although becoming nearly stable after about 70 h. A growing tendency is also manifested in the evolution of the EnR for MV-SOA and total OA, but only during the initial 25 hours, after which the EnRs

20 for both MV-SOA and total OA start~~s~~ to decrease. Since the BB OA concentration is typically much higher than 1 $\mu g\ m^{-3}$ (see Fig. ~~S8c~~S6c), LV-POA evaporates slowly, with its EnR decreasing by 30 % during the whole analysis period. The evaporation of LV-POA can be mainly driven by the loss of its gas phase-fraction due to reaction (R2).

It may be puzzling why EnR_{ext} is increasing twofold in the period until 30 h (see Fig. 7b), whereas no similar strong increase is demonstrated by the EnRs for any of the organic species. However, Fig. 8b also shows that the EnR for OA in particles

25 with sizes from 310 to 630 nm increases more than three times during the same period when EnR_{ext} increases twofold. According to Mie theory, this section corresponds to the particle diameters with the maximum scattering and extinction efficiencies at 550 nm. Hence, it is not surprising that the gain of mass by particles in this section of the accumulation mode results in an enhancement of AOD. Furthermore, Fig. 9 shows that the mass scattering efficiency (which is the main contributor to the mass extinction efficiency in our case) at the 550 nm wavelength increases by a comparable amount (almost by 70

30 %) in the same initial period of evolution. A similar, although relatively smaller, increase (~ 25 %) takes place in the mass scattering efficiency at 388 nm. In contrast, the mass absorption efficiency at 388 nm (also shown in Fig. 9) gradually decreases during the whole period of the evolution. Therefore, according to our simulation, the changes in the mass scattering and absorption efficiencies are the key drivers for the increases in both EnR for AOD at 550 nm and SSA at 388 nm. Our

further analysis indicates that the changes in the mass absorption and scattering efficiencies are indeed associated with changes in the size distribution of BB particles. Specifically, the particle size distribution shifts toward larger particles (see Fig. ~~S9~~S7) as the BB aerosol ages. Such a shift is apparently due to a complex interplay between the evaporation process (affecting predominantly smaller particles having a larger surface-to-volume ratio) and the dominating condensation process

5 (~~that~~ which can significantly affect also bigger particles, especially in the situation when smaller particles are partially evaporated). In the diluting plumes, condensation of organic material onto the particles occurs primarily as a result of oxidation processes driving the SOA formation. The growth of particles can also be caused by the uptake of water by both organic and inorganic components of the aerosol.

To get further insights into the role of the SOA formation in the analyzed evolution of the optical properties of BB aerosol,
10 we also performed simulations for a test scenario ('bb_poa') which has been briefly introduced in Sect. 2.3. In these simulations, the POA emissions had to be strongly (by a factor of 4.3) increased to keep the ~~balance~~agreement between the observed and simulated AOD. The 'bb_poa' simulations were performed by assuming that POA is hydrophilic with κ of 0.2 (whereas it was assumed to be hydrophobic in the 'bb_vbs' scenario). The corresponding results are presented in Sect. S5 and Fig. S8. Importantly, we found that neither EnR_{ext} nor the mass scattering efficiency considerably increase~~s~~ during the
15 period until 30 h, in striking contrast to the behavior of the same characteristics in the base case simulation. Changes in EnR_{ext}, which are due to the combined effect of evaporation of MV-POA and the uptake of water, are small (less than 15%) and negative during the whole period of evolution. There are decreasing trends in the mass absorption efficiency and EnR_{abs} and a gradual increase in SSA, which are apparently due to the limited lifetime of BrC in LV-POA. Overall, the simulations for the 'bb_poa' scenario confirm that the oxidation processes are the main driving force behind the major features in the re-
20 trieved evolution of AOD and SSA.

As could be expected, the simulated evolution of EnR_{abs} is also found to be driven by condensation and evaporation processes, but the impact of these processes on EnR_{abs} is mediated by several additional factors. In particular, one should take into account that AAOD is determined by BC, POA, and SOA species, each of which is characterized by a different value of the imaginary refractive index, and therefore equal relative changes in the mass concentrations of these components will have
25 different impacts on AAOD. Furthermore, changes in the POA and SOA mass concentrations can affect AAOD through the lensing effect (Lack et al., 2010). To examine these factors, we ran the OPTSIM module for several limiting cases representing different optical properties of the individual components of BB aerosol simulated within the 'bb_vbs" scenario. The main results are presented in Fig. 10, where the evolution of EnR_{abs} simulated under the different assumptions is compared with the corresponding trends derived from the OMI observations. Based on these results, we also evaluated the relative contribu-
30 tion of several factors to the BB aerosol absorption (see Sect. ~~S5~~ S6 and Fig. ~~S10~~S9).

Specifically, Fig. 10a shows the trend in EnR_{abs} for the sensitivity test where the refractive index of the shell of BB particles approaches that of ambient air. This is a ~~rather~~ relatively trivial case~~,~~ because the size distribution of BC particles should not be affected by evaporation and condensation of the POA and SOA species, and therefore AAOD associated with such parti-

47

cles is expected to behave almost as an inert tracer. And indeed, EnR$_{abs}$ computed for this case is found to be nearly constant (Fig. 10a). A minor increase in the EnR$_{abs}$ is likely due to different effects of dry deposition and coagulation on the size distribution of BB aerosol particles in the 'bb_vbs' and 'bb_trc' scenarios. Despite ~~being~~ looking ~~rather~~ trivial, this test confirms the integrity of our simulations and indicates that the evolution of AAOD in our simulations is almost fully determined by transformations of the organic fraction of BB aerosol. Note that in this case, the average AAOD in the selected dataset is much lower than in the base case: we estimated that "pure" BC (without the lensing effect) accounts on average for only 31% of the total absorption (see Sect. ~~S5~~S6).

Figure 10b presents results for the opposite sensitivity test, where the contribution of BC to the BB aerosol absorption was disregarded. In other words, AAOD was computed under the assumption that BC is not absorbing. In this case, the evolution of EnR$_{abs}$ is similar to that in the base case (see Fig. 7a), except that the amplitude of a variation of the nonlinear approximation is much larger in the test case. This test case further confirms a pivotal role played by OA in the simulated evolution of AAOD. As could be expected, constant BC absorption (see Fig. 10a) dampens, to a significant extent, the AAOD changes caused by the OA.

In principle, one would expect also that variations of the thickness of the organic shell, which are associated with the evolution of EnR$_{ext}$, lead to changes in EnR$_{abs}$ due to the lensing effect associated with the non-absorbing fraction of OA. To test this possibility, we set the imaginary refractive index for both POA and SOA to zero. The results of the corresponding computations are shown in Fig. 10c. According to these results, the lensing effect does not significantly contribute to the EnR$_{abs}$ variations in the base case. This can be due to the saturation of the absorption enhancement by a clear coating (Wu et al., 2018) and also ~~due to the fact that~~because the dilution-corrected variations of OA concentration in our simulations are ~~rather~~ relatively small (see Fig. 8b).

The test computations shown in Figs. 10a-10c clearly indicate that the key factor responsible for the changes of EnR$_{abs}$ in our simulation is the variable BrC absorption. Further insights into the mechanism of these changes are provided by a computation under the assumption that SOA is non-absorbing (while POA is still absorbing). The results of these computations are shown in Fig. 10d. Similar to the base case, EnR$_{abs}$ is decreasing with t_e, but at a much lower rate. Hence, we can conclude that the evolution of the aerosol absorption properties in our simulations is mainly driven by the formation and transformations of the SOA species.

Taking the entirety of the results of our analysis into account, we suggest the following qualitative interpretation of the main processes driving the evolution of EnRabs and EnRext in our simulations and, ultimately, in the real atmosphere. First, fast oxidation of NTVOCs results in the production of HV-SOA and MV-SOA. HV-SOA is mostly oxidized into MV-SOA and then LV-SOA during the initial period of a few hours, which is not represented in the satellite observations considered here. Oxidation of POA provides an additional source of both MV-SOA and LV-SOA. Evaporation (and subsequent transformation) of POA and HV-SOA and formation and condensation of LV-SOA and MV-SOA leads to a major increase of En-Rext, mainly as a result of an increase in the mass scattering efficiency at 550 nm due to a shift of the size distribution to-

wards bigger particles. In contrast, the mass absorption efficiency at 388 nm is not strongly affected by the indicated processes, and there is only a minor increase in EnRabs, which is caused by the formation of MV-SOA (as LV-SOA is assumed to be non-absorbing). As the sources of MV-SOA are depleted, its concentration decreases due to the oxidation reaction (R5). Since the fragmentation pathway is assumed to be dominating in this reaction, the depletion of MV-SOA is not com-

5 pensated by the production of LV-SOA; so the total concentration of the SOA species also decreases. This process can explain the decreasing stage in both the EnRabs and EnRext evolution. The decrease of the total SOA concentration – and the decrease of EnRabs and EnRext – slows down as the MV-SOA concentration decreases. Eventually, the BB aerosol consists predominantly of the lower volatility fractions of POA and SOA. This agrees with observations of low volatility of aged BB aerosols in field campaigns (Clarke and Kapustin, 2010; Thornberry et al., 2010; Andreae et al., 2018).

10 ~~We would like to emphasize that the presented interpretation is not necessarily unique. Although – based on our knowledge – we cannot propose any plausible alternative to oxidation processes associated with SOA formation and transformation as a driving force behind the major changes in the enhancement ratios for both AOD and AAOD, our interpretation involves considerable uncertainties with respect to many important features of these processes. For example, the evolution of the mass scattering efficiency (αs) is likely to depend on the initial size distribution of the BB aerosol particles, which may be very~~

15 ~~variable (Reid et al., 2005a). A smaller increase in αs would need to be compensated by a larger enhancement of the OA concentration (and vice versa). This could be achieved in our simulations by assuming a larger weight for the functionalization (or, alternatively, fragmentation) pathway of the oxidation reactions. Furthermore, the evolution of POA and SOA can depend on the phase state of the particles. While we assume in our simulations that particles are liquid, the critical temperature for the transition between the liquid and glassy states of the particles is estimated to be in the range of ambient tempera-~~

20 ~~tures in the boundary layer over Siberia (Shiraiwa et al., 2017), being a complex function of ambient relative humidity and particle composition. Slow diffusion of organic molecules within glassy or semi-solid particles could limit gas particle interactions but effectively expose larger amounts of SOA to gas phase photochemical processing. Taking the phase state transition processes into account would result in significant extensions of our simplified representation of BB aerosol aging, which could not be sufficiently constrained by the available observations in Siberia. However, we believe these extensionsare not~~

25 ~~likely to entail major qualitative changes in the proposed interpretation of the "observed" changes in the BB aerosol optical properties.~~

~~The evolution of the imaginary refractive index of BB aerosol is also represented in our simulation in a very simplified way. Although we differentiate between the several model species with respect to this properties, both primary and secondary real organic compounds are likely to feature a much wider spectrum of absorptive properties. Nonetheless, our interpretation will~~

30 ~~likely hold, if the low volatility SOA species formed in the real atmosphere from VOCs and POA as a result of a long chain of oxidation processes are much less absorptive than relatively fresh (and more volatile) SOA species. This assumption is supported by field observations (Forrister et al., 2015; Selimovic et al., 2019) and numerous laboratory experiments (e.g., Browne et al., 2019; Fan et al., 2019, Wong et al., 2017; 2019) indicating an eventual bleaching of BrC in BB aerosol as a~~

49

result of its exposure to the atmospheric oxidation processes and UV radiation. One more important simplifying assumption involved in our simulations concerns the evolution of the optical properties of the SOA species: as noted above, we assume that the imaginary refractive index for a given "virtual" SOA species, which represent the molecular weight and volatility of their real counterparts, does not change as long as this species exists. This assumption is obviously not true in a general case,

5 because destruction of chromophores by UV irradiation or as a result of aqueous heterogeneous oxidation is not necessarily associated with significant changes of the volatility or molecular weight of the affected compound. However, on the one hand, there is experimental evidence noted above (Fleming et al., 2020) that direct photodegradation of BrC in BB aerosol is a slow process with a characteristic time scale of at least several days – even though this observation, strictly speaking, applies only to fresh primary BB aerosol. On the other hand, aqueous heterogeneous oxidation can hardly be a significant pro-

10 cess in our situation, where water uptake by particles – as discussed above – is typically small, although the effect of ambient relative humidity on the atmospheric evolution of BrC in BB aerosol has yet to be investigated.

Overall, this discussion suggests that although our model representation of BB aerosol evolution involves strong assumptions (which yet need to be verified in future research), our qualitative interpretation of the inferred major changes of the optical properties of BB aerosol in Siberia is sufficiently robust and realistic. In turn, the applicability of this interpretation corrobo-

15 rates the reliability of our major findings from the analysis of the satellite observations.

3.4 Discussion of the uncertainties

In this section, we discuss possible sources of systematic errors in our retrieval and interpretation of the evolution of the optical properties of BB aerosol, which are associated both with our analysis of satellite data and CTM simulations. Random uncertainties (due to the spatial and temporal variability of satellite and model data corresponding to the same photochemical

20 age of BB aerosol) in the retrieved tendencies are taken into account in the confidence intervals as explained in Sect. 2.1.

To examine the main potential sources of systematic errors in our analysis of the satellite data, we performed several sensitivity tests. These tests and the corresponding results are presented in the Supplementary Material, Sect. S7 and Figs. S10-S12.

First, we tried to ensure that the major features in the retrieved evolution of the BB aerosol absorption properties are not

25 sensitive to possible biases in the simulated vertical profiles of BB aerosol, having in mind that such biases can affect the processing of the OMAERUV retrievals which are provided for five different altitudes of the aerosol center of mass (see Sect. 2.2). For this reason, we repeated our analysis with the 'final' OMAERUV retrievals, that is, without involving the simulated heights of the BB plumes. We found that the trends in EnR$_{abs}$ and SSA, which were obtained with the 'final' retrievals (see Fig. S10a, b) are only slightly different from those for the base case (see Fig. 5a, d, respectively).

30 Second, we examined to ~~which~~what extent our analysis is sensitive to the satellite and modeled data for the CO columns involved in the estimation of the correction factor f_c (see Eqs. 2 and 3) intended to compensate for possible model transport errors but possibly having biases of its own (see Sect. S7). To this end, we repeated our analysis of the satellite data with f_c

equal to 1. The derived trends (see Fig. S11) retained the main qualitative features of the tendencies obtained for the base case (see Fig. 5a, b). It is noteworthy that the tendency in EnR for AOD has wider confidence intervals corresponding to ~~the~~ photochemical ages larger than 70 h in the test case than in the base case, thereby indicating that the application of the CO columns is indeed helpful in reducing the uncertainties associated with model transport and BB emission errors in the simulations of the strongly aged BB plumes. This sensitivity test, therefore, provides strong evidence that the main derived qualitative features of the evolution of the BB aerosol optical characteristics are not an artifact of the model errors in the transport and BB emissions.

Third, we evaluated the sensitivity of the inferred tendencies in EnR_{ext} and EnR_{abs} to the assumptions regarding the background AOD and AAOD values (see Eq. 1) by neglecting the background AOD and assuming a constant value of 0.018 (based on the daily Level-3 OMAERUV data) for the background AAOD. This test indicated (see Fig. S12) that neither the increasing part in the trend in EnR_{ext} nor the decreasing parts in the trends in both EnR_{ext} and EnR_{abs} is due to possible biases in the background AOD and AAOD values. Overall, these tests confirm that our major qualitative findings obtained as a result of the analysis of the satellite data are not artifacts of the analysis procedure or model errors.

Potential systematic errors in the inferred tendencies in EnR_{ext} and EnR_{abs} can also be associated with biases in the satellite retrievals. However, as noted above (see Sect. 2.2), previous validation studies and analyse~~i~~s involving both the MODIS AOD and OMI AAOD retrievals for Siberian BB plumes did not reveal indications that these data are ~~considerably~~significantly biased. Accordingly, we have reason~~s~~ to ~~presume~~assume that the corresponding systematic errors in the inferred tendencies are relatively small in comparison ~~with~~to random errors and are covered by the estimated confidence intervals. Nonetheless, the lack of in situ measurements in Siberia does not allow us to properly evaluate and definitely rule out any effects of potential biases in the satellite retrievals on the results of our analysis. Validation of the satellite retrievals, especially ~~that~~ones distinguishing between fresh and aged BB aerosol, requires further dedicated studies.

As pointed out in the introduction and Sect. 2.4, our interpretation of the inferred evolution of the BB aerosol optical properties is based on the use of a highly simplified representation of the evolution of the organic fraction of BB aerosol. Accordingly, our analysis of the simulated data (see Sect. 3.3) was intended to identify only basic possible mechanisms underlying the main qualitative feature of the inferred tendencies and does not allow us to make any quantitative assessments. Although – based on our knowledge – we cannot propose any plausible alternative to oxidation processes associated with SOA formation and transformation as a driving force behind the major changes in the enhancement ratios for both AOD and AAOD, our interpretation involves considerable uncertainties with respect to many important features of these processes.

For example, the evolution of the mass scattering efficiency (α_s) is likely to depend on the initial size distribution of the BB aerosol particles, which may be very variable (Reid et al., 2005a). A smaller increase in α_s would need to be compensated by a larger enhancement of the OA concentration (and vice versa). This could be achieved in our simulations by assuming a larger weight for the functionalization (or, alternatively, fragmentation) pathway of the oxidation reactions. The evolution of POA and SOA can also depend on the phase state and viscosity of the particles. While we assume in our simulations that

particles are liquid and inviscid, the critical temperature for the transition between the liquid and glassy states of the particles is estimated to be in the range of ambient temperatures in the boundary layer over Siberia (Shiraiwa et al., 2017), being a complex function of ambient relative humidity and particle composition. Slow diffusion of organic molecules within highly viscous glassy or semi-solid particles could limit gas-particle interactions, thereby slowing down the POA and SOA evapora-

5   tion (e.g., Kim et al., 2019; Vaden et al., 2011) but also effectively exposing larger amounts of SOA species to gas-phase photochemical processing. The gas-particle partitioning and evolution of organic species forming BB aerosol can also depend on the mixing state of POA and SOA species. While there is experimental evidence supporting our simplifying assumption that POA and SOA species form a well-mixed solution (Asa-Awuku et al., 2009), there is also evidence (Song et al., 2007) that POA and SOA form separates solutionsexternal mixtures. If POA and SOA species do not mix in the real BB

10   aerosol and form two separate organic solutionsphases (as assumed, e.g., in Shrivastava et al., 2015), then our model is likely to prone to overestimateion of the concentrations of both POA and SOA species in particles. Taking the phase state transition processes, particle viscosity and possible scenarios concerning mixing of organic solutions into account would result in significant extensions of our simplified representation of BB aerosol aging. These extensions, which can hardlycannot be sufficiently constrained by available observations in Siberia, would probably require changes in the optimal values of the adjust-

15   able parameters and some other modifications (e.g., changes in the assumed volatility distribution or enthalpies of evaporation). However, we see no evidence in the literature that a more complex representation of BB aerosol could entailproduce qualitative changes in the simulated dynamics of BB aerosol, and thus an application of such a representation would not unlikely invalidate the proposed qualitative interpretation of the "observed" changes in the BB aerosol optical properties.

     One more potentially important factor that can affect the BB aerosol evolution in the real atmosphere but is not taken into

20   account in our simulations is the photolysis of SOA species, especially in particles. Based on a very limited amount of experimental data on the quantum yields for photolytic reactions of organic species in the particle phase, Hodzic et al. (2015) estimated the in-particle photolysis rate of SOA as 0.04 % of the photolysis rate of NO_2 and found – as a result of a global model simulation – that the SOA photolysis can remove aerosol from troposphere on time scales of several days. Although this mechanism of the SOA removal is very uncertain, we cannot rule out that it significantly contributed significantly to the

25   SOA depletion in the analyzed situation. If that was the case, then the SOA fragmentation rate in our simulations is likely overestimated. However, it should be noted that if the in-particle SOA photolysis were a primary driver for the decrease of AOD in our analysis (see Fig. 5b), then the rate of the decrease in EnR_{ext} would not be expected to strongly decelerate after about 70 h, as it does according to Fig. 5b (presuming that SOA and linked water are actually predominant components of aged BB aerosol). Hence, the brief inspection of our results suggests that the in-particle SOA photolysis could hardly be a

30   principal cause for the decreasing part of the trend in EnR_{ext}.

     The evolution of the imaginary refractive index of BB aerosol is also represented in our simulations in a very simplified way. Although we differentiate between the several model species with respect to these properties, both primary and secondary real organic compounds are likely to feature a much wider spectrum of absorptive properties. Nonetheless, our interpretation

will likely hold, if the low-volatility SOA species formed in the real atmosphere from VOCs and POA as a result of a long chain of oxidation processes are much less absorptive than relatively fresh (and more volatile) SOA species. This assumption is supported by field observations (Forrister et al., 2015; Selimovic et al., 2019) and numerous laboratory experiments (e.g., Browne et al., 2019; Fan et al., 2019, Wong et al., 2017; 2019) indicating eventual bleaching of BrC in BB aerosol as a result

5   of its exposure to the atmospheric oxidation processes and UV radiation. One more important simplifying assumption involved in our simulations concerns the evolution of the optical properties of the SOA species: as noted above, we assume that the imaginary refractive index for a given "virtual" SOA species, which represents the molecular weight and volatility of ~~their~~its real counterparts, does not change as long as this species exists. This assumption is not true in a general case, because the destruction of chromophores by UV irradiation or ~~as a result of~~ aqueous heterogeneous oxidation is not necessarily asso-

10   ciated with significant changes in the volatility or molecular weight of the affected compound. However, on the one hand, there is experimental evidence noted above (Fleming et al., 2020) that direct photodegradation of BrC in BB aerosol is a slow process with a characteristic time scale of at least several days – even though this observation, strictly speaking, applies only to fresh primary BB aerosol. On the other hand, aqueous heterogeneous oxidation can hardly be a significant process in our situation, where water uptake by particles – as discussed above – is typically small, although the effect of ambient rela-

15   tive humidity on the atmospheric evolution of BrC in BB aerosol has yet to be investigated.

Overall, this discussion suggests that although our model representation of BB aerosol evolution involves strong assumptions (which yet need to be verified in future research), our qualitative interpretation of the inferred major changes of the optical properties of BB aerosol in Siberia is sufficiently robust and realistic. In turn, the applicability of this interpretation corroborates the reliability of our major findings from the analysis of the satellite observations.

20   **4 Conclusions**

We have presented an analytical framework designed to advance the knowledge of changes in the optical properties of BB aerosol due to its atmospheric aging by using retrievals of AAOD, AOD, and SSA from satellite observations of BB plumes. This framework includes a method to evaluate nonlinear trends in the optical properties of BB aerosol due to the oxidation and gas-particle partitioning processes at the temporal scale (typically, several days) associated with ~~a~~ long-range transport

25   of BB plumes. It also involves using adjustable simulations of the sources and atmospheric evolution of BB aerosol with a chemistry transport model to reproduce and interpret the inferred trends.

We used this framework to get insights into the evolution of BB aerosol optical properties during a pronounced episode of a large-scale outflow of BB smoke plumes from Siberia towards Europe that occurred in July 2016. The analysis was based on the use of OMI AAOD and SSA retrievals combined with MODIS AOD retrievals. These retrievals were used together with

30   BB aerosol simulations and the CO columns derived from IASI observations to evaluate the enhancement ratios (EnR) for AAOD and AOD, which allows isolating the effects of oxidation and gas-particle partitioning processes from those of other processes, including transport, deposition, and wet scavenging. The simulations were performed with the CHIMERE chemis-

try transport model combined with the OPTSIM module enabling evaluation of the BB aerosol optical properties under the assumption of a core-shell morphology of the particles. The OA oxidation and gas-particle partitioning processes were represented in the simulation in the framework of a highly simplified but adjustable VBS scheme. Importantly, the evolution of BrC was simulated consistently with the evolution of the POA and SOA species, based on the assumptions that the POA

5   species are much more absorptive in the near-UV wavelength range than the SOA species and that the imaginary refractive index for a given SOA "virtual" species is constant. The EnR estimates and SSA data were analyzed as a function of model-based estimates of the BB aerosol photochemical age, which – in the situation considered – is found to be strongly associated with the geographical location of a BB plume.

We found that, while the EnR for AAOD does not change significantly during the first 20-30 hours of daytime evolution, the

10   EnR for AOD strongly (by more than a factor of 2) increases during the same period. The increase in EnR for AOD is accompanied by a statistically significant increase in SSA. Note that the first few hours of the atmospheric evolution of BB aerosol are not covered by our analysis. Further atmospheric processing of BB aerosol (up to a photochemical age of about 100 h) is found to be associated with statistically significant decreases (of about 45 %) of EnRs for both AAOD and AOD and insignificant changes of SSA. Note that while a similar increase in EnR for AOD was reported previously (Konovalov et

15   al., 2017a), our findings concerning the simultaneous changes in both the absorption and extinction characteristics of BB aerosol are novel.

By adjusting the imaginary refractive indexes for the SOA species, a few parameters of the simplified VBS scheme, and the emission factors, our simulations were brought into close agreement with the observed AAOD and AOD values and with the trends in EnRs for both AAOD and AOD. The analysis of our simulation results suggests that the upward trend in EnR for

20   AOD (which is associated with the initial increase in SSA) could be due to SOA formation and POA evaporation leading to a major increase in the mass scattering efficiency of BB aerosol through modulation of the particle size distribution. Evaporation of the semi-volatile SOA is indicated as a likely reason for the subsequent decrease of the EnR for both AAOD and AOD. We suggest that despite a highly simplified (mechanistic) character of our representation of BB aerosol our simulations, our conclusions regarding the basic factors behind the "observed" BB aerosol evolution are sufficiently robust. These

25   factors need to be adequately taken into account in chemistry transport and climate models to ensure reliable simulations of the BB aerosol optical properties and accurate estimates of associated radiative effects, specifically in Northern Eurasia. The proposed simplified representation of BB aerosol evolution can contribute to achieving such a goal, suggesting a reasonable compromise between over-complexity unconstrained by available observations and over-simplicity leading to major biases in the simulation results.

30   Overall, this study has demonstrated that the presented analytical framework can be helpful in identifying and interpreting manifestations of the BB aerosol aging processes far beyond the temporal time scales that can currently be addressed in aerosol chamber experiments. Although the application of the framework in the present study has been limited to a concrete episode of long-range transport of BB plumes, the proposed methods are rather sufficiently general and can be used in many

other studies of BB aerosol and applied to different sets of satellite data, including, for example, multi-spectral retrievals of aerosol absorptive properties from MISR (Multi-Angle Imaging Spectrometer) measurements (Junghenn Noyes et al., 2020). The framework was also shown to enable validation and optimization of model representations of BB aerosol evolution. Therefore, its future applications can help address current challenges associated with the representation of the evolution and optical properties of BB aerosol and its components in regional and global models (Shrivastava et al., 2017; Samset et al., 2018; Tsigaridis and Kanakidou, 2018; Konovalov et al., 2019).

References

Agarwal, S., Aggarwal, S. G., Okuzawa, K., and Kawamura, K.: Size distributions of dicarboxylic acids, ketoacids, α-dicarbonyls, sugars, WSOC, OC, EC and inorganic ions in atmospheric particles over Northern Japan: implication for long-range transport of Siberian biomass burning and East Asian polluted aerosols, Atmos. Chem. Phys., 10, 5839–5858, https://doi.org/10.5194/acp-10-5839-2010, 2010.

Ahern, A. T., Robinson, E. S., Tkacik, D. S., Saleh, R., Hatch, L. E., Barsanti, K. C., Stockwell, C. E., Yokelson, R. J., Presto, A. A., Robinson, A. L., Sullivan, R. C., and Donahue, N. M.: Production of secondary organic aerosol during aging of biomass burning smoke from fresh fuels and its relationship to VOC precursors, J. Geophys. Res., 124, 3583–3606, https://doi.org/10.1029/2018JD029068, 2019.

5 Ahn, C., Torres, O., and Jethva, H.: Assessment of OMI near-U aerosol optical depth over land, J. Geophys. Res.-Atmos., 119, 2457–2473, https://doi.org/10.1002/2013JD020188, 2014.

Akagi, S. K., Craven, J. S., Taylor, J. W., McMeeking, G. R., Yokelson, R. J., Burling, I. R., Urbanski, S. P., Wold, C. E., Seinfeld, J. H., Coe, H., Alvarado, M. J., and Weise, D. R.: Evolution of trace gases and particles emitted by a chaparral fire in California, Atmos. Chem. Phys., 12, 1397–1421, https://doi.org/10.5194/acp-12-1397-2012, 2012.

10 Andreae, M. O., and Gelencsér, A.: Black carbon or brown carbon? The nature of light-absorbing carbonaceous aerosols, Atmos. Chem. Phys., 6, 3131–3148, https://doi.org/10.5194/acp-6-3131-2006, 2006.

Andreae, M. O., Afchine, A., Albrecht, R., Holanda, B. A., Artaxo, P., Barbosa, H. M. J., Borrmann, S., Cecchini, M. A., Costa, A., Dollner, M., Fütterer, D., Järvinen, E., Jurkat, T., Klimach, T., Konemann, T., Knote, C., Krämer, M., Krisna, T., Machado, L. A. T., Mertes, S., Minikin, A., Pöhlker, C., Pöhlker, M. L., Pöschl, U., Rosenfeld, D., Sauer, D., Schlager, H.,
15 Schnaiter, M., Schneider, J., Schulz, C., Spanu, A., Sperling, V. B., Voigt, C., Walser, A., Wang, J., Weinzierl, B., Wendisch, M., and Ziereis, H.: Aerosol characteristics and particle production in the upper troposphere over the Amazon Basin, Atmos. Chem. Phys., 18, 921-961, https://doi.org/doi:10.5194/acp-18-921-2018, 2018.

Andreae, M. O.: Emission of trace gases and aerosols from biomass burning – an updated assessment, Atmos. Chem. Phys., 19, 8523–8546, https://doi.org/10.5194/acp-19-8523-2019, 2019.

20 Asa-Awuku, A., Miracolo, M. A., Kroll, J. H., Robinson, A. L., and Donahue, N. M.: Mixing and phase partitioning of primary and secondary organic aerosols, Geophys. Res. Lett., 36, L15827, https://doi.org/10.1029/2009GL039301, 2009.

Bekryaev, R. V., Polyakov, I. V., and Alexeev, V. A.: Role of polar amplification in long-term surface air temperature variations and modern Arctic warming, J. Clim., 23, 3888-3906, https://doi.org/10.1175/2010jcli3297.1, 2010.

Bessagnet, B., Menut, L., Curci, G., Hodzic, A., Guillaume, B., Liousse, C., Moukhtar, S., Pun, B., Seigneur, C., and Schulz,
25 M.: Regional modeling of carbonaceous aerosols over Europe – Focus on Secondary Organic Aerosols, J. Atmos. Chem., 61, 175–202, https://doi.org/10.1007/s10874-009-9129-2, 2008.

Bian, H., and Prather, M.: Fast-J2: Accurate simulation of stratospheric photolysis in global chemical models, J. Atmos. Chem., 41, 281–296, https://doi.org/10.1023/A:1014980619462, 2002.

Bian, Q., Jathar, S. H., Kodros, J. K., Barsanti, K. C., Hatch, L. E., May, A. A., Kreidenweis, S. M., and Pierce, J. R.: Sec-
30 ondary organic aerosol formation in biomass-burning plumes: theoretical analysis of lab studies and ambient plumes, Atmos. Chem. Phys., 17, 5459-5475, https://doi.org/10.5194/acp-17-5459-2017, 2017.

Brown, H., Liu, X., Feng, Y., Jiang, Y., Wu, M., Lu, Z., Wu, C., Murphy, S., and Pokhrel, R.: Radiative effect and climate impacts of brown carbon with the Community Atmosphere Model (CAM5), Atmos. Chem. Phys., 18, 17745–17768, https://doi.org/10.5194/acp-18-17745-2018, 2018.

Browne, E. C., Zhang, X., Franklin, J. P., Ridley, K. J., Kirchstetter, T. W., Wilson, K. R., Cappa, C. D., and Kroll, J. H., Effect of heterogeneous oxidative aging on light absorption by biomass burning organic aerosol: Aerosol Sci. Tech., 53, 663-674, doi:10.1080/02786826.2019.1599321, 2019.

Bond, T. C., Doherty, S. J., Fahey, D. W., Forster, P. M., Berntsen, T., DeAngelo, B. J., Flanner, M. G., Ghan, S., Kärcher, B., Koch, D., Kinne, S., Kondo, Y., Quinn, P. K., Sarofim, M. C., Schultz, M. G., Schulz, M., Venkataraman, C., Zhang, H., Zhang, S., Bellouin, N., Guttikunda, S. K., Hopke, P. K., Jacobson, M. Z., Kaiser, J. W., Klimont, Z., Lohmann, U., Schwarz, J. P., Shindell, D., Storelvmo, T., Warren, S. G. and Zender, C. S.: Bounding the role of black carbon in the climate system: A scientific assessment, J. Geophys. Res. Atmos., 118, 5380–5552, https://doi.org/10.1002/jgrd.50171, 2013.

Ciarelli, G., El Haddad, I., Bruns, E., Aksoyoglu, S., Möhler, O., Baltensperger, U., and Prévôt, A. S. H.: Constraining a hybrid volatility basis-set model for aging of wood-burning emissions using smog chamber experiments: a box-model study based on the VBS scheme of the CAMx model (v5.40), Geosci. Model Dev., 10, 2303-2320, https://doi.org/10.5194/gmd-10-2303-2017, 2017.

Clarke, A., and Kapustin, V.: Hemispheric aerosol vertical profiles: Anthropogenic impacts on optical depth and cloud nuclei, Science, 329, 1488-1492, https://doi.org/10.1126/science.1188838, 2010.

Clerbaux, C., Boynard, A., Clarisse, L., George, M., Hadji-Lazaro, J., Herbin, H., Hurtmans, D., Pommier, M., Razavi, A., Turquety, S., Wespes, C., and Coheur, P.-F.: Monitoring of atmospheric composition using the thermal infrared IASI/MetOp sounder, Atmos. Chem. Phys., 9, 6041–6054, https://doi.org/10.5194/acp-9-6041-2009, 2009.

Cubison, M. J., Ortega, A. M., Hayes, P. L., Farmer, D. K., Day, D., Lechner, M. J., Brune, W. H., Apel, E., Diskin, G. S., Fisher, J. A., Fuelberg, H. E., Hecobian, A., Knapp, D. J., Mikoviny, T., Riemer, D., Sachse, G. W., Sessions, W., Weber, R. J., Weinheimer, A. J., Wisthaler, A., and Jimenez, J. L.: Effects of aging on organic aerosol from open biomass burning smoke in aircraft and laboratory studies, Atmos. Chem. Phys., 11, 12049-12064, https://doi.org/10.5194/acp-11-12049-2011, 2011.

Di Lorenzo, R. A., Washenfelder, R. A., Attwood, A. R., Guo, H., Xu, L., Ng, N. L., Weber, R. J., Baumann, K., Edgerton, E., and Young, C. J.: Molecular-size-separated brown carbon absorption for biomass-burning aerosol at multiple field sites, Environ. Sci. Technol., 51, 3128–3137, https://doi.org/10.1021/acs.est.6b06160, 2017.

Donahue, N. M., Robinson, A. L., Stanier, C. O., and Pandis, S. N.: Coupled partitioning, dilution, and chemical aging of semivolatile organics, Environ. Sci. Technol., 40, 2635–2643, https://doi.org/10.1021/es052297c, 2006.

Efron, B. and Tibshirani, R. J.: An introduction to the bootstrap, Chapman & Hall, New York, 1993.

ESPRI: IASI retrievals, available at http://cds-espri.ipsl.fr/etherTypo/index.php?id=1707&L=1, last access: 15 April 2020.

Evangeliou, N., Balkanski, Y., Hao, W. M., Petkov, A., Silverstein, R. P., Corley, R., Nordgren, B. L., Urbanski, S. P., Eck-hardt, S., Stohl, A., Tunved, P., Crepinsek, S., Jefferson, A., Sharma, S., Nøjgaard, J. K., and Skov, H.: Wildfires in northern Eurasia affect the budget of black carbon in the Arctic – a 12-year retrospective synopsis (2002–2013), Atmos. Chem. Phys., 16, 7587–7604, https://doi.org/10.5194/acp-16-7587-2016, 2016.

5   Fan, X., Yu, X., Wang, Y., Xiao, X., Li, F., Xie, Y., Wei, S., Song, J., and Peng, P., The aging behaviors of chromophoric biomass burning brown carbon during dark aqueous hydroxyl radical oxidation processes in laboratory studies: Atmos. Envi-ron., 205, 9-18, doi:10.1016/j.atmosenv.2019.02.039, 2019.

Fleming, L. T., Lin, P., Roberts, J. M., Selimovic, V., Yokelson, R., Laskin, J., Laskin, A., and Nizkorodov, S. A.: Molecular composition and photochemical lifetimes of brown carbon chromophores in biomass burning organic aerosol, Atmos. Chem.

10 Phys., 20, 1105–1129, https://doi.org/10.5194/acp-20-1105-2020, 2020.

Folberth, G. A., Hauglustaine, D. A., Lathière, J., and Brocheton, F.: Interactive chemistry in the Laboratoire de Météorolo-gie Dynamique general circulation model: model description and impact analysis of biogenic hydrocarbons on tropospheric chemistry, Atmos. Chem. Phys., 6, 2273–2319, doi:10.5194/acp-6-2273-2006, 2006.

Forrister, H., Liu, J., Scheuer, E., Dibb, J., Ziemba, L., Thornhill, K. L., Anderson, B., Diskin, G., Perring, A. E., Schwarz, J.

15 P., Campuzano-Jost, P., Day, D. A., Palm, B. B., Jimenez, J. L., Nenes, A., and Weber, R. J.: Evolution of brown carbon in wildfire plumes, Geophys. Res. Lett., 42, 4623–4630, https://doi.org/10.1002/2015GL063897, 2015.

George, M., Clerbaux, C., Hurtmans, D., Turquety, S., Coheur, P.- F., Pommier, M., Hadji-Lazaro, J., Edwards, D. P., Worden, H., Luo, M., Rinsland, C., and McMillan, W.: Carbon monoxide distributions from the IASI/METOP mission: evaluation with other space-borne remote sensors, Atmos. Chem. Phys., 9, 8317–8330, https://doi.org/10.5194/acp-9-8317-

20 2009, 2009.

Giglio, L. and Justice, C.: MOD14 MODIS/Terra Thermal Anomalies/ Fire 5-Min L2 Swath 1km V006 [Data set], NASA EOSDIS LP DAAC, https://doi.org/10.5067/MODIS/MOD14.006, 2015a.

Giglio, L. and Justice, C.: MYD14 MODIS/Aqua Therma Anomalies/Fire 5-Min L2 Swath 1km V006 [Data set], NASA EOSDIS Land Processes DAAC, https://doi.org/10.5067/MODIS/MYD14.006, 2015b.

25 Gorchakov, G.I., Golitsyn, G.S., Sitnov, S.A., Karpov, A. V., Gorchakova, I. A., Gushchin, R.A., and Datsenko, O.I.: Large-Scale Haze over Eurasia in July 2016, Dokl. Earth Sc., 482, 1212, https://doi.org/10.1134/S1028334X1809012X, 2018.

Guenther, A., Karl, T., Harley, P., Wiedinmyer, C., Palmer, P. I., and Geron, C.: Estimates of global terrestrial isoprene emissions using MEGAN (Model of Emissions of Gases and Aerosols from Nature), Atmos. Chem. Phys., 6, 3181–3210,

30 https://doi.org/10.5194/acp-6-3181-2006, 2006.

Gupta, P., Doraiswamy, P., Levy, R., Pikelnaya, O., Maibach, J., Feenstra, B., Polidori, A., Kiros, F., and Mills, K. C.: Impact of California fires on local and regional air quality: the role of a low-cost sensor network and satellite observations, GeoHealth, 2, 172–181, https://doi.org/10.1029/2018GH000136, 2018.

Gustafsson, Ö., and Ramanathan, V.: Convergence on climate warming by black carbon aerosols, Proc. Natl. Acad. Sci., 113, 4243-4245, doi:10.1073/pnas.1603570113, 2016.

Hao, W. M., Petkov, A., Nordgren, B. L., Corley, R. E., Silverstein, R. P., Urbanski, S. P., Evangeliou, N., Balkanski, Y., and Kinder, B. L.: Daily black carbon emissions from fires in northern Eurasia for 2002–2015, Geosci. Model Dev., 9, 4461–4474, https://doi.org/10.5194/gmd-9-4461-2016, 2016.

Hennigan, C. J., Miracolo, M. A., Engelhart, G. J., May, A. A., Presto, A. A., Lee, T., Sullivan, A. P., McMeeking, G. R., Coe, H., Wold, C. E., Hao, W.-M., Gilman, J. B., Kuster, W. C., de Gouw, J., Schichtel, B. A., Collett Jr., J. L., Kreidenweis, S. M., and Robinson, A. L.: Chemical and physical transformations of organic aerosol from the photo-oxidation of open biomass burning emissions in an environmental chamber, Atmos. Chem. Phys., 11, 7669–7686, https://doi.org/10.5194/acp-11-7669-2011, 2011.

Hobbs, P. V., and Radke, L. F.: Cloud Condensation Nuclei from a Simulated Forest Fire, Science, 163 (3864), 279–280 https://doi.org/10.1126/science.163.3864.279, 1969

Hodshire, A. L., Bian, Q., Ramnarine, E., Lonsdale, C. R., Alvarado, M. J., Kreidenweis, S. M., Jathar, S. H., and Pierce, J. R.: More than emissions and chemistry: Fire size, dilution, and background aerosol also greatly influence near-field biomass burning aerosol aging, J. Geophys. Res.-Atmos., 124, 5589–5611, https://doi.org/10.1029/2018JD029674, 2019.

Hodzic, A., Jimenez, J. L., Madronich, S., Canagaratna, M. R., DeCarlo, P. F., Kleinman, L., and Fast, J.: Modeling organic aerosols in a megacity: Potential contribution of semi-volatile and intermediate volatility primary organic compounds to secondary organic aerosol formation, Atmos. Chem. Phys., 10, 5491–5514, https://doi.org/10.5194/acp-10-5491-2010, 2010.

Hodzic, A., Madronich, S., Kasibhatla, P. S., Tyndall, G., Aumont, B., Jimenez, J. L., Lee-Taylor, J., and Orlando, J.: Organic photolysis reactions in tropospheric aerosols: effect on secondary organic aerosol formation and lifetime, Atmos. Chem. Phys., 15, 9253–9269, https://doi.org/10.5194/acp-15-9253-2015, 2015.

Holloway, T., Levy, H., and Kasibhatla, P.: Global distribution of carbon monoxide, J. Geophys. Res., 105 (D10), 12123–12147, doi:10.1029/1999JD901173, 2000.

Hornik, K., Stinchcombe, M., and White, H.: Multilayer feedforward networks are universal approximators, Neural Networks, 2, 359-366, 1989.

Hurtmans, D., Coheur, P.-F., Wespes, C., Clarisse, L., Scharf, O., Clerbaux, C., Hadji-Lazaro, J., George, M., and Turquety, S.: FORLI radiative transfer and retrieval code for IASI, J. Quant. Spectrosc. Ra., 113, 1391–1408, 2012, https://doi.org/10.1016/j.jqsrt.2012.02.036.

Ikeda, K., and Tanimoto, H.: Exceedances of air quality standard level of PM2.5 in Japan caused by Siberian wildfires, Environ. Res. Lett., 10, 105001 , https://doi.org/10.1088/1748-9326/10/10/105001, 2015.

Jacobson, M. Z.: Effects of biomass burning on climate, accounting for heat and moisture fluxes, black and brown carbon, and cloud absorption effects, J. Geophys. Res.-Atmos., 119, 8980–9002, https://doi.org/10.1002/2014JD021861, 2014.

5 Janssens-Maenhout, G., Crippa, M., Guizzardi, D., Dentener, F., Muntean, M., Pouliot, G., Keating, T., Zhang, Q., Kurokawa, J., Wankmüller, R., Denier van der Gon, H., Kuenen, J. J. P., Klimont, Z., Frost, G., Darras, S., Koffi, B., and Li, M.: HTAP_v2.2: a mosaic of regional and global emission grid maps for 2008 and 2010 to study hemispheric transport of air pollution, Atmos. Chem. Phys., 15, 11411–11432, https://doi.org/10.5194/acp-15-11411-2015, 2015.

Jen, C. N., Hatch, L. E., Selimovic, V., Yokelson, R. J., Weber, R., Fernandez, A. E., Kreisberg, N. M., Barsanti, K. C., and
10 Goldstein, A. H.: Speciated and total emission factors of particulate organics from burning western US wildland fuels and their dependence on combustion efficiency, Atmos. Chem. Phys., 19, 1013–1026, https://doi.org/10.5194/acp-19-1013-2019, 2019.

Jethva, H. and Torres, O.: Satellite-based evidence of wavelength-dependent aerosol absorption in biomass burning smoke inferred from Ozone Monitoring Instrument, Atmos. Chem. Phys., 11, 10541–10551, https://doi.org/10.5194/acp-11-10541-
15 2011, 2011.

Jethva, H., Torres, O., and Ahn, C.: Global assessment of OMI aerosol single-scattering albedo using ground-based AERONET inversion, J. Geophys. Res.-Atmos., 119, 9020– 9040, https://doi.org/10.1002/2014JD021672, 2014.

Jiang, Y. Q., Lu, Z., Liu, X. H., Qian, Y., Zhang, K., Wang, Y. H., and Yang, X. Q., Impacts of global open-fire aerosols on direct radiative, cloud and surface-albedo effects simulated with CAM5: Atmos. Chem. Phys., 16, 14,805-14,824,
20 doi:10.5194/acp-16-14805-2016, 2016.

Jo, D. S., Park, R. J., Lee, S., Kim, S.-W., and Zhang, X.: A global simulation of brown carbon: implications for photochemistry and direct radiative effect, Atmos. Chem. Phys., 16, 3413–3432, https://doi.org/10.5194/acp-16-3413-2016, 2016.

Jolleys, M. D., Coe, H., McFiggans, G., Taylor, J. W., O'Shea, S. J., Le Breton, M., Bauguitte, S. J.-B., Moller, S., Di Carlo, P., Aruffo, E., Palmer, P. I., Lee, J. D., Percival, C. J., and Gallagher, M. W.: Properties and evolution of biomass
25 burning organic aerosol from Canadian boreal forest fires, Atmos. Chem. Phys., 15, 3077-3095, https://doi.org/10.5194/acp-15-3077-2015, 2015.

Junghenn Noyes, K.; Kahn, R., Sedlacek, A., Kleinman, L., Limbacher, J., and Li, Z.: Wildfire Smoke Particle Properties and Evolution, from Space-Based Multi-Angle Imaging, Remote Sens., 12, 769, https://doi.org/10.3390/rs12050769, 2020.

Keywood, M., Kanakidou, M., Stohl, A., Dentener, F., Grassi, G., Meyer, C. P., Torseth, K., Edwards, D., Thompson, A. M.,
30 Lohmann, U., and Burrows, J.: Fire in the air: biomass burning impacts in a changing climate, Crit. Rev. Env. Contr., 43, 40–83, https://doi.org/10.1080/10643389.2011.604248, 2013.

Kim, Y., Sartelet, K., and Couvidat, F.: Modeling the effect of non-ideality, dynamic mass transfer and viscosity on SOA formation in a 3-D air quality model, Atmos. Chem. Phys., 19, 1241–1261, https://doi.org/10.5194/acp-19-1241-2019, 2019.

Kleinman, L. I., Sedlacek Iii, A. J., Adachi, K., Buseck, P. R., Collier, S., Dubey, M. K., Hodshire, A. L., Lewis, E., Onasch, T. B., Pierce, J. R., Shilling, J., Springston, S. R., Wang, J., Zhang, Q., Zhou, S., and Yokelson, R. J., Rapid evolution of

5 aerosol particles and their optical properties downwind of wildfires in the western US: Atmos. Chem. Phys., 20, 13319-13341, doi:10.5194/acp-20-13319-2020, 2020.

Kleinman, L. I., Sedlacek Iii, A. J., Adachi, K., Buseck, P. R., Collier, S., Dubey, M. K., Hodshire, A. L., Lewis, E., Onasch, T. B., Pierce, J. R., Shilling, J., Springston, S. R., Wang, J., Zhang, Q., Zhou, S., and Yokelson, R. J., Rapid Evolution of Aerosol Particles and their Optical Properties Downwind of Wildfires in the Western U.S: Atmos. Chem. Phys. Discuss.,

10 2020, 1-52, doi:10.5194/acp-2020-239, 2020.

Konovalov, I. B., Beekmann, M., Richter, A., Burrows, J. P., and Hilboll, A.: Multi-annual changes of NO_x emissions in megacity regions: nonlinear trend analysis of satellite measurement based estimates, Atmos. Chem. Phys., 10, 8481–8498, https://doi.org/10.5194/acp-10-8481-2010, 2010.

Konovalov, I. B., Beekmann, M., Kuznetsova, I. N., Yurova, A., and Zvyagintsev, A. M.: Atmospheric impacts of the 2010

15 Russian wildfires: integrating modelling and measurements of an extreme air pollution episode in the Moscow region, Atmos. Chem. Phys., 11, 10031–10056, https://doi.org/10.5194/acp-11-10031-2011, 2011.

Konovalov, I. B., Beekmann, M., D'Anna, B., and George, C.: Significant light induced ozone loss on biomass burning aerosol: Evidence from chemistry-transport modeling based on new laboratory studies, Geophys. Res. Lett., 39, L17807, doi:10.1029/2012GL052432, 2012.

20 Konovalov, I. B., Berezin, E. V., Ciais, P., Broquet, G., Beekmann, M., Hadji-Lazaro, J., Clerbaux, C., Andreae, M. O., Kaiser, J. W., and Schulze, E.-D.: Constraining CO_2 emissions from open biomass burning by satellite observations of co-emitted species: a method and its application to wildfires in Siberia, Atmos. Chem. Phys., 14, 10383–10410, https://doi.org/10.5194/acp-14-10383-2014, 2014.

Konovalov, I. B., Beekmann, M., Berezin, E. V., Petetin, H., Mielonen, T., Kuznetsova, I. N., and Andreae, M. O.: The role

25 of semi-volatile organic compounds in the mesoscale evolution of biomass burning aerosol: a modeling case study of the 2010 mega-fire event in Russia, Atmos. Chem. Phys., 15, 13269-13297, https://doi.org/ 10.5194/acp-15-13269-2015, 2015.

Konovalov, I. B., Berezin, E. V., Ciais, P., Broquet, G., Zhuravlev, R. V., and Janssens-Maenhout, G.: Estimation of fossil-fuel CO_2 emissions using satellite measurements of "proxy" species, Atmos. Chem. Phys., 16, 13509–13540, https://doi.org/10.5194/acp-16-13509-2016, 2016.

30 Konovalov, I. B., Beekmann, M., Berezin, E. V., Formenti, P., and Andreae, M. O.: Probing into the aging dynamics of biomass burning aerosol by using satellite measurements of aerosol optical depth and carbon monoxide, Atmos. Chem. Phys., 17, 4513-4537, https://doi.org/10.5194/acp-17-4513-2017, 2017a.

Konovalov, I. B., Lvova, D. A., and Beekmann, M.: Estimation of the elemental to organic carbon ratio in biomass burning aerosol using AERONET retrievals, Atmosphere, 8, 122, https://doi.org/10.3390/atmos8070122, 2017b.

Konovalov, I. B., Lvova, D. A., Beekmann, M., Jethva, H., Mikhailov, E. F., Paris, J.-D., Belan, B. D., Kozlov, V. S., Ciais, P., and Andreae, M. O.: Estimation of black carbon emissions from Siberian fires using satellite observations of absorption and extinction optical depths, Atmos. Chem. Phys., 18, 14889-14924, https://doi.org/10.5194/acp-18-14889-2018, 2018.

Konovalov, I. B., Beekmann, M., Golovushkin, N. A., and Andreae, M. O.: Nonlinear behavior of organic aerosol in biomass burning plumes: a microphysical model analysis, Atmos. Chem. Phys., 19, 12091–12119, https://doi.org/10.5194/acp-19-12091-2019, 2019.

Kroll, J. H., Ng, N. L., Murphy, S. M., Flagan, R. C., and Seinfeld, J. H.: Secondary organic aerosol formation from isoprene photooxidation, Environ. Sci. Technol., 40, 1869–1877, https://doi.org/10.1021/es0524301, 2006.

Kumar, N. K., Corbin, J. C., Bruns, E. A., Massabó, D., Slowik, J. G., Drinovec, L., Močnik, G., Prati, P., Vlachou, A., Baltensperger, U., Gysel, M., El-Haddad, I., and Prévôt, A. S. H., Production of particulate brown carbon during atmospheric aging of residential wood-burning emissions: Atmos. Chem. Phys., 18, 17843-17861, doi:10.5194/acp-18-17843-2018, 2018.

Lack, D. A., and Cappa, C. D.: Impact of brown and clear carbon on light absorption enhancement, single scatter albedo and absorption wavelength dependence of black carbon, Atmos. Chem. Phys., 10, 4207–4220, https://doi.org/10.5194/acp-10-4207-2010, 2010.

Laing, J. R., Jaffe, D. A., and Hee, J. R.: Physical and optical properties of aged biomass burning aerosol from wildfires in Siberia and the Western USA at the Mt. Bachelor Observatory, Atmos. Chem. Phys., 16, 15185–15197, https://doi.org/10.5194/acp-16-15185-2016, 2016.

Lambe, A. T., Onasch, T. B., Massoli, P., Croasdale, D. R., Wright, J. P., Ahern, A. T., Williams, L. R., Worsnop, D. R., Brune, W. H., and Davidovits, P.: Laboratory studies of the chemical composition and cloud condensation nuclei (CCN) activity of secondary organic aerosol (SOA) and oxidized primary organic aerosol (OPOA), Atmos. Chem. Phys., 11, 8913–8928, https://doi.org/10.5194/acp-11-8913-2011, 2011.

Laskin, A., Laskin, J., and Nizkorodov, S. A., Chemistry of atmospheric brown carbon: Chem. Rev., 115, 4335-4382, doi:10.1021/cr5006167, 2015.

Lelieveld, J., Pozzer, A., Pöschl, U., Fnais, M., Haines, A., and Münzel, T., Loss of life expectancy from air pollution compared to other risk factors: a worldwide perspective: Cardiovascular Research, doi:10.1093/cvr/cvaa025, 2020.

Levelt, P. F., Hilsenrath, E., Leppelmeier, G. W., van den Oord, G. H. J., Bhartia, P. K., Tamminen, J., de Haan, J. F., and Veefkind, J. P.: Science objectives of the ozone monitoring instrument, IEEE T. Geosci. Remote, 44, 1199–1208, https://doi.org/10.1109/TGRS.2006.872336, 2006.

Levin, E. J. T., McMeeking, G. R., Carrico, C. M., Mack, L. E., Kreidenweis, S. M., Wold, C. E., Moosmuller, H., Arnott, W. P., Hao, W. M., Collett, J. L., and Malm, W. C., Biomass burning smoke aerosol properties measured during Fire Laboratory at Missoula Experiments (FLAME): J. Geophys. Res., 115, D18210, doi:10.1029/2009jd013601, 2010.

Levy, R. C., Remer, L. A., Kleidman, R. G., Mattoo, S., Ichoku, C., Kahn, R., and Eck, T. F.: Global evaluation of the Collection 5 MODIS dark-target aerosol products over land, Atmos. Chem. Phys., 10, 10399–10420, https://doi.org/10.5194/acp-10-10399-2010, 2010.

Levy, R. C., Mattoo, S., Munchak, L. A., Remer, L. A., Sayer, A. M., Patadia, F., and Hsu, N. C.: The Collection 6 MODIS aerosol products over land and ocean, Atmos. Meas. Tech., 6, 2989–3034, https://doi.org/10.5194/amt-6-2989-2013, 2013.

Levy, R. and Hsu, C.: MODIS Atmosphere L2 Aerosol Product. NASA MODIS Adaptive Processing System, Goddard Space Flight Center, USA, https://doi.org/10.5067/MODIS/MYD04_L2.006, 2015.

Li, C., He, Q., Schade, J., Passig, J., Zimmermann, R., Meidan, D., Laskin, A., and Rudich, Y., Dynamic changes in optical and chemical properties of tar ball aerosols by atmospheric photochemical aging: Atmos. Chem. Phys., 19, 139-163, doi:10.5194/acp-19-139-2019, 2019.

Lim, C. Y., Hagan, D. H., Coggon, M. M., Koss, A. R., Sekimoto, K., de Gouw, J., Warneke, C., Cappa, C. D., and Kroll, J. H.: Secondary organic aerosol formation from the laboratory oxidation of biomass burning emissions, Atmos. Chem. Phys., 19, 12797–12809, https://doi.org/10.5194/acp-19-12797-2019, 2019.

Liu, D., Whitehead, J., Alfarra, M. R., Reyes-Villegas, E., Spracklen, D. V., Reddington, C. L., Kong, S., Williams, P. I., Ting, Y.-C., Haslett, S., Taylor, J. W., Flynn, M. J., Morgan, W. T., McFiggans, G., Coe, H., and Allan, J. D.: Blackcarbon absorption enhancement in the atmosphere determined by particle mixing state, Nature Geoscience, 10, 184–188, https://doi.org/doi:10.1038/ngeo2901, 2017.

Liu, S., Aiken, A. C., Arata, C., Dubey, M. K., Stockwell, C. E., Yokelson, R. J., Stone, E. A., Jayarathne, T., Robinson, A. L., DeMott, P. J., and Kreidenweis, S. M., Aerosol single scattering albedo dependence on biomass combustion efficiency: Laboratory and field studies: Geophys. Res. Lett., 41, 742-748, doi:10.1002/2013GL058392, 2014.

Lu, Zi., Streets, D. G., Winijkul, E., Yan, F., Chen, Y., Bond, T. C., Feng, Y., Dubey, M. K., Liu, S., Pinto, J. P., and Carmichael, G. R.: Light absorption properties and radiative effects of primary organic aerosol emissions, Environ. Sci. Technol., 49, 4868–4877, https://doi.org/10.1021/acs.est.5b00211, 2015.

Lu, Zh., Liu, X., Zhang, Z., Zhao, C., Meyer, K., Rajapakshe, C., Wu, C., Yang, Z., and Penner, J. E.: Biomass smoke from southern Africa can significantly enhance the brightness of stratocumulus over the southeastern Atlantic Ocean, P. Natl. Acad. Sci. USA, 115, 2924–2929, https://doi.org/10.1073/pnas.1713703115, 2018.

Mailler, S., Menut, L., Khvorostyanov, D., Valari, M., Couvidat, F., Siour, G., Turquety, S., Briant, R., Tuccella, P., Bessagnet, B., Colette, A., Létinois, L., Markakis, K., and Meleux, F.: CHIMERE-2017: from urban to hemispheric chemistry-transport modeling, Geosci. Model Dev., 10, 2397-2423, https://doi.org/10.5194/gmd-10-2397-2017, 2017.

Majdi, M., Turquety, S., Sartelet, K., Legorgeu, C., Menut, L., and Kim, Y.: Impact of wildfires on particulate matter in the Euro-Mediterranean in 2007: sensitivity to some parameterizations of emissions in air quality models, Atmos. Chem. Phys., 19, 785–812, https://doi.org/10.5194/acp-19-785-2019, 2019.

Marelle, L., Raut, J.-C., Thomas, J. L., Law, K. S., Quennehen, B., Ancellet, G., Pelon, J., Schwarzenboeck, A., and Fast, J. D.: Transport of anthropogenic and biomass burning aerosols from Europe to the Arctic during spring 2008, Atmos. Chem. Phys., 15, 3831–3850, https://doi.org/10.5194/acp-15-3831-2015, 2015.

Matsui, H., Koike, M., Kondo, Y., Oshima, N., Moteki, N., Kanaya, Y., Takami, A., and Irwin, M.: Seasonal variations of Asian black carbon outflow to the Pacific: contribution from anthropogenic sources in China and biomass burning sources in Siberia and Southeast Asia, J. 20 Geophys. Res. Atmos., 118, 9948–9967, https://doi.org/10.1002/jgrd.50702, 2013.

May, A. A., Levin, E. J. T., Hennigan, C. J., Riipinen, I., Lee, T., Collett Jr., J. L., Jimenez, J. L., Kreidenweis, S. M., and Robinson, A. L.: Gas-particle partitioning of primary organic aerosol emissions: 3. Biomass burning, J. Geophys. Res. Atmos., 118, 11327–11338, https://doi.org/10.1002/jgrd.50828, 2013.

May, A. A., McMeeking, G. R., Lee, T., Taylor, J. W., Craven, J. S., Burling, I., Sullivan, A. P., Akagi, S., Collett, J. L., Flynn, M., Coe, H., Urbanski, S. P., Seinfeld, J. H., Yokelson, R. J., and Kreidenweis, S. M.: Aerosol emissions from prescribed fires in the United States: A synthesis of laboratory and aircraft measurements, J. Geophys. Res.-Atmos., 119, 11826–11849, https://doi.org/10.1002/2014JD021848, 2014.

May, A. A., Lee, T., McMeeking, G. R., Akagi, S., Sullivan, A. P., Urbanski, S., Yokelson, R. J., and Kreidenweis, S. M.: Observations and analysis of organic aerosol evolution in some prescribed fire smoke plumes, Atmos. Chem. Phys., 15, 6323-6335, https://doi.org/10.5194/acp-15-6323-2015, 2015.

Mazzoni, D., Logan, J. A., Diner, D., Kahn, R. A., Tong, L., and Li, Q.: A data-mining approach to associating MISR smoke plume heights with MODIS fire measurements, Remote Sens. Environ., 107, 138–148, https://doi.org/10.1016/j.rse.2006.08.014, 2007.

McClure, C. D., Lim, C. Y., Hagan, D. H., Kroll, J. H., and Cappa, C. D., Biomass-burning-derived particles from a wide variety of fuels – Part 1: Properties of primary particles: Atmos. Chem. Phys., 20, 1531-1547, doi:10.5194/acp-20-1531-2020, 2020.

McMeeking, G. R., Kreidenweis, S. M., Baker, S., Carrico, C. M., Chow, J. C., Collett, J. L., Hao, W. M., Holden, A. S., Kirchstetter, T. W., Malm, W. C., Moosmuller, H., Sullivan, A. P., and Wold, C. E., Emissions of trace gases and aerosols during the open combustion of biomass in the laboratory: J. Geophys. Res., 114, D19210, doi:10.1029/2009jd011836, 2009.

Menut, L., Bessagnet, B., Khvorostyanov, D., Beekmann, M., Blond, N., Colette, A., Coll, I., Curci, G., Foret, G., Hodzic, A., Mailler, S., Meleux, F., Monge, J.-L., Pison, I., Siour, G., Turquety, S., Valari, M., Vautard, R., and Vivanco, M. G.: CHIMERE 2013: a model for regional atmospheric composition modelling, Geosci. Model Dev., 6, 981–1028, https://doi.org/10.5194/gmd-6-981-2013, 2013.

Mikhailov, E. F., Mironova, S., Mironov, G., Vlasenko, S., Panov, A., Chi, X., Walter, D., Carbone, S., Artaxo, P., Heimann, M., Lavric, J., Pöschl, U., and Andreae, M. O.: Long-term measurements (2010–2014) of carbonaceous aerosol and carbon monoxide at the Zotino Tall Tower Observatory (ZOTTO) in central Siberia, Atmos. Chem. Phys., 17, 14365-14392, https://doi: 10.5194/acp-17-14365-2017, 2017.

5 Mok, J., Krotkov, N. A., Arola, A., Torres, O., Jethva, H., Andrade, M., Labow, G., Eck, T. F., Li, Z., Dickerson, R. R., Stenchikov, G. L., Osipov, S., and Ren, X.: Impacts of brown carbon from biomass burning on surface UV and ozone photochemistry in the Amazon Basin, Sci. Rep.-UK, 6, 36940, https://doi.org/10.1038/srep36940, 2016.

Morgan, W. T., Allan, J. D., Bauguitte, S., Darbyshire, E., Flynn, M. J., Lee, J., Liu, D., Johnson, B., Haywood, J., Longo, K. M., Artaxo, P. E., and Coe, H.: Transformation and ageing of biomass burning carbonaceous aerosol over tropical South 10 America from aircraft in situ measurements during SAMBBA, Atmos. Chem. Phys., 20, 5309–5326, https://doi.org/10.5194/acp-20-5309-2020, 2020.

NCEP: NCEP FNL Operational Model Global Tropospheric Analyses, continuing from July 1999, available at: https://rda.ucar.edu/datasets/ds083.2/ (last access: 1 April 2020), https://doi.org/10.5065/D6M043C6, 2017.

Omar, A. H., Winker, D. M., Vaughan, M. A., Hu, Y., Trepte, C. R., Ferrare, R. A., Lee, K. P., Hostetler, C. A., Kittaka, C., 15 Rogers, R. R., and Kuehn, R. E.: The CALIPSO Automated Aerosol Classification and Lidar Ratio Selection Algorithm, J. Atmos. Ocean. Tech., 26, 1994–2014, https://doi.org/10.1175/2009JTECHA1231.1, 2009.

Oris, F., Asselin, H., Ali, A., Finsinger, W., and Bergeron, Y.: Effect of increased fire activity on global warming in the boreal forest, Environ. Rev., 22, 206-219, https://doi.org/10.1139/er-2013-0062, 2014.

Park, R. J., Kim, M. J., Jeong, J. I., Youn, D., and Kim, S.: A contribution of brown carbon aerosol to the aerosol light ab-20 sorption and its radiative forcing in East Asia, Atmos. Environ., 44, 1414-1421, 2010.

Péré, J. C., Bessagnet, B., Mallet, M., Waquet, F., Chiapello, I., Minvielle, F., Pont, V., and Menut, L.: Direct radiative effect of the Russian wildfires and its impact on air temperature and atmospheric dynamics during August 2010, Atmos. Chem. Phys., 14, 1999–2013, https://doi.org/10.5194/acp-14-1999-2014, 2014.

Petrenko, M., Kahn, R., Chin, M., Soja, A., Kucsera, T., and Harshvardhan: The use of satellite-measured aerosol optical 25 depth to constrain biomass burning emissions source strength in the global model GOCART, J. Geophys. Res., 117, D18212, doi:10.1029/2012JD017870, 2012.

Petters, M. D., and Kreidenweis, S. M.: A single parameter representation of hygroscopic growth and cloud condensation nucleus activity, Atmos. Chem. Phys., 7, 1961–1971, https://doi.org/10.5194/acp-7-1961-2007, 2007.

Petters, M. D., Carrico, C. M., Kreidenweis, S. M., Prenni, A. J., DeMott, P. J., Collett, J. L., and Moosmuller, H.: Cloud 30 condensation nucleation activity of biomass burning aerosol, J. Geophys. Res., 114, D22205, https://doi.org/10.1029/2009JD012353, 2009.

Pokhrel, R. P., Beamesderfer, E. R., Wagner, N. L., Langridge, J. M., Lack, D. A., Jayarathne, T., Stone, E. A., Stockwell, C. E., Yokelson, R. J., and Murphy, S. M.: Relative importance of black carbon, brown carbon, and absorption enhancement from clear coatings in biomass burning emissions, Atmos. Chem. Phys., 17, 5063–5078, https://doi.org/10.5194/acp-17-5063-2017, 2017.

5 Press, W. H., Teukolsky, S. A., Vetterling, W. T., and Flannery, B. P.: Numerical Recipes, 2nd edition, Cambridge University Press, 1992.

Reddington, C. L., Spracklen, D. V., Artaxo, P., Ridley, D. A., Rizzo, L. V., and Arana, A.: Analysis of particulate emissions from tropical biomass burning using a global aerosol model and long-term surface observations, Atmos. Chem. Phys., 16, 11083–11106, https://doi.org/10.5194/acp-16-11083-2016, 2016.

10 Reid, J. S., Koppmann, R., Eck, T. F., and Eleuterio, D. P.: A review of biomass burning emissions part II: intensive physical properties of biomass burning particles, Atmos. Chem. Phys., 5, 799–825, https://doi.org/10.5194/acp-5-799-2005, 2005a.

Reid, J. S., Eck, T. F., Christopher, S. A., Koppmann, R., Dubovik, O., Eleuterio, D. P., Holben, B. N., Reid, E. A., and Zhang, J.: A review of biomass burning emissions part III: intensive optical properties of biomass burning particles, Atmos. Chem. Phys., 5, 827–849, https://doi.org/10.5194/acp-5-827-2005, 2005b.

15 Robinson, A. L., Donahue, N. M., Shrivastava, M. K., Weitkamp, E. A., Sage, A. M., Grieshop, A. P., Lane, T. E., Pierce, J. R., and Pandis, S. N.: Rethinking organic aerosols: Semivolatile emissions and photochemical aging, Science, 315, 1259–1262, https://doi.org/10.1126/science.1133061, 2007.

Sakamoto, K. M., Allan, J. D. Coe, H., Taylor, J. W., Duck, T. J., and Pierce, J. R.: Aged boreal biomass-burning aerosol size distributions from BORTAS 2011, Atmos. Chem. Phys., 15, 1633-1646, https://doi.org/10.5194/acp-15-1633-2015, 20 2015.

Saleh, R., Hennigan, C. J., McMeeking, G. R., Chuang, W. K., Robinson, E. S., Coe, H., Donahue, N. M., and Robinson, A. L.: Absorptivity of brown carbon in fresh and photo-chemically aged biomass-burning emissions, Atmos. Chem. Phys., 13, 7683–7693, https://doi.org/10.5194/acp-13-7683-2013, 2013.

Saleh, R., Robinson, E. S., Tkacik, D. S., Ahern, A. T., Liu, S., Aiken, A. C., Sullivan, R. C., Presto, A. A., Dubey, M. K., 25 Yokelson, R. J., Donahue, N. M., and Robinson, A. L.: Brownness of organics in aerosols from biomass burning linked to their black carbon content, Nat. Geosci., 7, 647–650, https://doi.org/10.1038/ngeo2220, 2014.

Saleh, R., Marks, M., Heo, J., Adams, P. J., Donahue, N. M., and Robinson, A. L.: Contribution of brown carbon and lensing to the direct radiative effect of carbonaceous aerosols from biomass and biofuel burning emissions, J. Geophys. Res.-Atmos., 120, 10285–10296, 2015.

30 Salomonson, V. V., Barnes, W. L., Maymon, P. W., Montgomery, H. E., and Ostrow, H.: MODIS: advanced facility instrument for studies of the Earth as a system, IEEE T. Geosci. Remote, 27, 145–153, 1989.

Samset, B. H., Stjern, C. W., Andrews, E., Kahn, R. A., Myhre, G., Schulz, M., and Schuster, G. L.: Aerosol absorption: progress towards global and regional constraints, Curr. Clim. Change Rep., 4 (2), 65–83, https://doi.org/10.1007/s40641-018-0091-42018, 2018.

Sand, M., Berntsen, T., von Salzen, K., Flanner, M., Langner, J., and Victor, D.: Response of Arctic temperature to changes in emissions of short-lived climate forcers, Nat. Clim. Change, 6, 286–289, https://doi.org/10.1038/nclimate2880, 2015.

Schepaschenko, D., McCallum, I., Shvidenko, A., Steffen, F., Kraxner, F., and Obersteiner, M.: A new hybrid land cover dataset for Russia: a methodology for integrating statistics, remote sensing and in-situ information, J. Land Use Sci., 6, 245–259, 2011.

Schmidt, H.C., Derognat, C., Vautard, R., and Beekmann, M.: A comparison of simulated and observed ozone mixing ratios for the summer of 1998 in western Europe, Atmos. Environ., 35, 6277-6297, https://doi.org/10.1016/S1352-2310(01)00451-4, 2001.

Schulze, E.-D., Wirth, C., Mollicone, D., von Lüpke, N., Ziegler, W., Achard, F., Mund, M., Prokushkin, A., and Scherbina, S.: Factors promoting larch dominance in central Siberia: fire versus growth performance and implications for carbon dynamics at the boundary of evergreen and deciduous conifers, Biogeosciences, 9, 1405–1421, https://doi.org/10.5194/bg-9-1405-2012, 2012.

Selimovic, V., Yokelson, R. J., McMeeking, G. R., and Coefield, S.: In situ measurements of trace gases, PM, and aerosol optical properties during the 2017 NW US wildfire smoke event, Atmos. Chem. Phys., 19, 3905–3926, https://doi.org/10.5194/acp-19-3905-2019, 2019.

Shi, S., Cheng, T., Gu X., Guo, H., Wu, Y., and Wang, Y.: Biomass burning aerosol characteristics for different vegetation types in different aging periods, Environ. Int., 126, 504-511, https://doi.org/10.1016/j.envint.2019.02.073, 2019.

Shiraiwa, M., Li, Y., Tsimpidi, A. P., Karydis, V. A., Berkemeier, T., Pandis, S. N., Lelieveld, J., Koop, T., and Pöschl, U.: Global distribution of particle phase state in atmospheric secondary organic aerosols, Nat. Commun., 8, 15002, https://doi.org/10.1038/ncomms15002, 2017.

Shrivastava, M., Easter, R., Liu, X., Zelenyuk, A., Singh, B., Zhang, K., Ma, P-L, Chand, D., Ghan, S., Jimenez, J. L., Zhang, Q., Fast, J., Rasch, P., and Tiitta, P.: Global transformation and fate of SOA: Implications of low volatility SOA and gas phase fragmentation reactions, J. Geophys. Res.-Atmos., 120, 4169–4195, https://doi.org/10.1002/2014JD022563, 2015.

Shrivastava, M., Cappa, C., Fan, J., Goldstein, A., Guenther, A., Jimenez, J., Kuang, C., Laskin, A., Martin, S., Ng, N., Petaja, T., Pierce, J., Rasch, P., Roldin, P., Seinfeld, J., Shilling, J., Smith, J., Thornton, J., Volkamer, R., Wang, J., Worsnop, D., Zaveri, R., Zelenyuk, A., and Zhang, Q.: Recent advances in understanding secondary organic aerosol: Implications for global climate forcing, Rev. Geophys., 55, 509–559, https://doi.org/10.1002/2016RG000540, 2017.

Sitnov, S.A., Mokhov, I.I., Gorchakov, G.I., Dzhola, A. V.: Smoke haze over the European part of Russia in the summer of 2016: A link to wildfires in Siberia and atmospheric circulation anomalies, Russ. Meteorol. Hydrol., 42, 518, https://doi.org/10.3103/S1068373917080052, 2017.

Sitnov, S.A., Mokhov, I.I., and Likhosherstova, A.A.: Exploring large-scale black-carbon air pollution over Northern Eurasia in summer 2016 using MERRA-2 reanalysis data, Atmos. Res., 235, 104763, DOI: 10.1016/j.atmosres.2019.104763, 2020.

Skamarock, W. C., Klemp, J. B., Dudhia, J., Gill, D. O., Barker, D. M., Duda, M. G., Huang, X.-Y., Wang, W., and Powers, J. G.: A Description of the advanced research WRF version 3, NCAR Tech. Notes–475CSTR, Boulder, Colorado, USA, 113 pp., 2008.

Sofiev, M., Ermakova, T., and Vankevich, R.: Evaluation of the smoke-injection height from wild-land fires using remote-sensing data, Atmos. Chem. Phys., 12, 1995–2006, https://doi.org/10.5194/acp-12-1995-2012, 2012.

Sofiev, M., Vankevich, R., Ermakova, T., and Hakkarainen, J.: Global mapping of maximum emission heights and resulting vertical profiles of wildfire emissions, Atmos. Chem. Phys., 13, 7039–7052, https://doi:10.5194/acp-13-7039-2013, 2013.

Song, C., Zaveri, R. A., Alexander, M. L., Thornton, J. A., Madronich, S., Ortega, J. V., Zelenyuk, A., Yu, X. -Y., Laskin, A., and Maughan, D. A.: Effect of hydrophobic primary organic aerosols on secondary organic aerosol formation from ozonolysis of α-pinene , Geophys. Res. Lett., 34, L20803, https://doi.org/10.1029/2007GL030720, 2007.

Stromatas, S., Turquety, S., Menut, L., Chepfer, H., Péré, J. C., Cesana, G., and Bessagnet, B.: Lidar signal simulation for the evaluation of aerosols in chemistry transport models, Geosci. Model Dev., 5, 1543–1564, https://doi.org/10.5194/gmd-5-1543-2012, 2012.

Sumlin, B. J., Pandey, A., Walker, M. J., Pattison, R. S., Williams, B. J., and Chakrabarty, R. K., Atmospheric photooxidation diminishes light absorption by primary brown carbon aerosol from biomass burning: Environmental Science & Technology Letters, 4, 540-545, doi:10.1021/acs.estlett.7b00393, 2017.

Taylor, J. W., Wu, H., Szpek, K., Bower, K., Crawford, I., Flynn, M. J., Williams, P. I., Dorsey, J., Langridge, J. M., Cotterell, M. I., Fox, C., Davies, N. W., Haywood, J. M., and Coe, H.: Absorption closure in highly aged biomass burning smoke, Atmos. Chem. Phys. Discuss., https://doi.org/10.5194/acp-2020-333, in review, 2020.

Thornberry, T., Froyd, K. D., Murphy, D. M., Thomson, D. S., Anderson, B. E., Thornhill, K. L., and Winstead, E. L.: Persistence of organic carbon in heated aerosol residuals measured during Tropical Composition Cloud and Climate Coupling (TC4), J. Geophys. Res., 115, D00J02, https://doi.org/10.1029/2009jd012721, 2010.

Tiitta, P., Leskinen, A., Hao, L., Yli-Pirilä, P., Kortelainen, M., Grigonyte, J., Tissari, J., Lamberg, H., Hartikainen, A., Kuuspalo, K., Kortelainen, A.-M., Virtanen, A., Lehtinen, K. E. J., Komppula, M., Pieber, S., Prévôt, A. S. H., Onasch, T. B., Worsnop, D. R., Czech, H., Zimmermann, R., Jokiniemi, J., and Sippula, O.: Transformation of logwood combustion emissions in a smog chamber: formation of secondary organic aerosol and changes in the primary organic aerosol upon daytime and nighttime aging, Atmos. Chem. Phys., 16, 13251-13269, https://doi.org/10.5194/acp-16-13251-2016, 2016.

Tsimpidi, A. P., Karydis, V. A., Pozzer, A., Pandis, S. N., and Lelieveld, J.: ORACLE 2-D (v2.0): an efficient module to compute the volatility and oxygen content of organic aerosol with a global chemistry-climate model, Geosci. Model Dev., 11, 3369-3389, https://doi.org/10.5194/gmd-11-3369-2018, 2018.

Toon, O. and Ackerman, T.: Algorithms for the calculation of scattering by stratified spheres, Appl. Optics, 20, 3657–3660, 1981.

Torres, O. O.: OMI/Aura Near UV Aerosol Optical Depth and Single Scattering Albedo 1-orbit L2 Swath 1324 km V003, Greenbelt, MD, USA, Goddard Earth Sciences Data and Information Services Center (GES DISC), https://doi.org/10.5067/Aura/OMI/DATA2004 (last access: 19 April 2020), 2006.

Torres, O., Tanskanen, A., Veihelmann, B., Ahn, C., Braak, R., Bhartia, P. K., Veefkind, P., and Levelt, P.: Aerosols and surface UV products from Ozone Monitoring Instrument observations: An overview, J. Geophys. Res., 112, D24S47, https://doi.org/10.1029/2007JD008809, 2007.

Torres, O., Ahn, C., and Chen, Z.: Improvements to the OMI near-UV aerosol algorithm using A-train CALIOP and AIRS observations, Atmos. Meas. Tech., 6, 3257–3270, https://doi.org/10.5194/amt-6-3257-2013, 2013.

Tosca, M. G., Randerson, J. T., and Zender, C. S.: Global impact of smoke aerosols from landscape fires on climate and the Hadley circulation, Atmos. Chem. Phys., 13, 5227–5241, https://doi.org/10.5194/acp-13-5227-2013, 2013.

Tsigaridis, K., Daskalakis, N., Kanakidou, M., Adams, P. J., Artaxo, P., Bahadur, R., Balkanski, Y., Bauer, S. E., Bellouin, N., Benedetti, A., Bergman, T., Berntsen, T. K., Beukes, J. P., Bian, H., Carslaw, K. S., Chin, M., Curci, G., Diehl, T., Easter, R. C., Ghan, S. J., Gong, S. L., Hodzic, A., Hoyle, C. R., Iversen, T., Jathar, S., Jimenez, J. L., Kaiser, J. W., Kirkevag, A., Koch, D., Kokkola, H., Lee, Y. H., Lin, G., Liu, X., Luo, G., Ma, X., Mann, W., Mihalopoulos, N., Morcrette, J. J., Mueller, J. F., Myhre, G., Myriokefalitakis, S., Ng, N. L., O'Donnell, D., Penner, J. E., Pozzoli, L., Pringle, K. J., Russell, L. M., Schulz, M., Sciare, J., Seland, O., Shindell, D. T., Sillman, S., Skeie, R. B., Spracklen, D., Stavrakou, T., Steenrod, S. D., Takemura, T., Tiitta, P., Tilmes, S., Tost, H., van Noije, T., van Zyl, P. G., von Salzen, K., Yu, F., Wang, Z., Wang, Z., Zaveri, R. A., Zhang, H., Zhang, K., Zhang, Q., and Zhang, X.: The AeroCom evaluation and intercomparison of organic aerosol in global models, Atmos. Chem. Phys., 14, 10845–10895, https://doi.org/10.5194/acp-14-10845- 2014, 2014.

Tsigaridis, K. and Kanakidou, M.: The Present and Future of Secondary Organic Aerosol Direct Forcing on Climate, Current Climate Change Reports, 4, 1–15, https://doi.org/10.1007/s40641-018-0092-3, 2018.

Vaden, T. D., Imre, D., Beránek, J., Shrivastava, M., and Zelenyuk, A.: Evaporation kinetics and phase of laboratory and ambient secondary organic aerosol, Proc. Natl. Acad. Sci., 108, 2190–2195, https://doi.org/10.1073/pnas.1013391108, 2011.

Vakkari, V., Beukes, J. P., Dal Maso, M., Aurela, M., Josipovic, M., and van Zyl, P. G.: Major secondary aerosol formation in southern African open biomass burning plumes, Nature Geosci., 11, 580–583, https://doi.org/10.1038/s41561-018-0170-0, 2018.

van der Werf, G. R., Randerson, J. T., Giglio, L., van Leeuwen, T. T., Chen, Y., Rogers, B. M., Mu, M., van Marle, M. J. E., Morton, D. C., Collatz, G. J., Yokelson, R. J., and Kasibhatla, P. S.: Global fire emissions estimates during 1997–2016, Earth Syst. Sci. Data, 9, 697–720, https://doi.org/10.5194/essd-9-697-2017, 2017.

Wang, R., Balkanski, Y., Boucher, O., Ciais, P., Schuster, G. L., Chevallier, F., Samset, B. H., Liu, J., Piao, S., Valari, M., and Tao, S., Estimation of global black carbon direct radiative forcing and its uncertainty constrained by observations: J. Geophys. Res., 121, 5948-5971, doi:10.1002/2015JD024326, 2016.

Wang, X., Heald, C. L., Sedlacek, A. J., de Sá, S. S., Martin, S. T., Alexander, M. L., Watson, T. B., Aiken, A. C., Springston, S. R., and Artaxo, P.: Deriving brown carbon from multiwavelength absorption measurements: method and application to AERONET and Aethalometer observations, Atmos. Chem. Phys., 16, 12733–12752, https://doi.org/10.5194/acp-16-12733-2016, 2016.

Wang, X., Heald, C. L., Liu, J., Weber, R. J., Campuzano-Jost, P., Jimenez, J. L., Schwarz, J. P., and Perring, A. E.: Exploring the observational constraints on the simulation of brown carbon, Atmos. Chem. Phys., 18, 635–653, https://doi.org/10.5194/acp-18-635-2018, 2018.

Warneke, C., Bahreini, R., Brioude, J., Brock, C. A., de Gouw, J. A., Fahey, D. W., Froyd, K. D., Holloway, J. S., Middlebrook, A., Miller, L., Montzka, S., Murphy, D. M., Peischl, J., Ryerson, T. B., Schwarz, J. P., Spackman, J. R., and Veres, P.: Biomass burning in Siberia and Kazakhstan as an important source for haze over the Alaskan Arctic in April 2008, Geophysical Research Letters, 36, https://doi.org/10.1029/2008GL036194, 2009.

Wild, O., Zhu, X., and Prather, J.: Fast-J: accurate simulation of the in- and below-cloud photolysis in tropospheric chemical models, J. Atmos. Chem., 37, 245–282, 2000.

Wong, J. P. S., Nenes, A., and Weber, R. J.: Changes in light absorptivity of molecular weight separated brown carbon due to photolytic aging, Environ. Sci. Technol., 51, 8414–8421, https://doi.org/10.1021/acs.est.7b01739, 2017.

Wong, J. P. S., Tsagkaraki, M., Tsiodra, I., Mihalopoulos, N., Violaki, K., Kanakidou, M., Sciare, J., Nenes, A., and Weber, R. J.: Atmospheric evolution of molecular-weight-separated brown carbon from biomass burning, Atmos. Chem. Phys., 19, 7319–7334, https://doi.org/10.5194/acp-19-7319-2019, 2019.

Wu, C., Wu, D., and Yu, J. Z.: Quantifying black carbon light absorption enhancement with a novel statistical approach, Atmos. Chem. Phys., 18, 289–309, https://doi.org/10.5194/acp-18-289-2018, 2018.

Yasunari, T., Kim, K.-M., Da Silva, A., Hayasaki, M., Akiyama, M., Murao, N., Extreme air pollution events in Hokkaido, Japan, traced back to early snowmelt and large-scale wildfires over East Eurasia: Case studies, Scientific Reports, 8, 6413, https://doi.org /10.1038/s41598-018-24335-w, 2018.

Yokelson, R. J., Crounse, J. D., DeCarlo, P. F., Karl, T., Urbanski, S., Atlas, E., Campos, T., Shinozuka, Y., Kapustin, V., Clarke, A. D., Weinheimer, A., Knapp, D. J., Montzka, D. D., Holloway, J., Weibring, P., Flocke, F., Zheng, W., Toohey, D., Wennberg, P. O., Wiedinmyer, C., Mauldin, L., Fried, A., Richter, D., Walega, J., Jimenez, J. L., Adachi, K.,

Buseck, P. R., Hall, S. R., and Shetter, R.: Emissions from biomass burning in the Yucatan, Atmos. Chem. Phys., 9, 5785–5812, https://doi.org/10.5194/acp-9-5785-2009, 2009.

Zhang, A., Wang, Y., Zhang, Y., Weber, R. J., Song, Y., Ke, Z., and Zou, Y.: Modeling the global radiative effect of brown carbon: a potentially larger heating source in the tropical free troposphere than black carbon, Atmos. Chem. Phys., 20, 1901–1920, https://doi.org/10.5194/acp-20-1901-2020, 2020.

Zhang, L., Gong, S., Padro, J., and Barrie, L.: A size-segregated particle dry deposition scheme for an atmospheric aerosol module, Atmos. Environ., 35, 549–560, 2001.

Zhang, L., Henze, D. K., Grell, G. A., Carmichael, G. R., Bousserez, N., Zhang, Q., Torres, O., Ahn, C., Lu, Z., Cao, J., and Mao, Y.: Constraining black carbon aerosol over Asia using OMI aerosol absorption optical depth and the adjoint of GEOS-Chem, Atmos. Chem. Phys., 15, 10281–10308, https://doi.org/10.5194/acp-15- 10281-2015, 2015.

Zhang, Y., Huang, J.-P., Henze, D. K., and Seinfeld, J. H.: Role of isoprene in secondary organic aerosol formation on a regional scale, J. Geophys. Res. Atmos., 112, D20207, https://doi.org/10.1029/2007JD008675, 2007.

Zhong, M. and Jang, M.: Dynamic light absorption of biomass-burning organic carbon photochemically aged under natural sunlight, Atmos. Chem. Phys., 14, 1517–1525, https://doi.org/10.5194/acp-14-1517-2014, 2014.

Zhou, S., Collier, S., Jaffe, D. A., Briggs, N. L., Hee, J., Sedlacek III, A. J., Kleinman, L., Onasch, T. B., and Zhang, Q.: Regional influence of wildfires on aerosol chemistry in the western US and insights into atmospheric aging of biomass burning organic aerosol, Atmos. Chem. Phys., 17, 2477–2493, https://doi.org/10.5194/acp-17-2477-2017, 2017.

Table 1. Parameters of the species representing the evolution of BB OA in the framework of the simplified VBS scheme

Species name	Volatility, C^* $(\mu g\ m^{-3})$	Molar mass	Enthalpy of evaporation, ΔH_{vap} $(kJ\ mol^{-1})$
LV-POA	10^0	216	85
MV-POA	10^2	216	77
LV-SOA	10^0	144	85
MV-SOA	10^2	135	77
HV-SOA	10^3	131	73
NTVOCs	∞	113	-

5

Table 2. Reactions representing the evolution of BB OA in the simplified VBS scheme and their OH reaction rates (k_{OH})

	Reaction	k_{OH} $(cm^3\ molec^{-1}\ s^{-1})$
(R1)	MV-POA + OH → 1.3 LV-SOA + OH	4×10^{-11}
(R2)	LV-POA + OH → 1.3 LV-SOA + OH	4×10^{-11}
(R3)	NTVOC + OH → $\xi_1^{(a)}$ 0.33 HV-SOA + (1-ξ_1) 0.30 LV-SOA + OH	4×10^{-11}
(R4)	HV-SOA + OH → MV-SOA + OH	4×10^{-11}
(R5)	MV-SOA+ OH → $\xi_2^{(a)}$ LV-SOA + OH	1×10^{-11}
(R6)	LV-SOA+ OH → ξ_2 LV-SOA + OH	1×10^{-11}

[a] ξ_1 and ξ_2 are adjustable parameters, which have been evaluated as: ξ_1=0.85, ξ_2=0.15

10

Table 3. Key features of the configuration of the simulations with the CHIMERE model

Simulation scenario	Key features
'bb_vbs'	- POA and SOA processing is represented using a simplified 6-component VBS scheme (see Tables 1 and 2) with two adjustable parameters - Gas-particle partitioning of the POA and SOA species is calculated assuming these species to form an ideal inviscid liquid solution; - BB POA and BC emissions are derived from the FRP measurements and constrained by the AOD and AAOD satellite observations with the injection heights parameterized[a] as a function of FRP; the mass emission ratio of NTVOCs to POAs is an adjustable parameter estimated as 14.2; - Spherical core/shell structure of particles, with BC forming the core and the other (homogeneously mixed) components forming the shell, is assumed to calculate the BB aerosol optical properties using the OPTSIM module[b] - Light absorption by LV-POA, HV-SOA, and MV-SOA with k_{poa}[c] $=0.03\times\exp(-t_e/82)$ (where t_e is the BB aerosol photochemical age [hours]) and k_{soa}[c] estimated as 9×10^{-3} is taken into account, while MV-POA and LV-SOA are treated as non-absorbing species - Uptake of water by SOA is computed[d] assuming the hygroscopicity parameter κ_{org} of 0.2, whereas BC and POA are assumed to be hydrophobic - Photochemical age of BB aerosol is estimated using two model tracers, one of which is inert and another is decaying with a constant rate - Biogenic and anthropogenic emissions of aerosols and gases are turned off - Zero concentrations are taken for the boundary conditions
'bb_trc'	- SOA formation is turned off and the organic fraction of BB aerosol is treated as being chemically inert, refractory, non-absorbing, and hydrophobic - Other features and assumptions are the same as in the 'bb_vbs' scenario
'bgr'	- BB emissions are turned off but both the biogenic and anthropogenic emissions of aerosols and gases are taken into account using the HTAP[e] and MEGAN[f] emission inventories, respectively - SOA formation from both the anthropogenic and biogenic precursors is taken into account using simplified representations[g] provided in the standard version of CHIMERE - AOD is calculated with the in-built FAST-JX module[h] of CHIMERE with the standard settings[i] - Boundary conditions for aerosol and gaseous components are specified using the monthly climatology from the LMDZ-INCA global model[j]
'bb_poa' (a test scenario)	- SOA formation is turned off but POA is treated in the same way as in the 'bb_vbs' scenario except that POA is assumed to be hydrophilic (κ_{org}=0.2) - Other features and assumptions are the same as in the 'bb_vbs' scenario
All scenarios	- Simulations are performed on a $1°\times 1°$ model grid with 12 non-equidistant layers extending up to 200 hPa pressure level - Gas-phase chemical processes are simulated using the MELCHIOR2 chemical mechanism (in-build into CHIMERE) - Dry deposition of gases, wet scavenging of aerosol and gases are taken into account using parameterizations implemented in the standard version of CHIMERE[i] - Meteorological fields are computed "off-line" with the WRF (version 3.9) model[k]

[a] according to Sofiev et al. (2012); [b] Stromatas et al. (2012); [c] k_{poa} and k_{soa} are the imaginary parts of the refractive indexes (at 388 nm) for the POA and SOA species, respectively; [d] according to Petter and Kreidenweis et al. (2007); [e] Janssens-Maenhout et al. (2015); [f] Guenther et al. (2006); [g] Kroll et al. (2006), Zhang et al. (2007), Bessagnet et al. (2008); [h] Wild et al., (2000); [i] Mailler et al. (2017); [j] Folberth et al. (2006); [k] Skamarock et al., (2008)
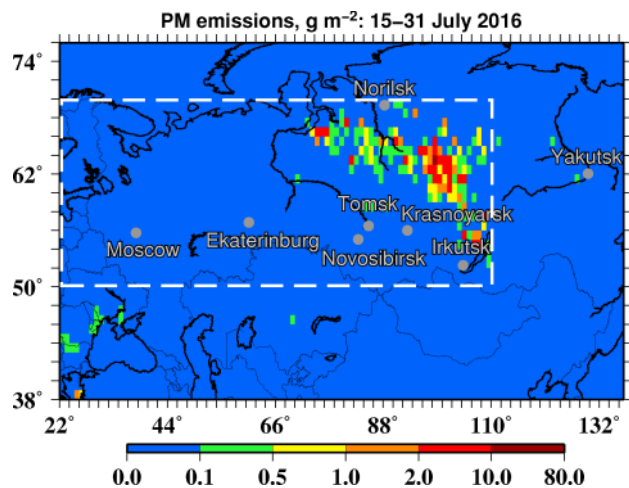
Figure 1. Spatial distribution of the total emissions (g m⁻²) of particulate matter from fires in the period from 15 to 31 July 2016. The emissions were computed using the MODIS FRP data (see Sect. 2.3) and are shown over the CHIMERE domain specified in this study. A dashed white rectangle indicates the study region.

(a)

AOD at 550 nm : MODIS : 15–31 July 2016

AOD at 550 nm : MODIS : 15–31 July 2016

(b)

AOD at 550 nm : MODIS : 15 June – 14 July 2016

AOD at 550 nm : MODIS : 15 June – 14 July 2016

(c)

AOD at 550 nm : CHIMERE : 15–31 July 2016

(d)

AOD at 550 nm : CHIMERE : 15 June – 14 July 2016
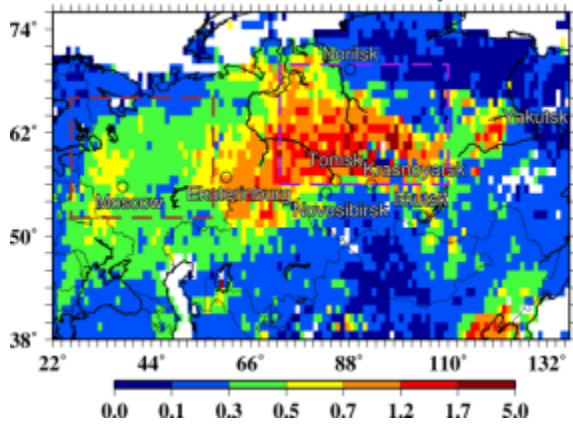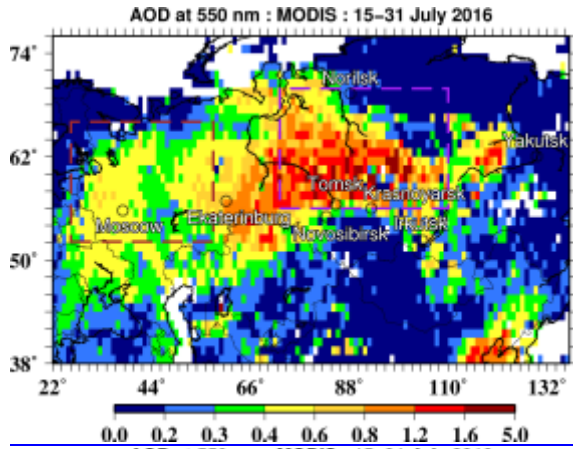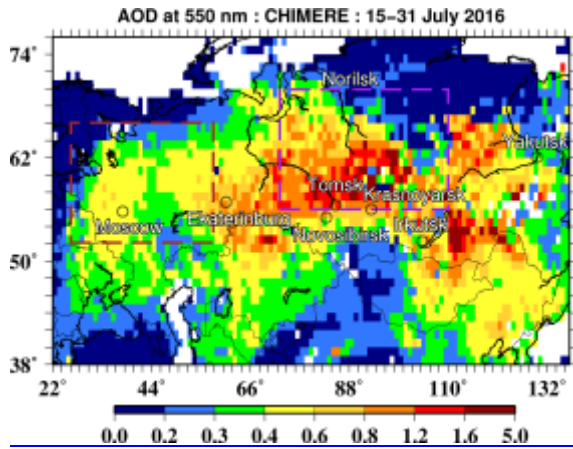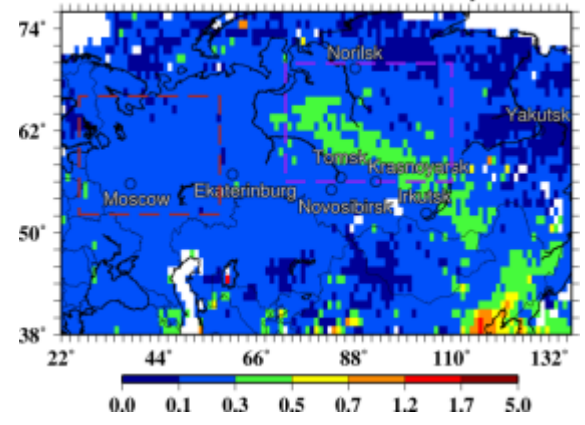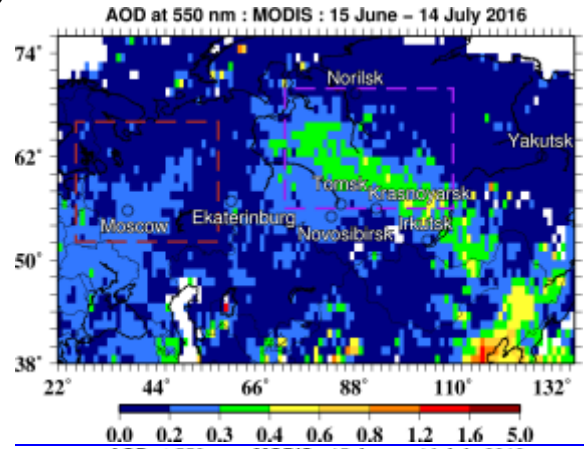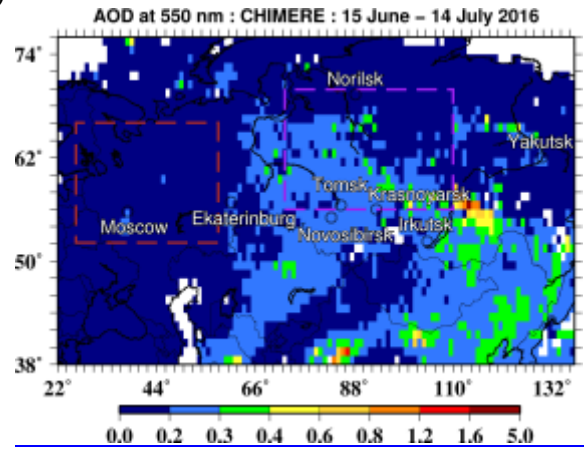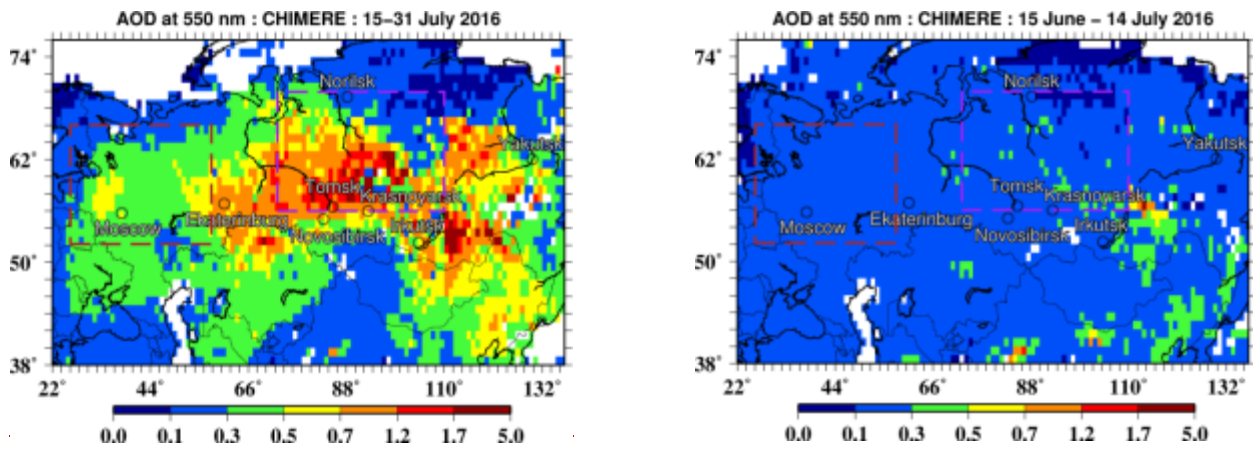
Figure 2. Spatial distributions of the temporal averages of AOD (at 550 nm) in the periods (a, c) from 15 to 31 July 2016 and (b, d) from 15 June to 14 July 2016 according to (a, b) the MODIS observations and (c, d) the combined CHIMERE simulations for the 'bb_vbs' and 'bgr' scenarios. The distributions represent the ancillary sets of AOD data that were selected irrespective of the availability of the corresponding AAOD retrievals. The rectangles depict the "source" (purple lines) and "receptor" (dark red lines) regions covering parts of Siberia and (mostly) the European territory of Russia, respectively.

(a)

(b)
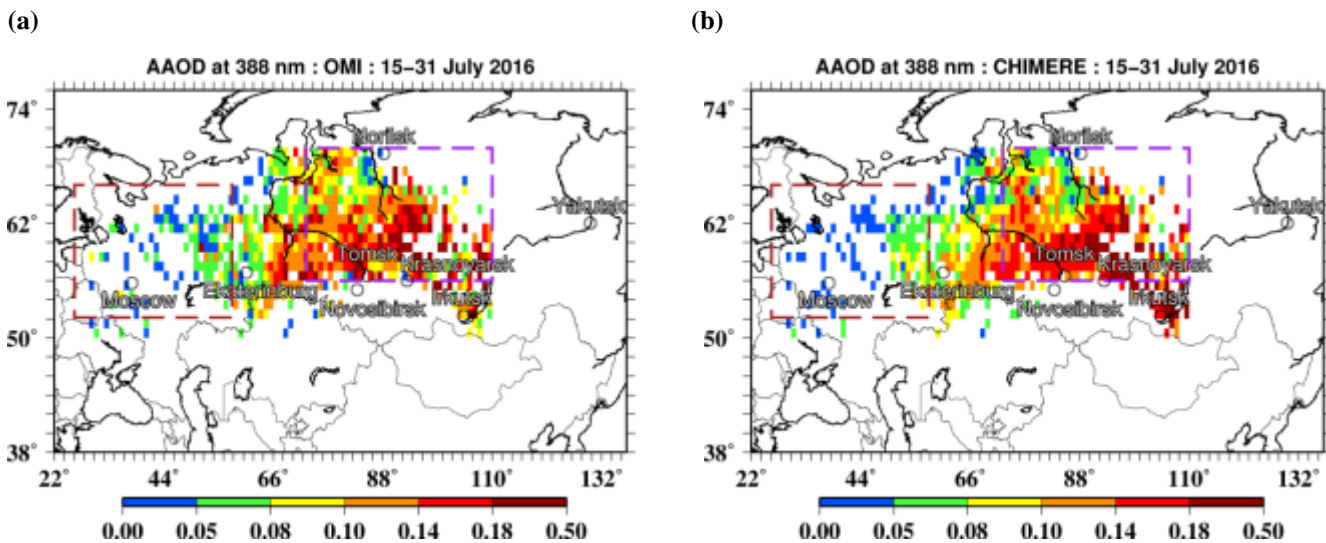
Figure 3. Spatial distributions of temporal averages of AAOD (at 388 nm) in the period from 15 to 31 July 2016 according to (a) the OMI observations and (b) CHIMERE simulations for the 'bb_vbs' scenario. The AAOD data represent only BB aerosol in the study region according to the selection criterion specified in the OMAERUV data product. The rectangles depict the source and receptor regions as in Fig. 2.

5
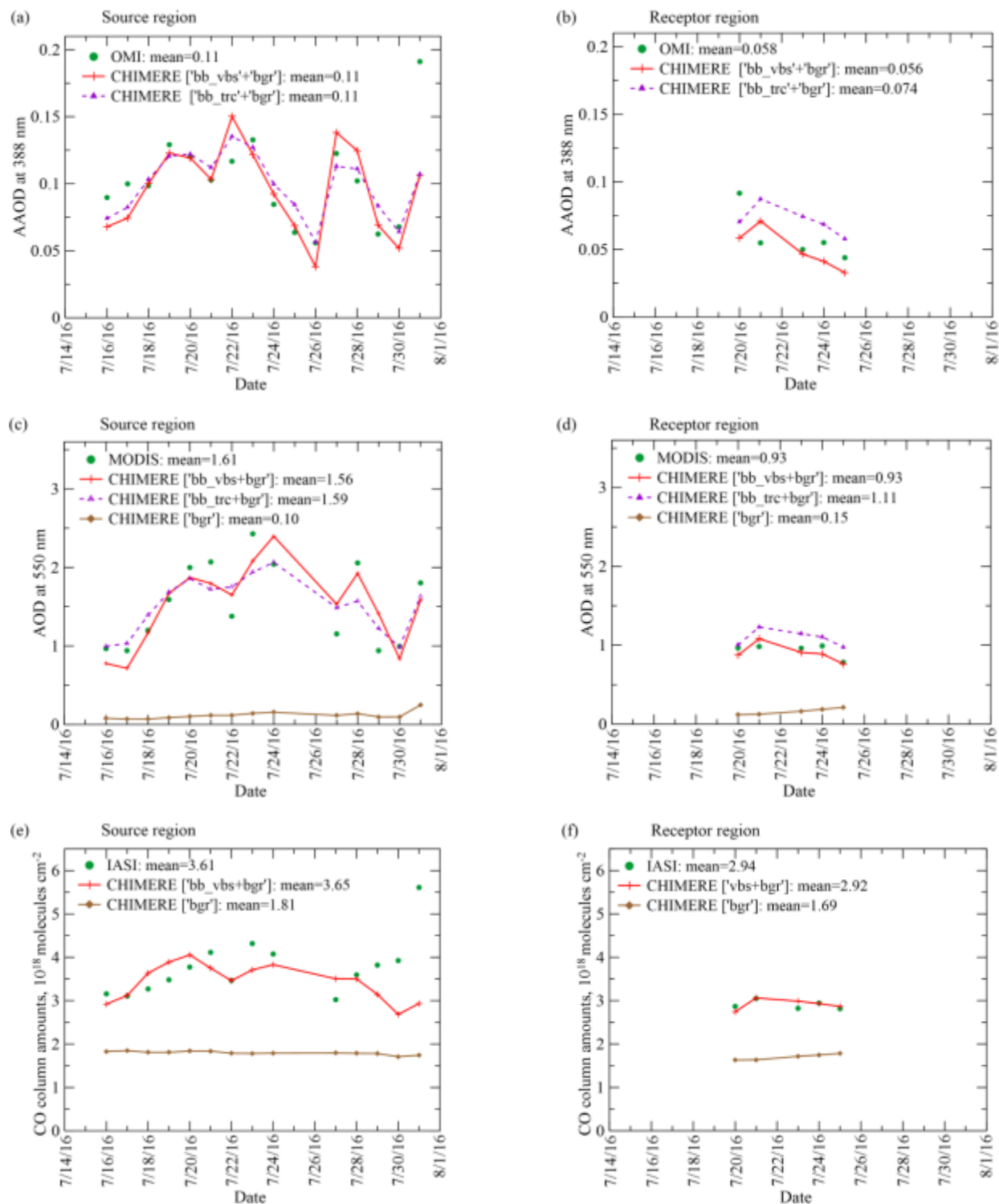
Figure 4. Time series of the daily (a, b) AAOD, (c, d) AOD, and (e, f) CO values averaged over the study region according to the satellite

observations and the CHIMERE simulations under the different model scenarios for the (a, c, e) "source" and (b, d, f) "receptor" regions indicated in Fig. 2. All the data were selected consistently. Note that the simulations for the 'bgr' (background) scenario are shown after applying the de-biasing procedure (see Sect. 2.5). The background AAOD is not evaluated in this study and therefore not shown. Taking into account that the time series are very short, the correlation coefficient has not been evaluated (as its values are not sufficiently robust).
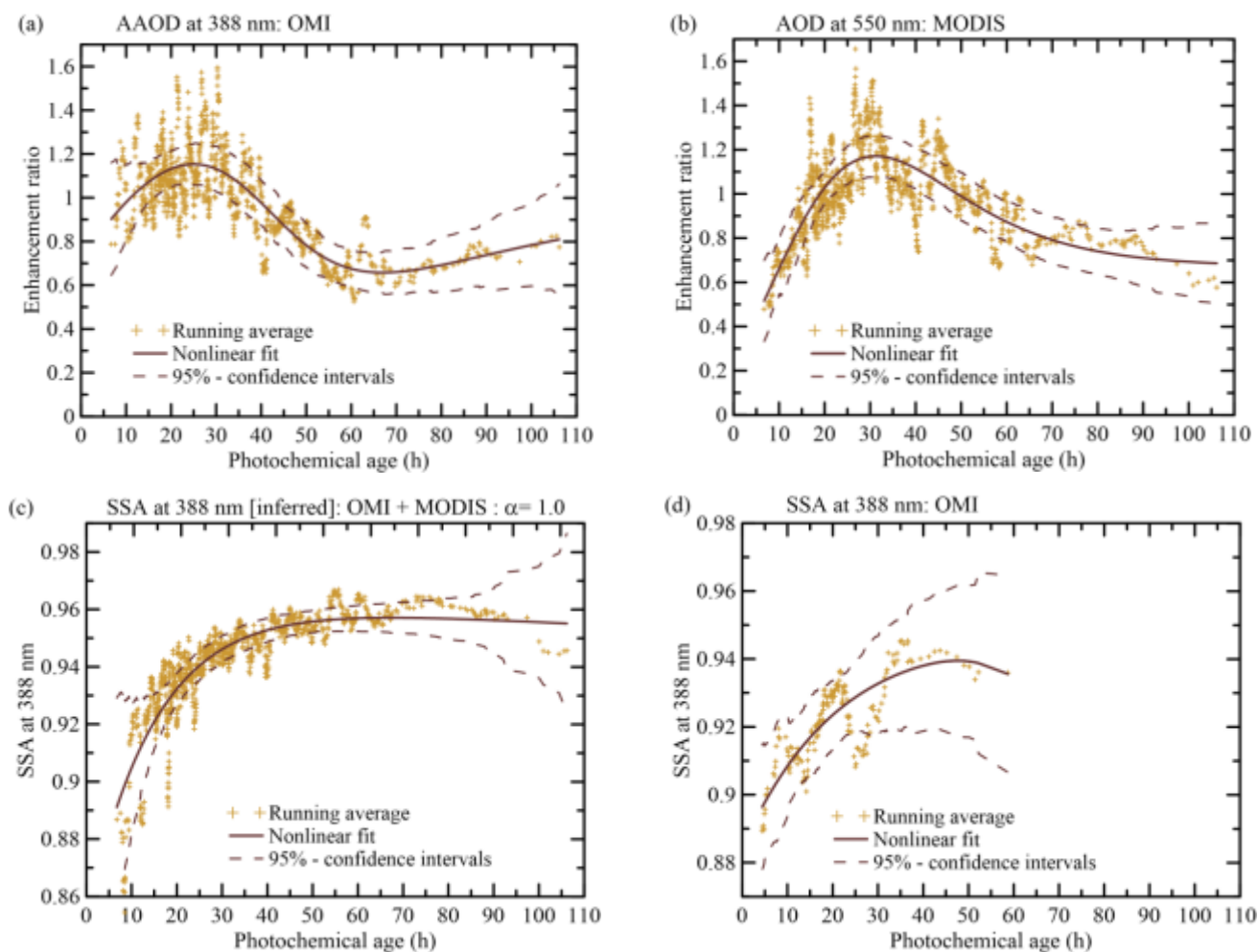
Figure 5. Nonlinear approximations (see Eq. 5) of the dependencies of (a, b) EnRs for AAOD (388 nm) and AOD (550 nm) and (c, d) SSA (388 nm) on the photochemical age of BB aerosol. Also shown are the running averages over each consecutive 15 data points (for EnRs or SSA) arranged with respect to the photochemical age as well as the 95 % confidence intervals for the approximations. The SSA values approximated in panel (c) are inferred from the OMI AAOD and MODIS AOD observations, while those presented in panel (d) are provided directly in the OMAERUV data product.

5
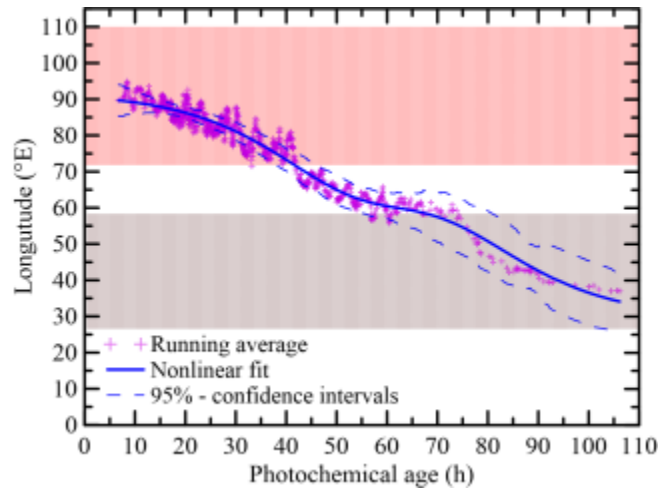
Figure 6. Dependence of the longitude of the instant location of a given BB plume on its photochemical age. The shaded areas indicate the ranges of longitudes of the source (red shade) and receptor (brown shade) regions shown in Fig. 2.

5
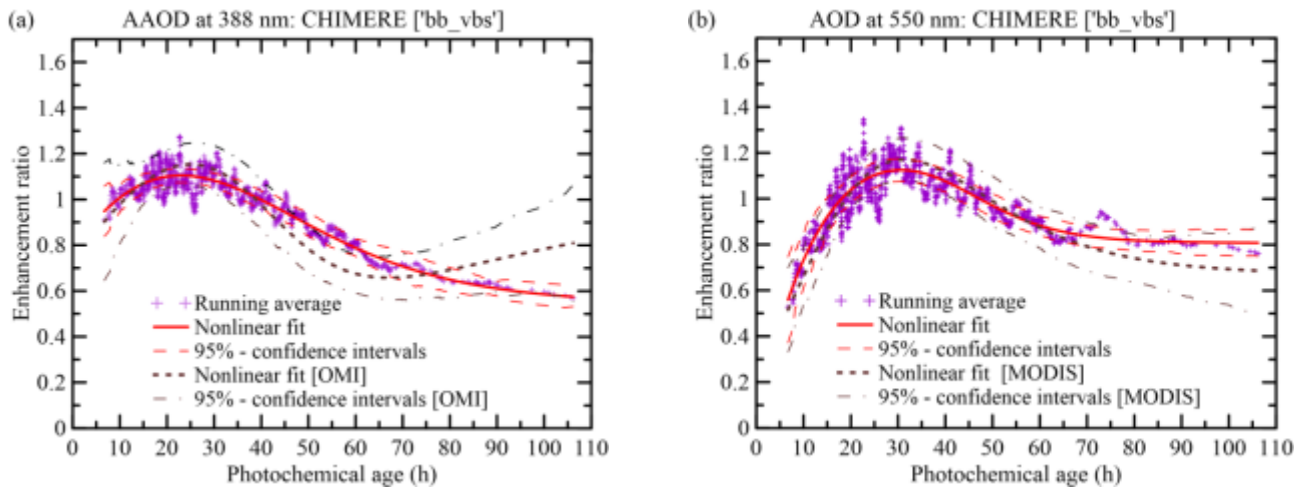
Figure 7. The same as in Figs. 6a5a, b but obtained using the CHIMERE simulations for the 'bb_vbs' scenario. The dependencies from Figs. 6a5a, b, and their confidence intervals are also shown for comparison.
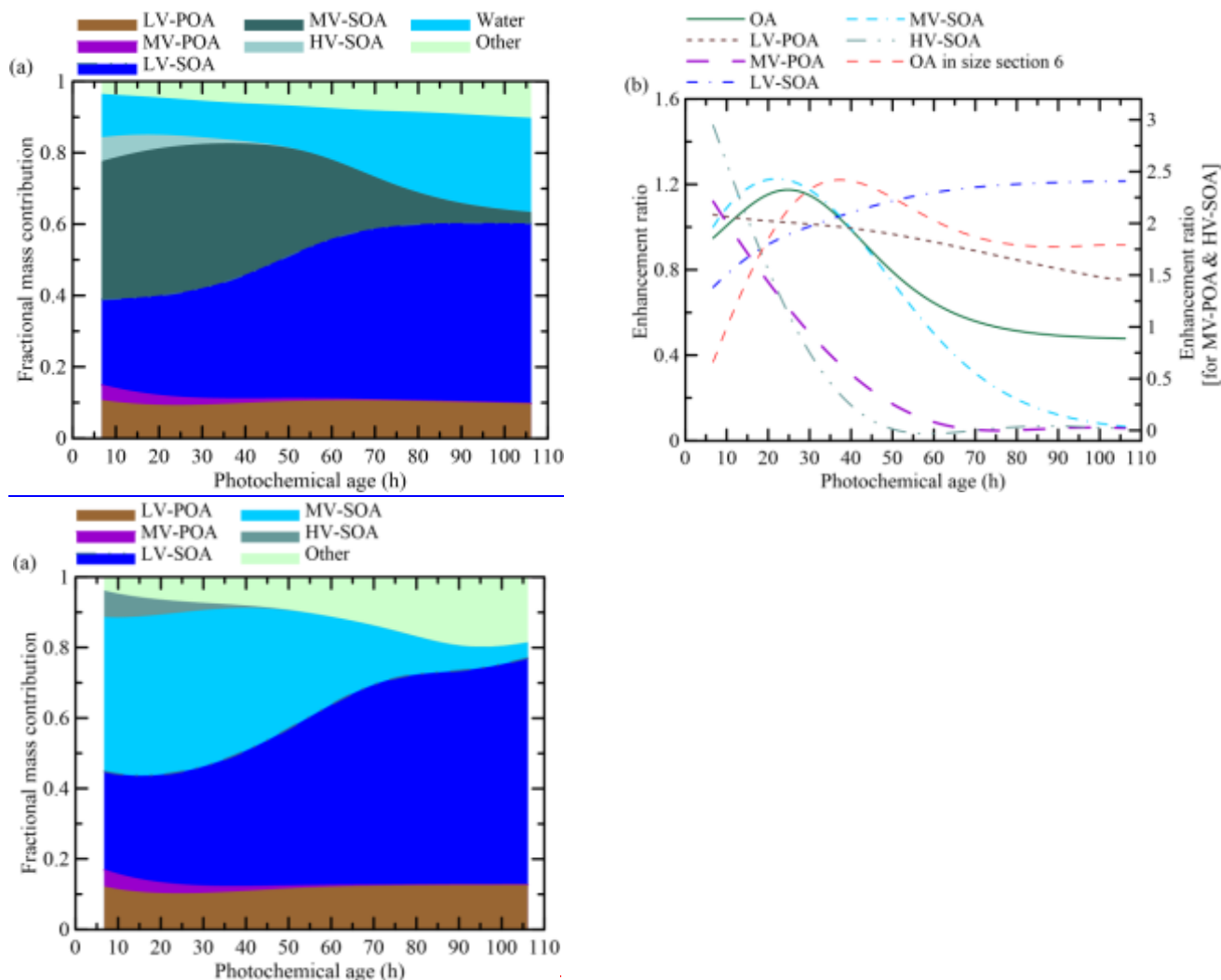
Figure 8. Evolution of the key model species determining the composition of BB aerosol in the CHIMERE simulation for the 'bb_vbs' scenario: (a) fractional contributions of the model species in the mass columnar concentration of BB aerosol, (b) the normalized EnRs of columnar concentrations of organic species in the particulate phase in the simulations for the 'bb_vbs' scenario with respect to OA concentration in the simulations for the 'bb_trc' scenario, along with similar enhancement ratios for the total columnar OA concentration and OA concentration in the 6th bin (310-630 nm) of the particle size distribution in CHIMERE. Note that the EnRs for MV-POA and HV-SOA are presented using the right ordinate axis.
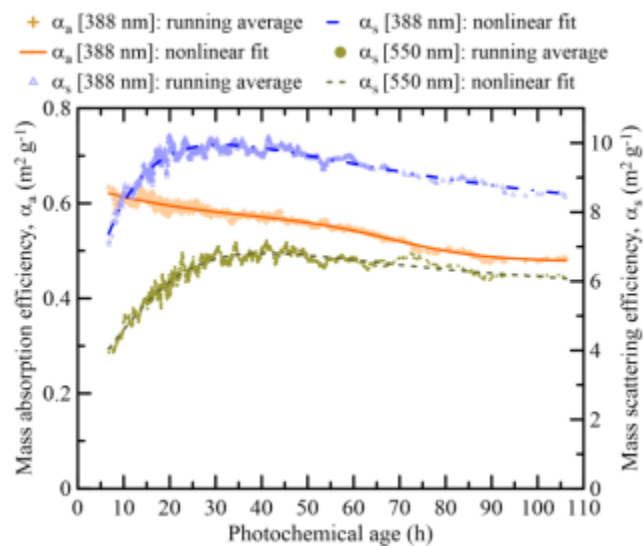
Figure 9. Evolution of the mass absorption efficiency at 388 nm (left axis) and mass scattering efficiency at 388 and 550 nm (right axis) according to the simulations with the CHIMERE CTM and OPTSIM module for the 'bb_vbs' scenario.
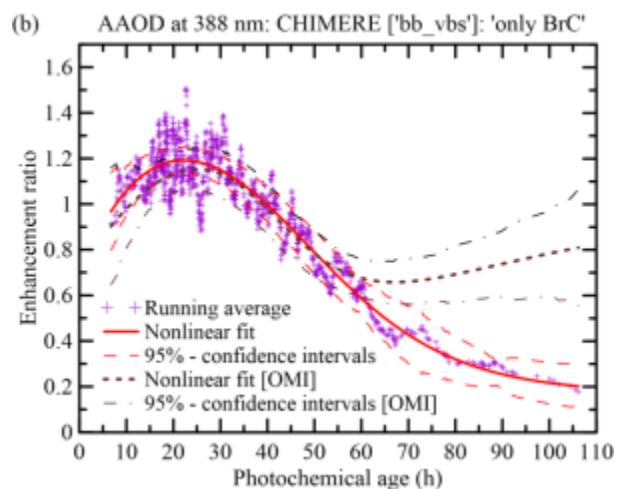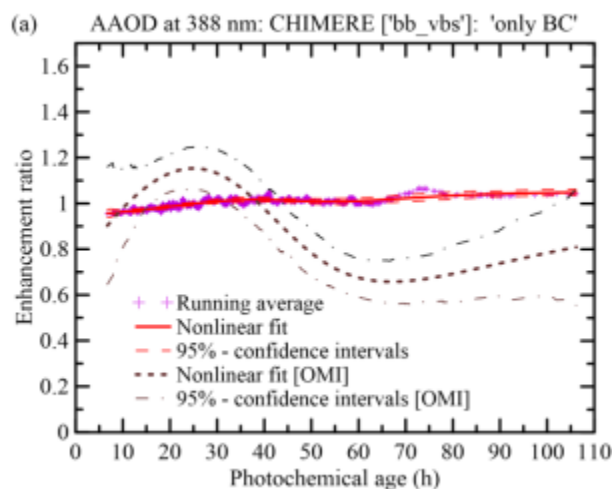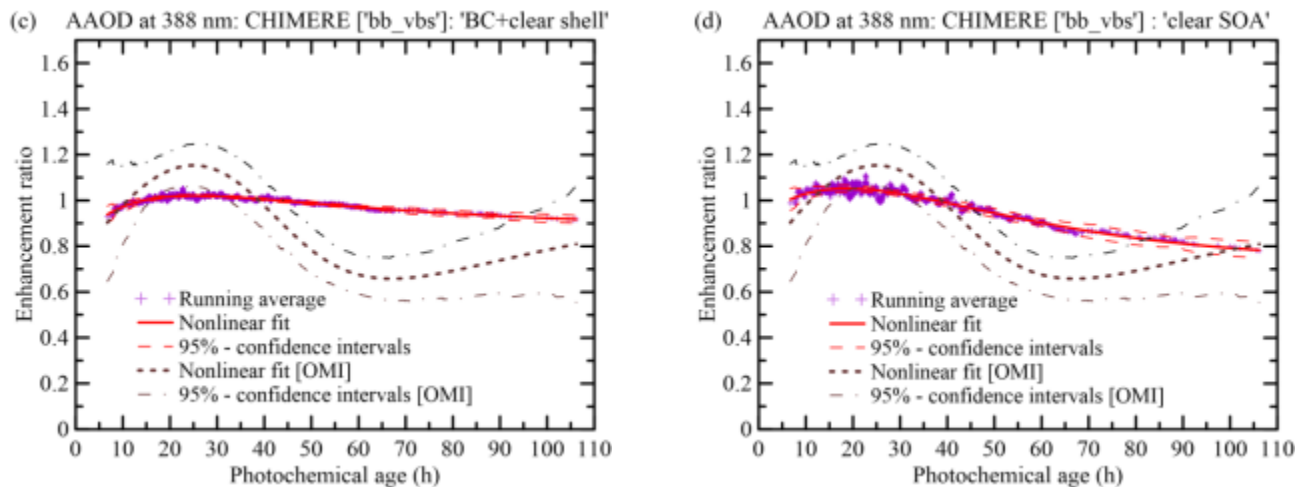
Figure 10. Evolution of EnR$_{abs}$ according to model results for several limiting cases involving different specifications of the optical properties of the individual components of BB aerosol: (a) absorption is determined only by BC, (b) absorption is determined only by BrC, (c) absorption is determined only by the BC core surrounded by ~~a~~the non-absorbing shell, (d) absorption is determined only by both the BC core and OA shell, but SOA is non-absorbing. The trends in EnR$_{abs}$ according to the analysis of satellite observations (Figs. ~~6a~~5a) and its confidence intervals are also shown for comparison. The corresponding model results for the base case where the BC core is surrounded by the absorbing shell are shown in Fig. 7a.

Insights into the aging of biomass burning aerosol from satellite observations and 3D atmospheric modeling: Evolution of the aerosol optical properties in Siberian wildfire plumes

Igor B. Konovalov et al.

Correspondence to: Igor B. Konovalov (konov@ipfran.ru)

S1. A note on the differences between the analysis method used in this study and by Konovalov et al. (2017)

While the analysis procedure developed in this study (see Sect. 2.1) is similar to that used by Konovalov et al. (2017), there are also notable differences between these procedures. A major distinctive feature of the analysis in Konovalov et al. (2017) is splitting the available data into several bins, each of which covered a fixed range of photochemical ages. Consequently, the results of the analysis depended on the chosen width of the photochemical age bin. In this study, we avoided the intrinsic uncertainty associated with a choice of the photochemical age bin width by fitting all the available data at once with a "universal approximator". The optimal approximation still depends on the structural parameter (N), but the choice of the optimal parameter value in this study is rather straightforward and objective, as described in Sect. 2.1. Overall, we believe that the analysis procedure used in the framework of this study is superior to the procedure employed in the previous study, enabling more reliable detection of the aging changes in the BB aerosol properties.

S2. Box model simulations

Here we present the simulations performed with a microphysical dynamic (box) model of organic aerosol. The model is described in detail in Konovalov et al. (2019), where five different VBS schemes were used to simulate the BB OA evolution in an isolated plume under the prescribed ambient conditions. In the present study, box model simulations were performed using our simplified adaptive VBS scheme as well as the original 1.5-dimensional (C17) one (Ciarelli et al., 2017) from which our scheme was derived. Air temperature and the initial BB OA mass concentration were chosen to be representative of the conditions of the four "high-temperature" chamber experiments reported by Ciarelli et al. (2017). These experiments were conducted at a temperature of 288.15 K, with the initial BB OA mass concentration varying in the narrow range from 17.55 to 22.63 µg m^{-3}. In our model runs, we set the temperature accordingly at 288.15 K and assumed the fixed value of 19 µg m^{-3} for the initial BB OA mass concentration. Note that the "low-temperature" experiments conducted by Ciarelli et al. (2017) at 263.15 K are not considered here because according to our simulations (see Sect. S4 below), the typical ambient temperature at the locations of the center of mass of the analyzed BB plumes was significantly higher than 263.15 K (ranging from about 280 to 285 K). Dilution and the background OA concentration, which were taken into account in the analysis reported in Konovalov et al. (2019), were disregarded in the simulations presented here, which are intended to replicate the conditions of chamber experiments. The parameters of our simplified VBS scheme (the reaction rates, enthalpies of evaporation, stoichiometric coefficients, and the ratio of the initial mass concentration of NTVOCs to the sum of the initial mass concentrations of the POA species) were chosen to be the same as those reported in Sect. 2.4 and Tables 1 and 2. As explained in Sects. 2.4 and 2.6, a few parameters (specifically those defining HV-SOA and LV-SOA yields, the product yields from the oxidation reactions of MV-SOA and LV-SOA, and the emission ratio of mass concentration of NTVOCs to the sum of mass concentrations of the POA species) were optimized in this study using satellite observations. The parameters of the C17 scheme were adopted from Ciarelli et al. (2017, see Table 1 therein). Note that these parameter values were partly constrained by data from both the low-temperature and high-temperature experiments (see Ciarelli et al., 2017 for details). The model runs were performed for a period of 110 hours. This period corresponds to the estimated maximum duration of the exposure of smoke plumes to sunlight in the analyzed region and period (see Sect 3.2). The OH concentration was fixed at 5×10^6 molec cm^{-3}.

The results of our simulations are presented in Fig. S1. Specifically, the figure shows the time series of the total BB OA mass concentration and also illustrates changes in the fractional composition of BB OA. The calculations can be compared to measurements of the BB OA mass concentrations at the high-temperature experiments. The BB OA concentration initially enhances more rapidly in the simulation with our scheme (Fig. S1a) than in the simulation with the original scheme (Fig. S1b). As a result, the BB OA concentration predicted by our scheme after about 10 hours of evolution is about 40 % larger than the corresponding concentration predicted by the original C17 scheme. It is also about 15% larger than the maximum concentration obtained in the chamber experiments. However, it should be noted that these particular experiments are not representative of the wide range of burning conditions and large variety of fuels in the Siberian forest. Moreover, there was significant variability in BB OA concentrations even under the controlled conditions of the chamber experiments (Fig. S1). Taking these observations into account, we consider the comparison presented in Fig. S1a as additional evidence that the simulations of the BB OA evolutions with our simplified scheme are sufficiently reasonable. A comparison of the results obtained with the simplified and original schemes (cf. Fig. S1a and Fig. S1b) reveals that the simulations are qualitatively different. Indeed, while the original scheme demonstrates a monotonic saturating increase of BB OA concentration, the simplified scheme yields a non-monotonic behavior of BB OA concentration (a rapid increase followed by a gradual decrease due to fragmentation of SOA). These two types of behavior of BB OA were earlier identified and discussed in Konovalov et al. (2019). However, the available chamber experiments, which are representative of only relatively small OH exposures, do not allow us to exclude any of these types of behavior of BB OA aerosol.

Since the definitions of surrogate organic species in our VBS scheme and C17 schemes are considerably different, a direct comparison of the simulated compositions of OA is not feasible. Nonetheless, the comparison of Fig. S1a and S1b reveals some obvious similarities between the simulations with the two schemes. In particular, there is a decreasing trend of POA in

the both simulations; there is also a steep increase in the concentration of the secondary compounds in the medium volatility range during the first several hours and eventual disappearance of these compounds. In both simulations, the low –volatility components (C*<10^0 µg m^{-3}) provide predominant contributions to the BB OA composition at the end of the evolution period. Overall, this comparison indicates that the BB OA behavior predicted by our scheme is not strikingly different from that predicted by the C17 scheme and is physically reasonable. The major differences are associated with the dynamics of the medium-volatility components.

~~S2~~S3. Time series of AOD and CO data from the ancillary data set

Figure ~~S2~~S3 shows the time series of AOD retrieved from the MODIS measurements and simulated with CHIMERE for all the three main modeling scenarios considered in this study. The time series for the MODIS AOD observations and the simulations for "bb_vbs' scenario correspond to the spatial distributions shown in Fig. 2. Similar time series for the CO columns corresponding to the spatial distributions shown in Fig. ~~S1~~S2 are presented in Fig. ~~S3~~S4. The time series are shown separately for the source and receptor regions. The differences between the simulations performed with and without fire emissions are indicative of the BB fraction of AOD or CO columns. Note that these time series represent the ancillary dataset (see Sect. 2.5), which does not include the OMI observations. Both the observations and simulations exhibit strong AOD and CO enhancements, which (according to our simulations) were caused predominantly by fire emissions in Siberia. In the source region, the fires strongly affected AOD and CO from the end ~~to~~ of June until the end of July, and the enhancements were particularly strong during the analysis period (from 15 to 31 July). In the receptor region, considerable AOD and CO enhancements were observed only in the period from 18 to 31 July. These enhancements caused by the major outflow of BB plumes from Siberia are in striking contrast with much lower values of both characteristics outside of the analysis period.

The simulations taking fire emissions into account are in good agreement with the observations, with the correlation coefficient typically exceeding 0.85. There are, however, some noticeable differences between the simulations for the "bb_vbs" and 'bb_stn' scenarios. In particular, while the simulations for the 'bb_vbs' scenario slightly (by ~7 % percent on average) underestimate AOD in the source region, they are in nearly perfect agreement (again on average) with the observations in the receptor region. In contrast, the "standard" simulations agree with the observations in the source regions but are biased high (by ~18 %) in the receptor region. Note that the fire emissions used in our simulations were optimized (see Sect. 2.6) using the main dataset, which is consistent with the OMI AAOD observations and contains much fewer data points than the ancillary dataset (which includes AOD and CO observations irrespective of the availability of the corresponding AAOD retrievals) presented in Figs. 2, and ~~S1~~S2-~~S3~~S4. This explains some noticeable differences between the average AOD or CO values from the observations and simulations in the source region.

~~## S3. Sensitivity analysis~~

~~As noted above (see Sect. 2.2), one of the important features of the OMAERUV data products is that the AAOD and SSA retrievals are dependent on the BB plume height, which needs to be assumed a priori and can be a source of systematic uncertainty in the results of our analysis. While the base case results presented above are obtained using the BB plume heights predicted by our model independently for each grid cell and hour, we also tested the 'final' OMAERUV retrievals based on the monthly aerosol layer height climatology derived from CALIOP measurements (Torres et al., 2013). Assuming a constant aerosol layer height for a whole month is effectively equivalent to disregarding possible dependences of this parameter on the intensity of fires and plume age and can, therefore, result in some systematic errors in our analysis. On the other hand, the emission injection heights estimates involved in our simulations are likely affected by the uncertainty dominated by random errors associated with the corresponding parameterization (Sofiev et al., 2012). Accordingly, we consider the differences between the BB aerosol absorption trends inferred from the different subsets of the OMAERUV data as an indicator of the robustness of the results of our analysis with respect to both possible systematic and random uncertainties in the aerosol layer height. We find that the results obtained with the 'final' retrievals of both AAOD and SSA (see Fig. S5a, b) are only slightly different from those for the base case (see Fig. 5a, d, respectively). Specifically, the amplitude of the variation of the AAOD trend is insignificantly smaller, and the SSA values are slightly higher in the test case than in the base case.~~

~~One more potential source of systematic uncertainty in our analysis is associated with the use of the IASI CO data to correct possible transport errors by applying the correction factor f_c (see Sect. 2.1 and Eqs. 2 and 3). This uncertainty may appear for two main reasons. First, the IASI CO columns are likely to be underestimated close to emissions (Turquety et al., 2009). And second, our estimates of f_c can be affected by uncertainties in the background part of the CO columns. In the situation addressed in this study, a negative bias in the IASI CO columns in the source region — since the CO emissions from fires were fitted to the IASI observations in the source region — would likely result in underestimation of CO columns in our simulations for the receptor region. However, our analysis does not reveal any significant biases in our simulations (see Figs. 4f and S3). The potential bias in the simulated data could hardly be compensated by the transport errors because the data are averaged over many grid cells representing the source and receptor regions. So we do not see any evidence of the impact of potential biases in the IASI CO columns on our estimates of the correction factors f_c. The effects of potential uncertainties in the background CO columns on our estimates are more difficult to evaluate, particularly because these uncertainties can vary in both space and time. Underestimation of the background CO would result in overestimation of f_c, making the downward trends of EnR$_{abs}$ and EnR$_{ext}$ stronger, and vice versa. However, the de-biasing procedure used in our analysis (see Sect. 2.5) is expected to ensure that such effects are overall not considerable. Indeed, we find that the de-biased CO columns simulated without fire emissions are in good agreement with the IASI CO columns both in the source and receptor regions on the days when the contribution of fire emissions was negligible (see Fig. S3). To test the overall impact of the CO data on the derived trends in EnR$_{abs}$ and EnR$_{ext}$, we repeated the analysis of the AAOD and AOD data with f_c equal to 1. The results of the test (see Fig. S6) are qualitatively (although not necessarily quantitatively) rather similar to those for the base case (see Fig. 5a,b). We regard these sensi-~~

S4. Evolution of ambient parameters

Here we consider the behavior of several characteristics that can affect the gas-particle partitioning and oxidation processes in the BB plumes as well as the estimates of the AAOD and AOD enhancement ratios. To this end, Figure ~~S8~~ S6 presents the simulated trends in several quantities, including ambient temperature and relative humidity (Fig. ~~S8a~~S6a), the height of the BB plume mass center and OH concentration (Fig. ~~S8b~~S6b), and total BB OA concentration (Fig. ~~S8c~~S6c). All the characteristics are calculated as the weighted average over the vertical profile of the plume, with BB aerosol mass concentration being used as weights. Additionally, Fig. ~~S8c~~ S6c shows the trend in the normalized ratio of the BB tracer's AAOD (τ_{abs}^t) involved in Eq. (1) to the column amount of the inert gaseous tracer of BB OA emissions, T_1 (see Sect. 2.3). This ratio characterizes the changes in AAOD due to dry deposition, wet scavenging, and coagulation of particles.

It can be seen that the average temperature fluctuates around 10° C and does not exhibit any considerable trend. The relative humidity (RH) is typically very low, with the average values being below 50% for the BB aerosol aged less than 70 h. The BB plume height initially increases from about 1.5 to 1.8 km during the initial 30 h of the daytime evolution and then slightly decreases. There is also only a slight downward trend ~~of~~ in the OH concentration during the initial period. The regular changes in all these characteristics are overall rather small and could hardly induce the significant trends in AAOD and AOD that are identified above. In contrast, rather significant changes occur in the simulated average concentration of BB OA, which drops from 62 to 13 µg m^{-3} (see Fig ~~S8c~~S6c). This is an expected effect of the dilution of BB plumes. The dilution is associated with increasing the equilibrium concentration of SVOCs, favoring evaporation of particulate organic material and more rapid losses of SVOCs as a result of gas-phase fragmentation reactions. ~~This~~ These process~~es~~ ~~is~~ are driving the decrease of both AAOD and AOD after t_e of ~30 h (see Fig 5a, b).

Figure S8c also indicates that the basic aerosol processes included in the "tracer" simulation could not significantly affect the BB aerosol evolution. As could be expected, the ratio of AAOD computed for the inert aerosol tracer (τ_{abs}^t) to the column mass concentration, [T1], of the inert gaseous tracer decreases with time, apparently mostly as a result of dry deposition (as according to our meteorological simulations, there were almost no precipitation events in the region and period considered), but coagulation could also contribute to this trend (Sakamoto et al., 2015). Virtually the same dependence, which is not shown, is found for τ_{ext}^t. The rate of the decrease of the τ_{abs}^t-to-[T1] ratio is much slower than the expected rate of the loss of BB BC from the lower atmosphere: indeed, the atmospheric lifetime of BC in Siberia was estimated to be only about 5 days under typical conditions (Paris at al., 2009). However, this lifetime is partly determined by wet deposition, and it also should be taken into account that τ_{abs}^t at 388 nm is mostly determined by relatively small and thus long-lived particles in the accumulation mode, whereas the total BC concentration can be dominated by larger particles. This consideration implies, in particular, that the appearance of the decreasing parts of the EnR trends derived from the observed values of AAOD and AOD (see Fig. 5a, b) cannot be due to underestimation of dry deposition of BB aerosol in our simulations of the BB aerosol tracers. Note again that coagulation can also contribute to the changes of τ_{abs}^t and τ_{ext}^t due to aging by modulating the size distribution, but the corresponding effects have not been isolated in this study.

S5. Simulation results for the 'bb_poa' simulation scenario

The 'bb_poa' simulation test scenario that was introduced in Sect. 2.3 and discussed in Sect. 3.3 addresses a hypothetical situation where the organic components of BB aerosol are not affected by any oxidation reactions. For this scenario, we also postulated that the POA species are hygroscopic instead of being hydrophobic as in the bb_vbs scenario to compensate for the water uptake by the SOA species. The simulations were performed using the same model configuration as for the 'bb_vbs' scenario

3

except that all the reaction rates reported in Table 2 were set to zero, the hygroscopicity parameter κ_{org} for both LV-POA and MV-POA was assumed to be 0.2, and the POA emissions were increased by a factor of 4.3. Using the simulated concentrations for this scenario, we also performed an additional calculation with the OPTSIM module for a test case in which the contribution of water to the BB aerosol composition was neglected. The main simulation results are presented in Fig. S8.

According to these results, EnRs for both AAOD and AOD (see Fig. S8a, b) demonstrate monotonous decreasing dependencies, in striking contrast to the non-monotonous dependencies obtained from satellite observations (cf. with Fig. 5a, b) and simulations for the 'bb_vbs' scenario (cf. with Fig. 7a, b). The decrease in EnR_{abs} is substantial (~50 %), while that in EnR_{ext} is small (~10 %). Consistently with the monotonous changes in AOD and AAOD, SSA gradually increases (Fig. S8c), instead of demonstrating a hyperbolic (saturable) dependence on the BB aerosol photochemical age as in our analysis of the satellite data (see Figs. 5c). The corresponding values of the mass absorption and scattering efficiencies (α_a and α_s, respectively) indicate (see Fig S8d) that the decrease in α_a (which is expected to occur due to the limited lifetime of BrC in the primary aerosol, see Sect. 2.4) is the main factor responsible for the strong decrease in EnR for AAOD. The main process underlying the decrease in EnR for AOD is apparently the evaporation of MV-POA, since in contrast to α_a, α_s increases as a result of the BB evolution (by 44 %). The increase in α_s can be due to changes in the particle size distribution upon the evaporation of MV-POA, as well as due to an increase in the water uptake as a result of the rise in RH (see Fig. S6a). The test OPTSIM calculation, in which the contribution of water to BB aerosol was disregarded and α_s is found to increase by 27 % (see a brown line in Fig. S8d), confirms that the increase in the water uptake is important but not the major factor underlying changes in α_s. It may be noteworthy that the initial – for the period considered – value of α_s in the 'bb_poa' scenario (6.4 m^2 g^{-1}) is found to be larger than that in the 'bb_vbs' scenario (4.0 m^2 g^{-1}, see Fig. 9). A more detailed examination of the simulation data reveals that this difference is associated with the differences in the corresponding particle volume size distributions. Specifically, the 'bb_vbs' simulation allocates a much larger fraction of the particle mass to the particles with diameters around 100 nm or less, which have a relatively small scattering efficiency, than the 'bb_poa' simulation. In the 'bb_vbs' simulation, these particles consist predominantly of the SOA species and are, therefore, formed as a result of oxidation of NTVOC and POA. Further SOA formation results in the growth of these particles, pushing the size distribution toward larger values as illustrated in Fig. S7. The difference between values of the absorption efficiency for the 'bb_vbs' and 'bb_poa' scenarios is determined by the difference in the absorptive properties of the POA and SOA species and is not of interest in the context of this study.

Overall, the simulation results presented in Fig. S8 indicate that the evaporation of POA and the water uptake by BB aerosol particles cannot explain a prominent increase in EnR for AOD, which is found both in the analysis of satellite data and in our simulations for the base case ('bb_vbs') scenario. Accordingly, the simulation for the 'bb_poa' scenario confirms that the strong increase in AOD is primarily a result of oxidation processes leading to the SOA formation. The analysis presented here may also have a wider implication when considered together with the OC emission estimates discussed in Sect. 2.6. Specifically, it provides further evidence that if a given model strongly underestimates AOD (with respect to satellite observations), this fact does necessarily mean that the underestimation is due to a negative bias in BB emission inventory data. Instead, it may be due to insufficiently strong SOA formation in the model. The proposed joint analysis of satellite and model data allows distinguishing between the two possible reasons for the underestimation of AOD by the model. If AOD is underestimated as a result of missing SOA formation processes, the adjustment of the POA emissions in the model would not enable it to reproduce the major features of the retrieved evolution of the BB aerosol optical properties, as demonstrated in our analysis presented in this section.

~~S5~~S6. The relative contribution of BC, lensing effect, and BrC to the BB aerosol absorption

Figure ~~S10~~ S9 shows the fractional contributions of BC, lensing effect, and BrC to absorption at 388 nm as a function of BB aerosol photochemical age according to our simulations for the 'bb_vbs' scenario with different assumptions examined in Fig. 10. These computations are carried out using two approaches. First (see Fig. ~~S10a~~S9a), we computed the absorption determined by BC and the OA lensing by setting the imaginary refractive indexes for POA and SOA to zero. The difference between the "base case" simulation (Fig. 7a) and the test case simulation with non-absorbing OA (Fig. 10c) is regarded as a contribution of BrC to absorption. Second (see Fig. ~~S10b~~S9b), we computed the absorption determined only by BrC (Fig. 10b) and regarded the difference between the "base case" simulation and this test case simulation as a contribution of BC (with the OA lensing) to absorption. These approaches are not expected to yield identical results because of the "sunglasses effect" of BrC, that is, the blocking effect of an absorbing coating on the absorption associated with the BC core (Luo et al., 2018). An optically thick BrC shell could account for virtually all the absorption according to the second approach, irrespective of the BC content. However, our absorption estimates for the second approach turned out to be only insignificantly larger than those for the first approach, thereby indicating that the sunglasses effect does not play a major role in our situation.

According to our computations (Fig. ~~S10a~~S9a), "pure" BC accounts on average (over the study region and analysis period) for only 31% of the total absorption. The BC contribution is the smallest (28 %) at t_e of 17 h and largest (54 %) at the end of the evolution period. The lensing effect (see Fig. 10c) leads to an enhancement of the BC absorption by 80 % on average, contributing about 20 % to the absorption. Finally, compared to the sensitivity case with non-absorbing OA, the base case absorption that includes the contribution of BrC is, on average, 78 % larger. According to Fig. ~~S10b~~S9b, BrC contributes about 50 % to the BB aerosol absorption at the beginning of the evolution period considered, but less than 15% at the end of the period. Based on our additional computations, the percentage contribution of BrC to absorption ~~BrC~~ by POA in fresh BB aerosol (which is not covered by our analysis) is also about 50%, which is within the broad range of values (21-80%) reported by Pokhrel et al. (2017) for aerosol originating from combustion of samples of pine and black spruce trees. Accordingly, we estimate that the BrC contribution to the BB aerosol absorption is reduced by more than a factor of 3 after about 100 hours of daytime evolution. Hence, our simulations suggest that~~,~~ consistent with observational findings (Forrister et al., 2015; Selimovic et al., 2019), BrC absorption is strongly decreasing when BB aerosol is exposed to atmospheric processing under daytime condi-

4

tions. On the other hand, consistent with the analysis of the AERONET data by Wang et al. (2016), our results indicate that a sizeable BrC fraction is resistant to both photooxidation and photobleaching. According to our analysis, this fraction, which is likely associated with high-molecular-weight chromophores (Di Lorenzo et al., 2017, Wong et al., 2017, Fleming et al., 2020), remains a significant contributor to the absorptive properties of BB aerosol even after several days of atmospheric aging.

S7. Sensitivity analysis

As noted in Sect. 2.2, one of the important features of the OMAERUV data products is that the AAOD and SSA retrievals are dependent on the BB plume height, which needs to be assumed a priori and can be a source of systematic uncertainty in the results of our analysis. While the base case results presented above are obtained using the BB plume heights predicted by our model independently for each grid cell and hour, we also tested the 'final' OMAERUV retrievals based on the monthly aerosol layer height climatology derived from CALIOP measurements (Torres et al., 2013). Assuming a constant aerosol layer height for a whole month is effectively equivalent to disregarding possible dependencies of this parameter on the intensity of fires and plume age and could, therefore, result in some systematic errors in our analysis. On the other hand, the emission injection heights estimates involved in our simulations are likely affected by the uncertainty dominated by random errors associated with the corresponding parameterization (Sofiev et al., 2012). Accordingly, we consider the differences between the BB aerosol absorption trends inferred from the different subsets of the OMAERUV data as an indicator of the robustness of the results of our analysis with respect to both possible systematic and random uncertainties in the aerosol layer height. We find that the results obtained with the 'final' retrievals of both AAOD and SSA (see Fig. S10a, b) are only slightly different from those for the base case (see Fig. 5a, d, respectively). Specifically, the amplitude of the variation of the AAOD trend is insignificantly smaller, and the SSA values are slightly higher in the test case than in the base case.

One more potential source of systematic uncertainty in our analysis is associated with the use of the IASI CO data to correct possible transport errors by applying the correction factor f_c (see Sect. 2.1 and Eqs. 2 and 3). This uncertainty may appear for two main reasons. First, the IASI CO columns are likely to be underestimated close to emissions (Turquety et al., 2009). Second, our estimates of f_c can be affected by uncertainties in the background part of the CO columns. In the situation addressed in this study, a negative bias in the IASI CO columns in the source region – since the CO emissions from fires were fitted to the IASI observations in the source region – would likely result in underestimation of CO columns in our simulations for the receptor region. However, our analysis does not reveal any significant biases in our simulations (see Figs. 4f and S4). The potential bias in the simulated data could hardly be compensated by the transport errors because the data are averaged over many grid cells representing the source and receptor regions. Thus we do not see any evidence of the impact of potential biases in the IASI CO columns on our estimates of the correction factors f_c. The effects of potential uncertainties in the background CO columns on our estimates are more difficult to evaluate, particularly because these uncertainties can vary in both space and time. Underestimation of the background CO would result in overestimation of f_c, making the downward trends of EnR_{abs} and EnR_{ext} stronger, and vice versa. However, the de-biasing procedure used in our analysis (see Sect. 2.5) is expected to ensure that such effects are not considerable overall. Indeed, we find that the de-biased CO columns simulated without fire emissions are in good agreement with the IASI CO columns both in the source and receptor regions on the days when the contribution of fire emissions was negligible (see Fig. S4). To test the overall impact of the CO data on the derived trends in EnR_{abs} and EnR_{ext}, we repeated the analysis of the AAOD and AOD data with f_c equal to 1. The results of the test (see Fig. S11) are qualitatively (although not necessarily quantitatively) similar to those for the base case (see Fig. 5a,b). We regard these sensitivity test results as strong evidence that the main features of the inferred trends in EnR_{abs} and EnR_{ext} are not an artifact of the proposed correction of the aerosol tracers and possible uncertainties associated with it, and are not significantly affected by uncertainties in the observations and simulations of the CO columns.

Finally, we examined the sensitivity of the inferred evolution of EnR_{abs} and EnR_{ext} to the assumptions about the background AAOD and AOD values involved in Eq. (1). It may be useful first to recall that we assumed the background AAOD values to be negligible when compared to the OMI AAOD retrievals, mainly because it is not known how the background part can be accounted for in the OMI AAOD retrievals for the "biomass burning" type of aerosol (see Sect. 2.3). Nonetheless, we roughly estimated to which degree our estimates could change if the OMI AAOD retrievals included an additive "background" part. The OMAERUV algorithm identifies – as noted above – three types of aerosol, but only one ("biomass burning") type is used in our analysis presented above. To get an idea about the typical magnitude of AAOD at 388 nm under background conditions, we used – in addition to the Level-2 BB aerosol data – the daily Level-3 OMAERUV data which combine all three aerosol types and are available from the Giovanni online application (https://giovanni.gsfc.nasa.gov/giovanni/, last access 11 April 2020) on a 1-by-1-degree grid. According to these data, the mean AAOD in the receptor region in the period from 15 June to 15 July (where and when there was no discernable fire activity) was about 0.018. This value was used as an estimate of τ_{abs}^{bgr} in Eq. (1). Not surprisingly, the resulting approximation (see Fig. S12a) exhibits a stronger downward trend, but the AAOD evolution remained qualitatively the same as in the base case (see Fig. 5a). It should be noted that the Level-3 AAOD data are expected to provide an upper limit for the background AAOD because the clean scenes typically dominating in the receptor region cannot be associated with any of the three aerosol types. To examine the sensitivity of EnR_{ext} to the background values of AOD, we repeated our analysis by assuming that τ_{ext}^{bgr} equals to zero. In this case, the decline of EnR_{ext} is smaller (see Fig. S12b) than in the base case (see Fig. 5b), but is still statistically significant. Hence, based on the results of the tests involving different assumptions on the background values of AAOD and AOD, we can conclude that (i) the impact of the unknown true background AAOD in Eq. (1) on the results of our analysis of EnR_{abs} is probably small and (ii) the declining part of the estimated trend in EnR_{abs} is not due to any bias in our estimates of τ_{ext}^{bgr}.
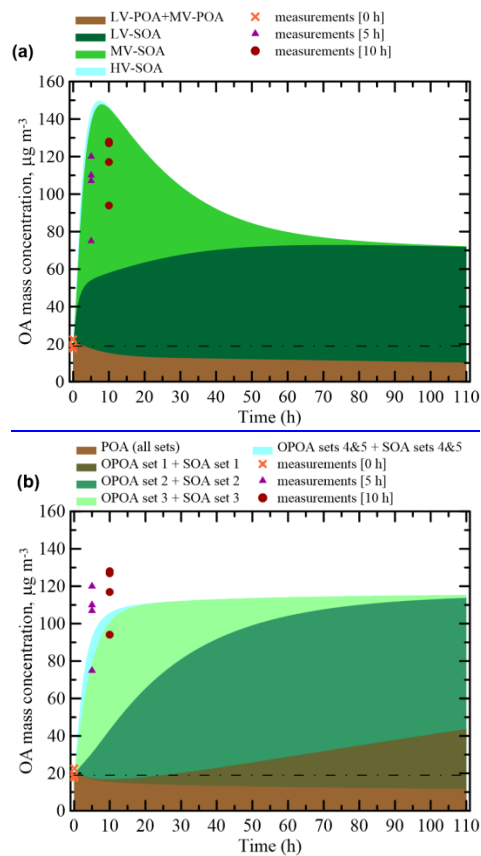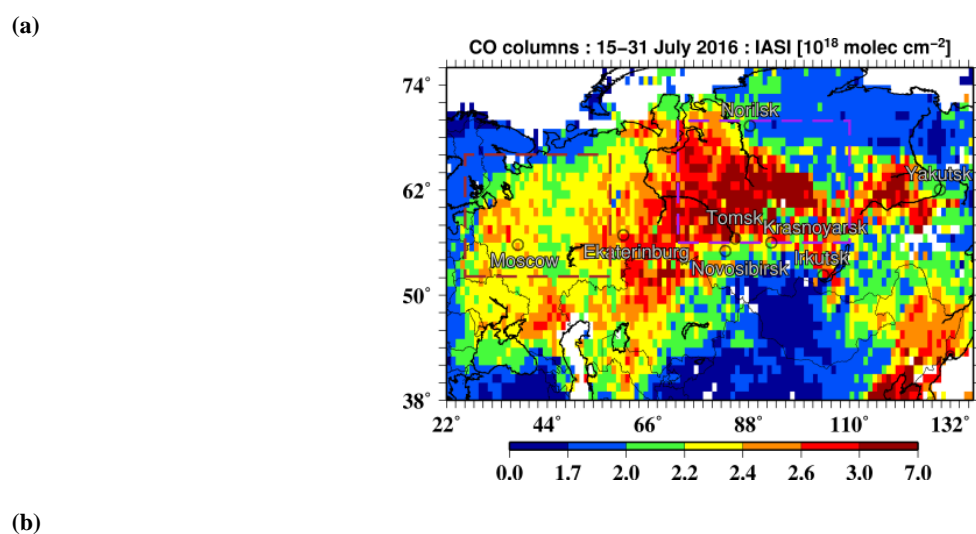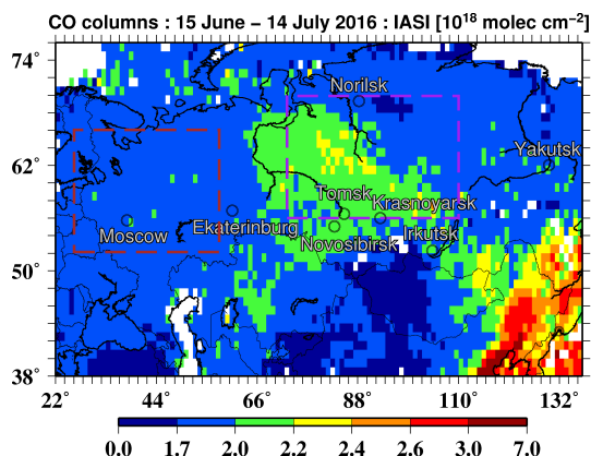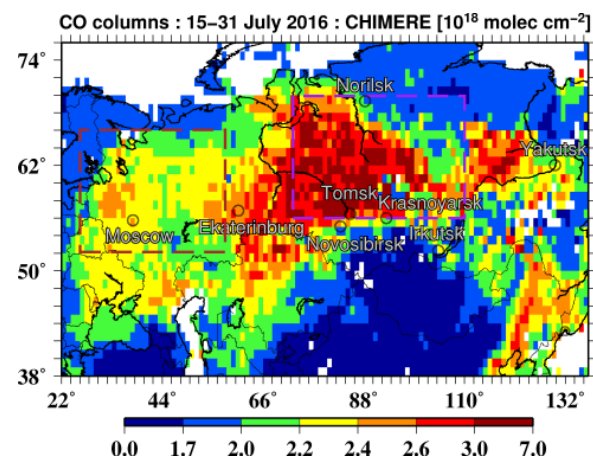
Supplementary figures

5

(a)

(b)

Figure S1. The dynamics of the mass concentration of BB OA and several groups of its components according to the simulations performed with a box model using (a) the simplified VBS parameterization introduced in this paper (see Sect. 2.4) and (b) 1.5-dimensional VBS scheme proposed by Ciarelli et al. (2017). The crosses, triangles, and dots depict the BB OA mass concentration measurements (Ciarelli et al., 2017) originally reported for the OH exposures of 0, 30×10^6, and 50×10^6 molec cm^{-3} h, respectively, and corresponding to 0, 5, and 10 hours of the exposure of BB aerosol to oxidation processes under the assumption that OH concentration equals to 5×10^6 molec cm^{-3}.

(a)

(b)

6

CO columns : 15 June – 14 July 2016 : IASI [10^{18} molec cm^{-2}]

(c)

CO columns : 15–31 July 2016 : CHIMERE [10^{18} molec cm^{-2}]

(d)

CO columns : 15 June – 14 July 2016 : CHIMERE [10^{18} molec cm^{-2}]
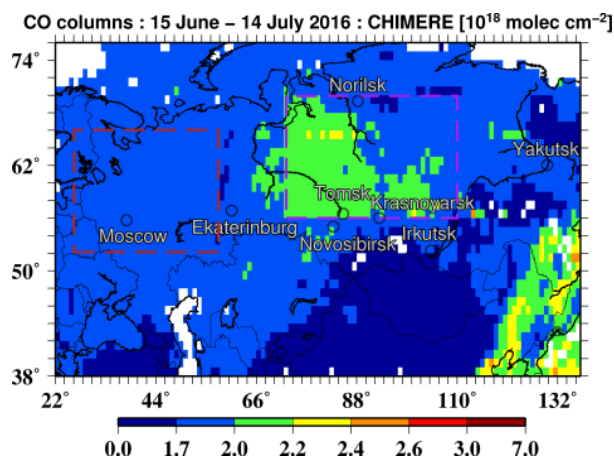
Figure S1S2. Spatial distributions of temporal averages of CO columns in the periods (a,c) from 15 to 31 July 2016 and (b,d) from 15 June to 14 July 2016 according to (a,b) the IASI observations and (c,d) the combined CHIMERE simulations for the 'bb_vbs' and 'bgr' scenarios. The distributions represent the ancillary sets of CO data that were selected irrespective of the availability of the corresponding AAOD retrievals. The rectangles depict the "source" (purple lines) and "receptor" (dark red lines) regions covering parts of Siberia and (mostly) the European territory of Russia, respectively.

7

(a) Source region
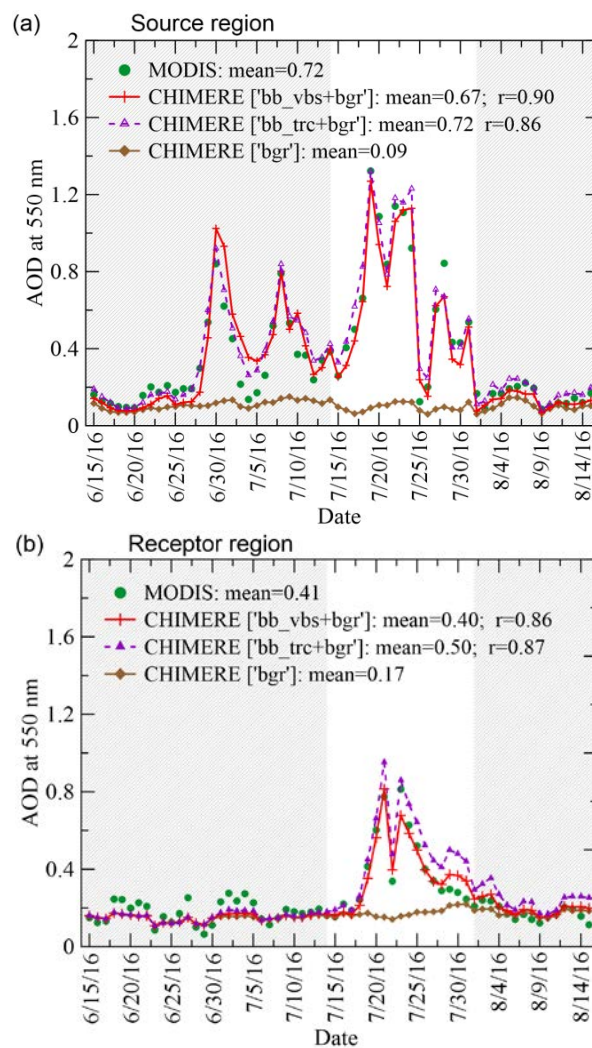
(b) Receptor region

Figure S2S3. Time series of the daily AOD values averaged over the study region according to the MODIS observations and the CHIMERE simulations under the different model scenarios for the (a) "source" and (b) "receptor" regions indicated in Figs. 2 and S1S2. Note that the simulations for the 'bgr' (background) scenario are shown after applying the de-biasing procedure (see Sect. 2.5). The shaded areas indicate the days that are outside of the analysis period (15-31 July 2016) in the given study. The mean and correlation coefficient are evaluated for the analysis period.

(a) Source region

8
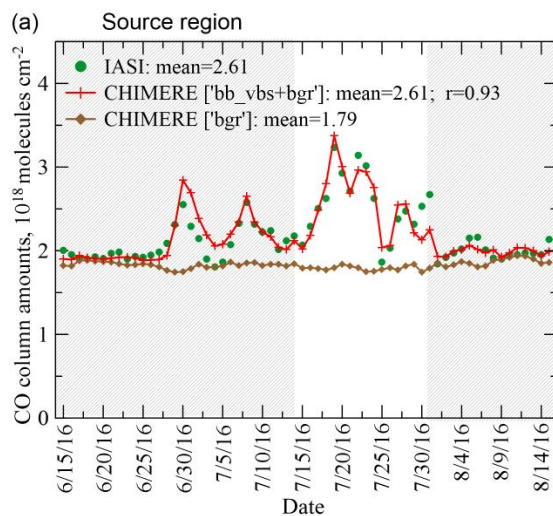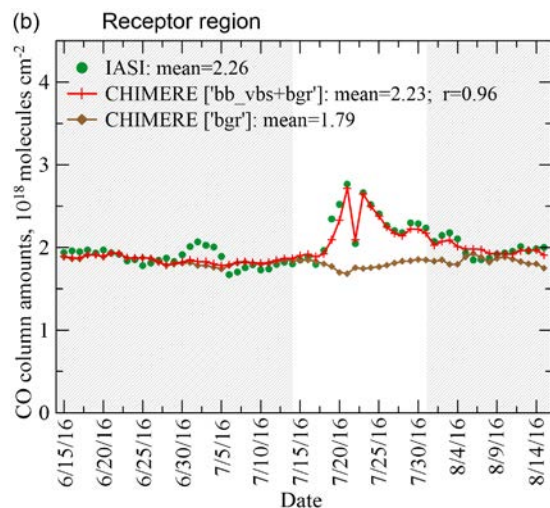
Figure S3S4. Time series of the daily CO column values averaged over the study region according to the IASI observations and the CHI-MERE simulations for the (a) "source" and (b) "receptor" regions. Note that the CO simulations for the 'bb_vbs' and 'bb_trc' scenarios are almost indistinguishable, so only simulations for the 'bb_vbs' scenario (combined with the simulations for the 'bgr' scenario) are shown. Note also that the simulations for the 'bgr' (background scenario) are shown after applying the de-biasing procedure (see Sect. 2.5). The shaded areas indicate the days that are outside of the analysis period (15-31 July 2016) in our study. The mean and correlation coefficient are evaluated for the analysis period.
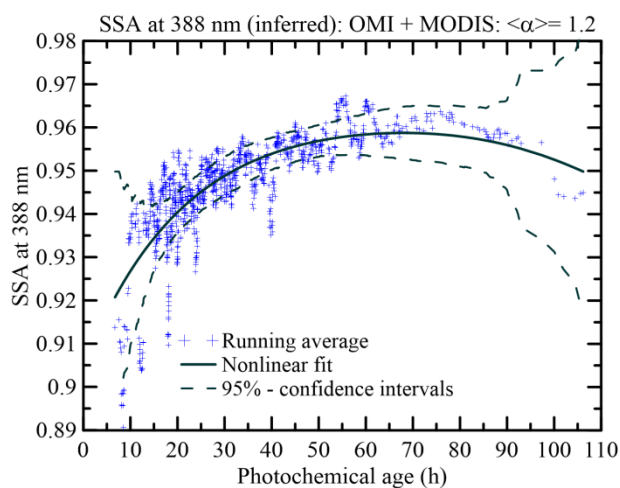
Figure S4S5. Nonlinear approximation (see Eq. 5) of the dependence of SSA (388 nm) on the photochemical age of BB aerosol. The SSA values were inferred from the OMI AAOD (388 nm) and MODIS AOD (550 nm) observations using the variable extinction Ångström exponent (α) estimates based on the CHIMERE simulations for the 'bb_vbs' scenario.

9

(a) AAOD at 388 nm: OMI [OMAERUV_"final"]

(b) SSA at 388 nm: OMI [OMAERUV_"final"]

(a) AAOD at 388 nm: OMI: $f_c = 1$

(b) AOD at 550 nm: MODIS: $f_c = 1$
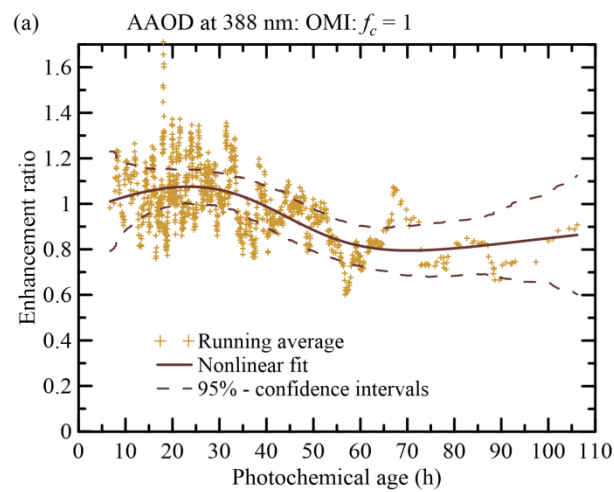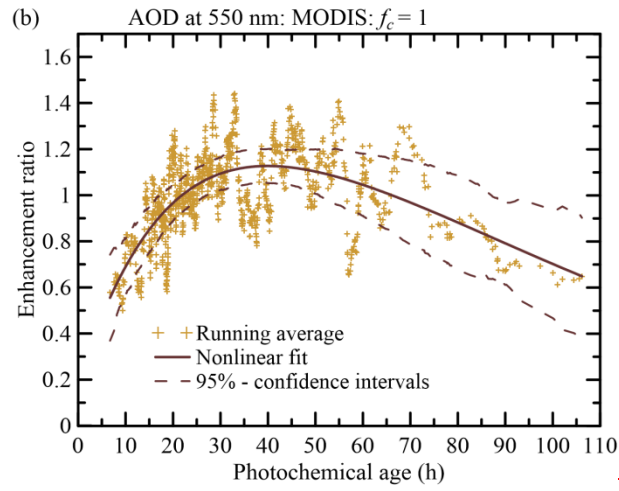
Figure S6. Nonlinear approximations of the dependencies of EnRs for (a) AAOD (388 nm) and (b) AOD (550 nm) on the photochemical age of BB aerosol. The dependencies are similar to those shown in Fig. 5a and 5b except that they are obtained without applying the correction involving CO columns (see Eqs.2 and 3).

(a) AAOD at 388 nm: OMI: $AAOD_{bgr} = 0.018$

(b) AOD at 550 nm: MODIS: $AOD_{bgr} = 0$

Figure S7. Nonlinear approximations of the dependencies of EnRs for (a) AAOD (388 nm) and (b) AOD (550 nm) on the photochemical age of BB aerosol. The dependencies are similar to those shown in Fig. 5a and 5b except that they are obtained assuming that the background AAOD ($AAOD_{bgr}$) equals to 0.018 and that the background AOD (AOD_{bgr}) equals to zero, respectively.

11
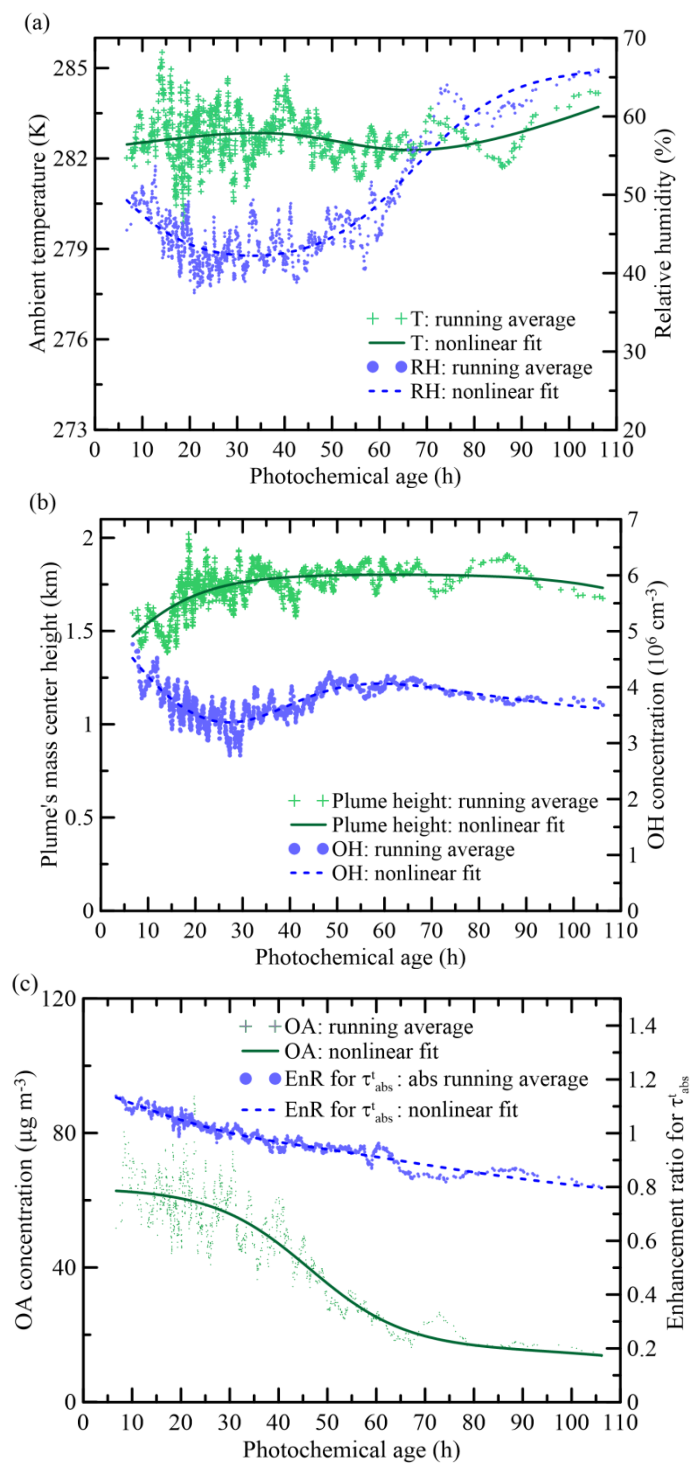
Figure S8S6. Nonlinear trends in several parameters characterizing the conditions of the atmospheric evolution of BB aerosol in the plumes considered: (a) ambient temperature and relative humidity, (b) the height of the BB plume mass center and OH concentration within a plume. Also shown (c) the trends in total BB OA concentration and the normalized ratio of BB tracer's AAOD (τ_{abs}^{t}) to the column amount of the inert gaseous tracer of BB OA emissions (T_1).
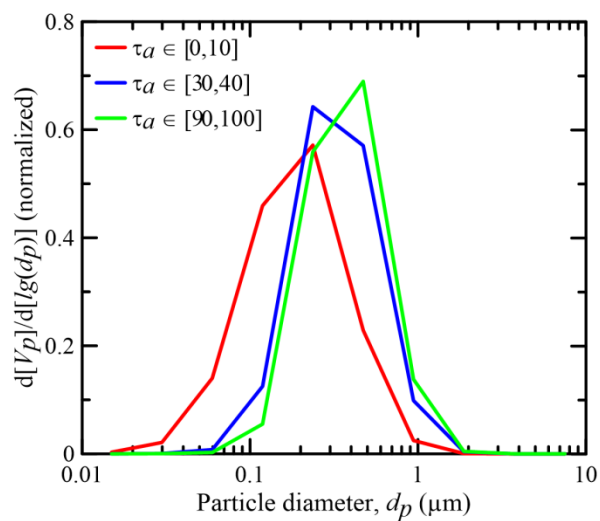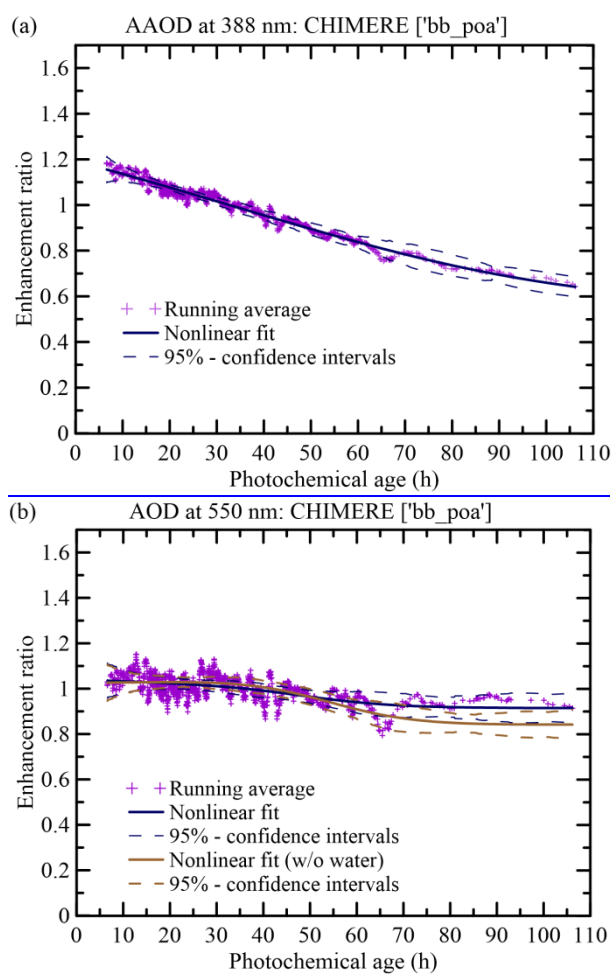
Figure S9S7. Normalized particle volume size distributions averaged over three intervals – [0,10], [30,40], [90,100] – of the BB aerosol photochemical age (h) according to the simulations for the 'bb_vbs' scenario.
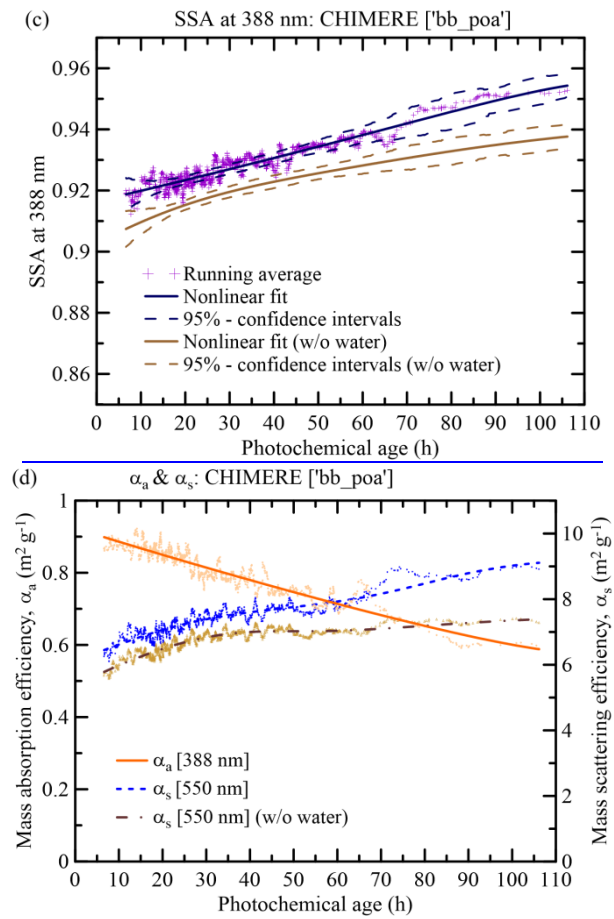
Figure S8. Dependencies of (a, b) EnRs for AAOD (388 nm) and AOD (550 nm) (respectively), (c) SSA (388 nm), and (d) mass absorption and scattering efficiencies (388 nm and 550 nm, respectively) on the photochemical age of BB aerosol according to the simulation for 'bb_poa' scenario. Also shown (brown lines in panels b-d) are the corresponding dependencies of EnRs for AOD, SSA and the mass scattering efficiency according to the OPTSIM calculations with the neglected contribution of water to the particle composition; similar dependencies of the AAOD and the mass absorption efficiency are not shown as they visually merge with the dependencies shown by blue and orange lines in panels (a) and (d), respectively.

14
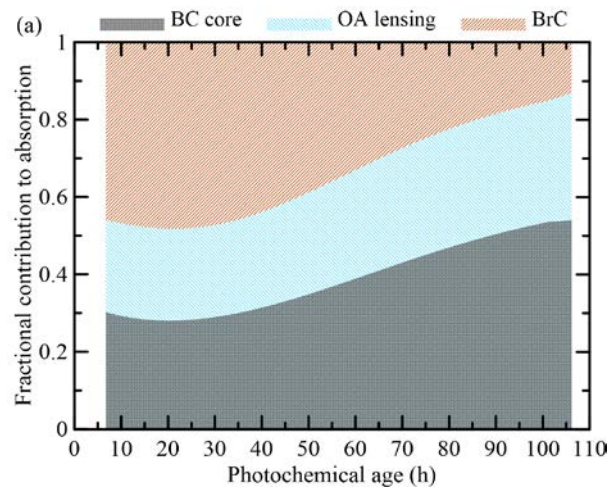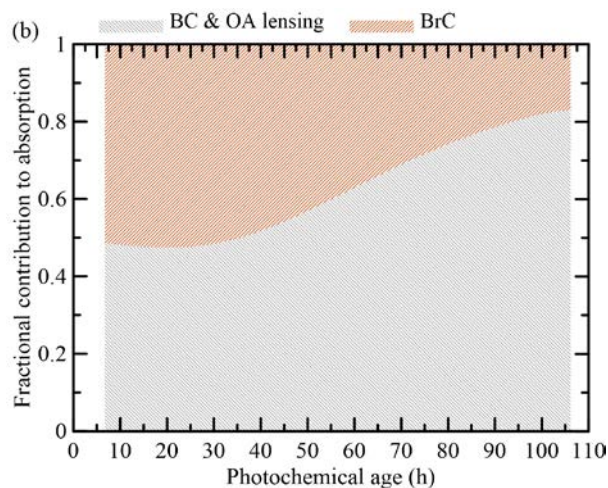
Figure S~~10~~9. Fractional contributions of BC, lensing effect and BrC to absorption at 388 nm as a function of BB aerosol photochemical age according to the simulations for the 'bb_vbs' scenario with the CHIMERE CTM and OPTSIM software. The contributions shown in panels (a) and (b) are evaluated using the first and second approaches described in Sect. ~~S5~~S6.
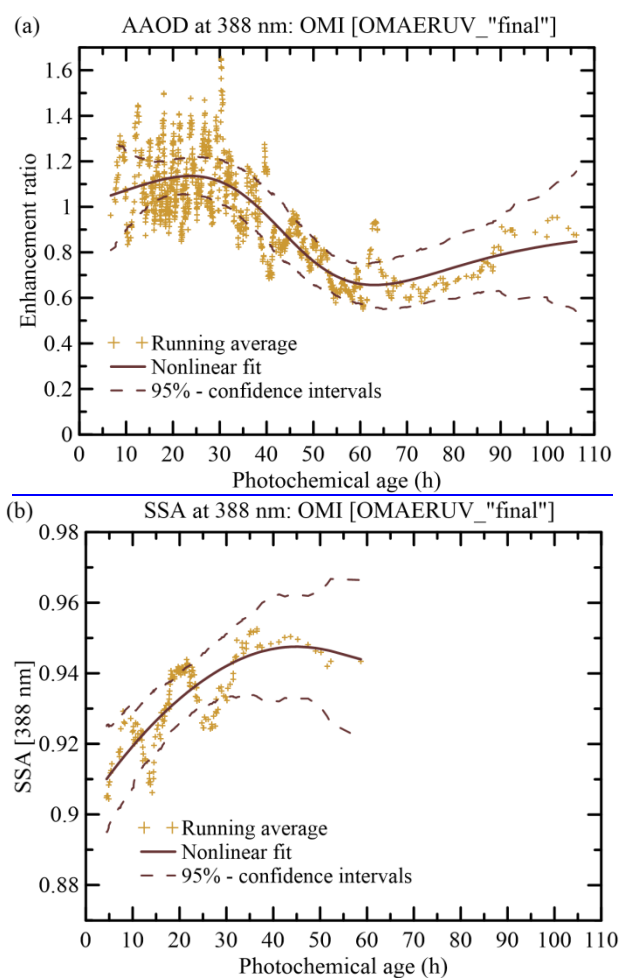

Figure S10. Nonlinear approximations (see Eq. 5) of the dependencies of EnRs for (a) AAOD (388 nm) and (b) SSA (388 nm) on the photochemical age of BB aerosol. The dependencies are similar to those shown in Fig. 5a and 5d except that they are obtained using the "final" OMAERUV data product.
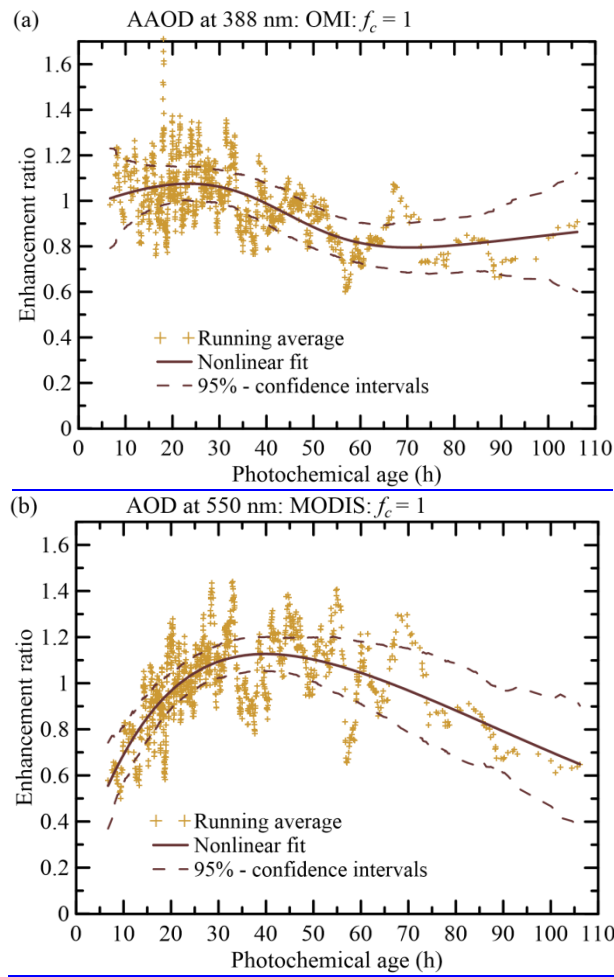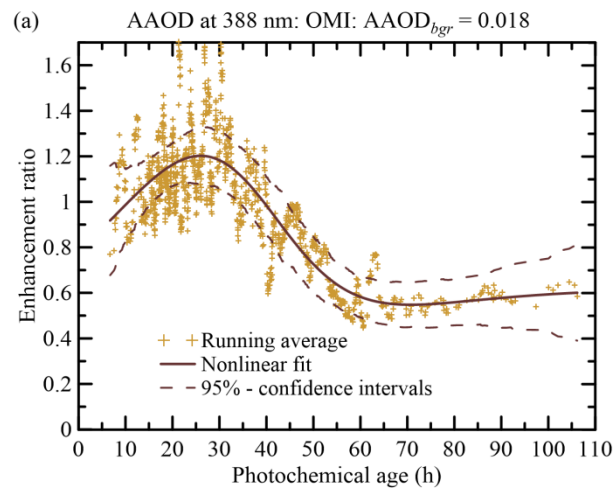
Figure S11. Nonlinear approximations of the dependencies of EnRs for (a) AAOD (388 nm) and (b) AOD (550 nm) on the photochemical age of BB aerosol. The dependencies are similar to those shown in Fig. 5a and 5b except that they are obtained without applying the correction involving CO columns (see Eqs. 2 and 3).
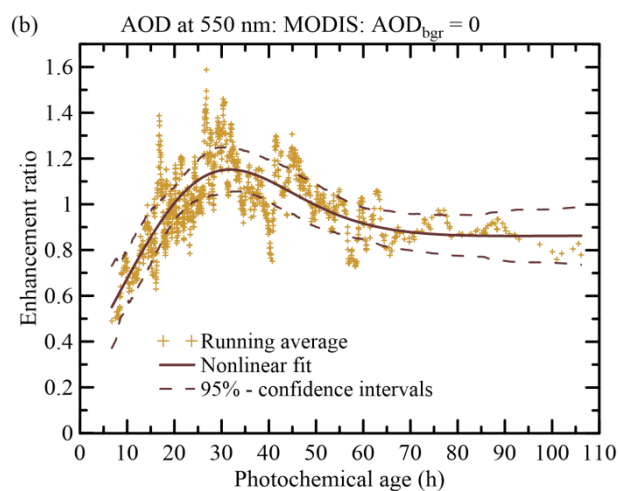
Figure S12. Nonlinear approximations of the dependencies of EnRs for (a) AAOD (388 nm) and (b) AOD (550 nm) on the photochemical age of BB aerosol. The dependencies are similar to those shown in Fig. 5a and 5b except that they are obtained assuming that the background AAOD (AAOD$_{bgr}$) equals to 0.018 and that the background AOD (AOD$_{bgr}$) equals to zero, respectively.

References

Ciarelli, G., El Haddad, I., Bruns, E., Aksoyoglu, S., Möhler, O., Baltensperger, U., and Prévôt, A. S. H.: Constraining a hybrid volatility basis-set model for aging of wood-burning emissions using smog chamber experiments: a box-model study based on the VBS scheme of the CAMx model (v5.40), Geosci. Model Dev., 10, 2303-2320, https://doi.org/10.5194/gmd-10-2303-2017, 2017.

Di Lorenzo, R. A., Washenfelder, R. A., Attwood, A. R., Guo, H., Xu, L., Ng, N. L., Weber, R. J., Baumann, K., Edgerton, E., and Young, C. J.: Molecular-size-separated brown carbon absorption for biomass-burning aerosol at multiple field sites, Environ. Sci. Technol., 51, 3128–3137, https://doi.org/10.1021/acs.est.6b06160, 2017.

Fleming, L. T., Lin, P., Roberts, J. M., Selimovic, V., Yokelson, R., Laskin, J., Laskin, A., and Nizkorodov, S. A.: Molecular composition and photochemical lifetimes of brown carbon chromophores in biomass burning organic aerosol, Atmos. Chem. Phys., 20, 1105–1129, https://doi.org/10.5194/acp-20-1105-2020, 2020.

Forrister, H., Liu, J., Scheuer, E., Dibb, J., Ziemba, L., Thornhill, K. L., Anderson, B., Diskin, G., Perring, A. E., Schwarz, J. P., Campuzano-Jost, P., Day, D. A., Palm, B. B., Jimenez, J. L., Nenes, A., and Weber, R. J.: Evolution of brown carbon in wildfire plumes, Geophys. Res. Lett., 42, 4623–4630, https://doi.org/10.1002/2015GL063897, 2015.

Konovalov, I. B., Beekmann, M., Berezin, E. V., Formenti, P., and Andreae, M. O.: Probing into the aging dynamics of biomass burning aerosol by using satellite measurements of aerosol optical depth and carbon monoxide, Atmos. Chem. Phys., 17, 4513-4537, https://doi.org/10.5194/acp-17-4513-2017, 2017.

Konovalov, I. B., Beekmann, M., Golovushkin, N. A., and Andreae, M. O.: Nonlinear behavior of organic aerosol in biomass burning plumes: a microphysical model analysis, Atmos. Chem. Phys., 19, 12091–12119, https://doi.org/10.5194/acp-19-12091-2019, 2019.

Luo, J., Zhang, Y., Wang, F., and Zhang, Q.: Effects of brown coatings on the absorption enhancement of black carbon: a numerical investigation, Atmos. Chem. Phys., 18, 16897–16914, https://doi.org/10.5194/acp-18-16897-2018, 2018.

Paris, J.-D., Stohl, A., Nédélec, P., Arshinov, M. Yu., Panchenko, M. V., Shmargunov, V. P., Law, K. S., Belan, B. D., and Ciais, P.: Wildfire smoke in the Siberian Arctic in summer: source characterization and plume evolution from airborne measurements, Atmos. Chem. Phys., 9, 9315–9327, https://doi.org/10.5194/acp-9-9315-2009, 2009.

Pokhrel, R. P., Beamesderfer, E. R., Wagner, N. L., Langridge, J. M., Lack, D. A., Jayarathne, T., Stone, E. A., Stockwell, C. E., Yokelson, R. J., and Murphy, S. M.: Relative importance of black carbon, brown carbon, and absorption enhancement from clear coatings in biomass burning emissions, Atmos. Chem. Phys., 17, 5063–5078, https://doi.org/10.5194/acp-17-5063-2017, 2017.

Sakamoto, K. M., Allan, J. D. Coe, H., Taylor, J. W., Duck, T. J., and Pierce, J. R.: Aged boreal biomass-burning aerosol size distributions from BORTAS 2011, Atmos. Chem. Phys., 15, 1633-1646, https://doi.org/10.5194/acp-15-1633-2015, 2015.

Selimovic, V., Yokelson, R. J., McMeeking, G. R., and Coefield, S.: In situ measurements of trace gases, PM, and aerosol optical properties during the 2017 NW US wildfire smoke event, Atmos. Chem. Phys., 19, 3905–3926, https://doi.org/10.5194/acp-19-3905-2019, 2019.

Sofiev, M., Ermakova, T., and Vankevich, R.: Evaluation of the smoke-injection height from wild-land fires using remote-sensing data, Atmos. Chem. Phys., 12, 1995–2006, https://doi.org/10.5194/acp-12-1995-2012, 2012.

Turquety, S., Hurtmans, D., Hadji-Lazaro, J., Coheur, P.-F., Clerbaux, C., Josset, D., and Tsamalis, C.: Tracking the emission and transport of pollution from wildfires using the IASI CO retrievals: analysis of the summer 2007 Greek fires, Atmos. Chem. Phys., 9, 4897–4913, https://doi.org/10.5194/acp-9-4897-2009, 2009.

Wong, J. P. S., Nenes, A., and Weber, R. J.: Changes in light absorptivity of molecular weight separated brown carbon due to photolytic aging, Environ. Sci. Technol., 51, 8414–8421, https://doi.org/10.1021/acs.est.7b01739, 2017.